Design and Development of polyfluorene Based Conjugated Polyelectrolytes for Sensing Applications

A thesis submitted by

Akhtar Hussain Malik

Roll No. 126122024

to

Indian Institute of Technology Guwahati

for the award of the degree of

Doctor of Philosophy

Department of Chemistry
Indian Institute of Technology Guwahati
Guwahati - 781039
India

June-2017

Dedicated To My Grandparents

INDIAN INSTITUTE OF TECHNOLOGY GUWAHATI
Department of Chemistry

STATEMENT

I do hereby declare that the work contained in the thesis entitled **"Design and Development of Polyfluorene Based Conjugated Polyelectrolytes for Sensing Applications"** is the result of investigations carried out by me in the Department of Chemistry, Indian Institute of Technology Guwahati, Guwahati, Assam India under the supervision of Prof. Parameswar Krishnan Iyer, Professor, Department of Chemistry, Indian Institute of Technology Guwahati, Guwahati, Assam, India. This work has not been submitted elsewhere for the award of any degree.

June, 2017
IIT Guwahati

Akhtar Hussain Malik

INDIAN INSTITUTE OF TECHNOLOGY GUWAHATI
Department of Chemistry

CERTIFICATE

This is to certify that the work contained in the thesis entitled **"Design and Development of Polyfluorene Based Conjugated Polyelectrolytes for Sensing Applications "** by **Akhtar Hussain Malik**, a Ph.D. student of Department of Chemistry, Indian Institute of Technology Guwahati, for the award of degree of Doctor of Philosophy has been carried out under my supervision and this work has not been submitted elsewhere for any degree.

June, 2017
Guwahati

Prof. Parameswar Krishnan Iyer
Thesis Supervisor
Department of Chemistry
Indian Institute of Technology Guwahati
Guwahati – 781039
Assam, India.

Acknowledgements

Foremost, I would like to express my earnest gratitude to my supervisor Prof. Parameswar Krishnan Iyer for his expert supervision, encouragement, advice, prudent suggestions and without whom this work would not have been possible. I am fortunate enough to have worked under his expert guidance which has taught me a lot about scientific research and life in general. I could not have imagined having a better advisor and mentor for my Ph.D.

I am indebited to my doctoral committee members, Prof. Bhisma Kumar Patel (Chairman), Prof. Aditya Narayan Panda and Dr. Vishal Trivedi for their ingenious advices, suggestions and critique which helped me a lot in improving my thesis work.

I am grateful to all faculty members of the Department of Chemistry, IIT Guwahati for their help and encouragement and also the non-teaching staff of the Department for their technical support. I am thankful to the Central Instruments Facility (CIF), IIT Guwahati for various characterization facilities.

I gratefully acknowledge all my teachers at AMU, Aligarh especially Prof. Shamsuzzaman, Prof. Mushfiq Prof. Suhail Sabir, Prof. Aminul Islam, Prof. Farukh Arjmand, Prof. Syed Mashhood, Dr. M. Shahid, Dr. Anamika Gupta for their friendly nature, best teachings, proper guidance, continuous encouragement, motivation and treasurable advices which certainly have great impact on me to pursue my higher studies.

I convey my special thanks to Sameer Hussain, Anamika Kalita, Ajaz Ahmad Dar and Adil Afroz for their continuing encouragement, invaluable advices and assistance in my thesis work. My best regards with Arvin, Sayan, Niranjan, Maimur, Nehal, Debasish, Ravindra for their unconditional love, respect, assistance and moral support.

It is a pleasure to express my deep sense of gratitude to all my dear labmates Sameer Bhai, Radha Bhai, Suresh Bhai, Bhim Bhai, Anamika Kalita, Anamika Dey, Ashish, Dipjyoti, Arvin, Sayan, Gopi, Rahul, Niranjan, Raman, Indrani, Ramesh Babu, Subrata, Maimur, Nystha, Nehal, Rithesh, Debasish, Ravinder, Priyanka Di, Himani Di and Ekta Di, for providing a friendly environment in lab and making my days memorable. Thanks also to all other departmental seniors, batch mates, juniors and friends (Saugata Da, Upashi, Anushree, Nawami, Radika, Deepanjali, Nevideta, Asif, Randeep, Somerjet, all the members of Chemistry Circket Association) for sharing valuable experiences and unforgettable moments.

I am highly obliged to all my seniors at AMU Aligarh especially Niyaz bhai, Khurshed bhai, Haider bhai, Khalid bhai, Firdouse bhai, Ayaz bhai,Yasir bhai, Tawseef bhai,

Nayeem bhai, Sajad bhai Naveed bhai, Ashiq bahi, Rouf bhai, Zeeshan bhai, Shameem bhai, Palash Bhai, for their continuous guidance, affection and care during my graduation and masters.

I am highly thankful to Almighty who bestowed me friends like Mudasir, Azhar, Mohasin, Javid, Firdose, Hamidulla, Tafazul, Habibi, Maggie, Faiza, Altaf, Ibrahim, Shafi, without whom my life would have been incomplete.

I would also like to express deep gratitude to my seniors, colleagues and juniors from AMU, Ajaz bhai, Palash bhai, Sameer bhai Wajid, Sahnawaz, Krapa, Zia, Faheem, Adil Bhai, Shaad, Kafeel, Maimur, Akhtar Alam, Adil Rather, Bilal, Tasleem, Munendra, Nehal, Rabiul, Shoaib, Shavez for giving me unforgettable experiences and cherishable moments. I will especially miss the wonderful moments shared with Sameer bhai, Ajaz bhai, Shaad, Adil bhai, Adil Rather, Bilal Mir, Wajid, Shahnawaz, Arvin, during my stay at Brahmaputra hostel IITG.

Finally, my PhD endeavour could not be completed without the boundless love, unending support, tolerance and blessings of my family. I would like to express my sincere gratitude with great honour to my family members who give me lots of love, strength, kind support and prayers which made me to reach this stage. I am fortunate and blessed enough to have such a caring and supportive parents Mrs. Misra Begum and Mr. Gh Mohi ud din, it is because of their prayers, sacrifice and struggle I am able to live my dream to complete my higher education from a prestigious institute. I am grateful to my younger sisters (Ulfat & Sufaya) and brother (Afaq) for their eternal love, cooperation and emotional support which were immensely needed to complete this work.

Last but not the least, I would like to thank the Almighty Allah for continuously showering his blessings and for providing me an expert supervisor cum mentor, a loving and supportive family, and wonderful friends who have sincerely helped me to achieve my intellectual destiny.

Akhtar Hussain Malik

Synopsis

The content of this synopsis report entitled **"Design and Development of Polyfluorene Based Conjugated Polyelectrolytes for Sensing Applications"** is divided into five chapters. Chapter 1 described the respective research area where the scope and significance of the subsequent chapters are discussed. Chapter 2 discussed about the synthesis and characterization of spontaneously formed conjugated polymer nanoparticles (CPNs) PFMI and its application in the detection of potent nitroexplosive-picric acid (PA) in multiple environments including 100% aqueous media, solid support using portable paper strips and vapor phase detection *via* two terminal devices. Chapter 3 described the synthesis of a new anionic conjugated polyelectrolyte PFPT and its application in the detection and removal of broad spectrum antibiotic tetracycline hydrochloride (Tc) from water. Chapter 4 highlights the synthesis of cationic CPE PFBT-MI *via* Suzuki cross-coupling polymerization which has been applied for the detection of widely used anionic surfactants SDS/SDBS in aqueous solution *via* the phenomenon of FRET. Furthermore, the polymer-surfactant nanoaggregates thus formed *via* electrostatic as well as hydrophobic interactions has been explored for the sensitive detection of spermine (considered as an excellent biomarker for early cancer diagnosis) in urinary samples. Chapter 5 discussed the synthesis of a new AIEE active CPE PFTPEBT-MI which finds it's practicability in the development of latent fingerprints on various substrates including plastic, glass, aluminium foil, metallic substrates, etc. without any additional treatment.

Chapter 1: Introduction

Conjugated polymers (CPs) have been developed and widely used since Shirakawa *et al.* discovered in 1977 that polyacetylenes obtained unusual conductivity, as high as 10 million times, upon halogen doping. The stable charge-transfer π complexes were believed to be formed during the halogen doping to achieve the systematically controllable electrical properties. As the first step of making plastics electrically conductive, this discovery led to the 2000 Nobel Prize in Chemistry, which was awarded to Hideki Shirakwa of the University of Tsukuba in Japan, Alan MacDiarmid of the University of Pennsylvania at Philadelphia and Alan Heeger of the University of California at Santa Barbara. In the past decades, we have witnessed revolutionary applications of conducting polymers, such as flat panel displays using OLEDs, light-emitting electrochemical cells (LECs), polymer solar cells, field-effect transistors (FETs), and chemical and bio-sensors.

Conjugated polyelectrolytes (CPEs) have emerged as excellent materials in the field of sensing due to their numerous features such as remarkable sensitivity, high quantum efficiency, photostability etc. These materials combine the optoelectronic properties of neutral conjugated polymers (CPs) as well as electrostatic behaviour of polyelectrolytes because CPEs consists of a hydrophobic π backbone responsible for its unique optical properties and a hydrophilic ionic side group which not only enhances its solubility in aqueous solution but also makes it liable to exhibit strong electrostatic interactions with various charged species and biological molecules like proteins, amino acids, DNA, nucleosides, surfactants, explosives etc. Thus, CPEs have arisen as promising resources in the fields of biological sensors and bioimaging entities because of their excellent biocompatibility, low cytotoxicity, and resistance to photo bleaching. Some of the well-known CP system are poly (*p*-phenylene vinylene) (PPV), poly (*p*-phenylenes) (PPP), poly(*p*-phenylene ethynylene) (PPE), polyfluorene (PF), polythiophene (PT), polypyrrole (PPy), etc. as shown in **Figure 1.**

Amplifying signal response

CPs exhibit strong absorption and emission due to the migration of excitons along the conjugated backbone chain. These excitons can be transferred to low energy/electron acceptor sites over a particular distance that subsequently results in signal amplification of the acceptors or amplified quenching of the fluorescence of CPs.

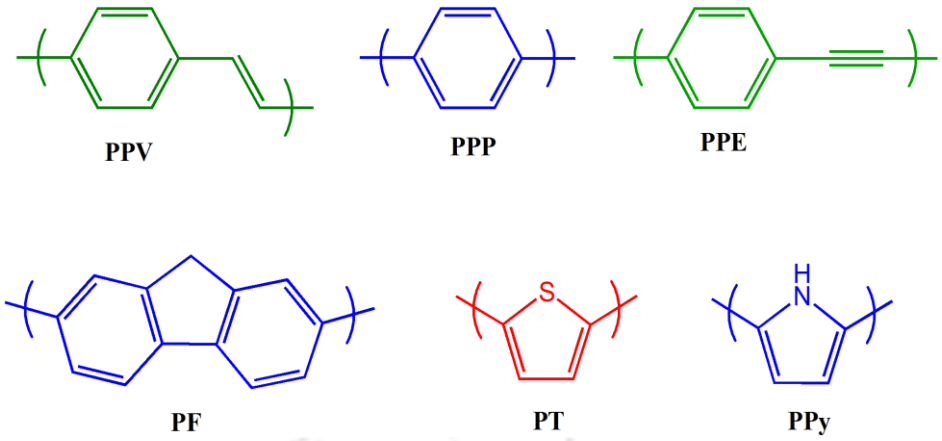

Figure 1. Structures of some well-known fluorescent conjugated polymer system.

The photophysical properties of CPs depend on effective conjugation length, chemical nature, intramolecular arrangements and intermolecular packing that provide suitable mechanisms for sensing applications. Sensors based on CPs are considered much more sensitive than small molecule based indicator due to their ability to amplify the signal from a recognition event. On binding of an analyte to a receptor attached to CP, the conducting properties of the entire backbone or various absorbing units are collectively affected as shown in **Figure 2**. Such recognition process ultimately results in signal amplification or super quenching (turn-off) of the fluorescence compared to small molecule based sensors where change in fluorescence usually occurred due to single chromophore after binding to that indicator only (**Figure 2**). This signal amplification process in CPs was first discovered by Swager in 1995 and termed as "molecular-wire effect". Such remarkable feature of CPs is important for chemo- and biosensing applications, since extremely dilute concentrations of the probe is required. When "turn-on" sensing mechanism is implemented, the analyte binding perturbs the electron density along the polymer backbone or alter the conformation of the polymer chain that subsequently results in appearance of emission.

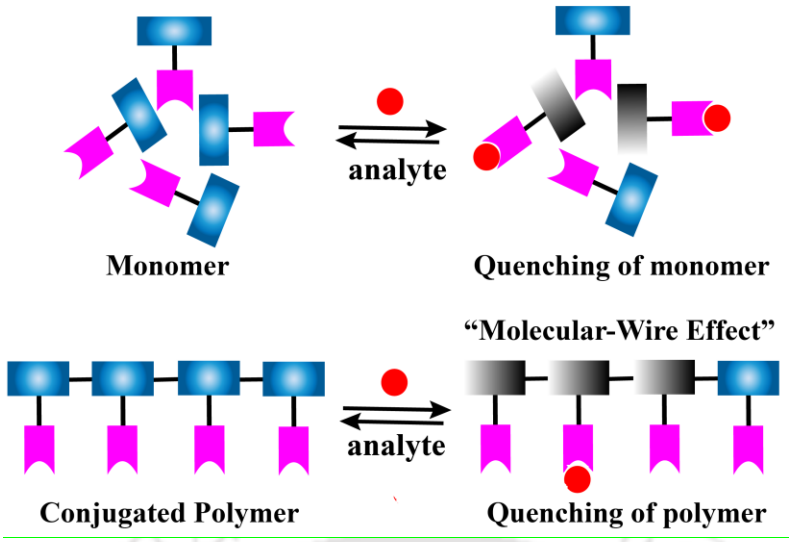

Figure 2. Pictorial representation of fluorescence quenching in monomer and polymer by analyte molecules.

Applications of conjugate polyelectrolytes as sensors

In recent years, the conjugated polymers provide unique optical properties and have triggered tremendous exploration for their use in sensing chemical and biological materials. For example, the conjugated polymers have been effectively employed as sensors to detect metal ions, anions, explosives, small biomolecules, proteins and DNA, etc. Due to the amplification occurred from the conjugated backbones of these polymers, the chemical and biosensors are able to achieve extraordinary sensitivity. Typically, the detection limits for CPE based biosensors are in the nanomolar range. In a few cases, sensors can even detect the target analytes at the zeptomole level.

Chapter 2: Conjugated polymer nanoparticles for the amplified detection of nitro-explosive picric acid on multiple platforms

This chapter described the synthesis of new cationic conjugated polyelectrolyte (CPE) poly(3,3'-((2-phenyl-9H-fluorene-9,9-diyl)bis(hexane-6,1-diyl))bis(1-methyl-1H-imidazol-3-ium)bromide) (PFMI) as shown in **Figure 3** *via* Suzuki coupling polymerization followed by post functionalization method without employing any hectic purification technique. Spontaneously formed conjugated polymer nanoparticles (PFMI-PNs) displayed remarkable fluorescence response towards nitroexplosive-picric acid (PA) in multiple environments including 100% aqueous media, solid support using portable paper strips and vapor phase detection *via* two terminal device. Highest quenching constant value (K_{sv}) of 1.12×10^8 M^{-1} and a very low detection limit of 30.9 pM/7.07 ppt

were obtained exclusively for PA in 100% aqueous environment which is rare and unique for any CPE/CPNs. Contact mode detection of PA was also performed using simple, cost-effective and portable fluorescent paper strips for achieving on-site detection. Furthermore, the two terminal sensor device fabricated PFMI-NPs provide an exceptional and unprecedented platform for the vapor mode detection of PA under ambient conditions. The mechanism for the ultra-sensitivity of PFMI-NPs probe to detect PA is attributed to the "molecular-wire effect", electrostatic interaction, photoinduced electron transfer (PET) and/or possible resonance energy transfer (RET) as shown in **Figure 4.**

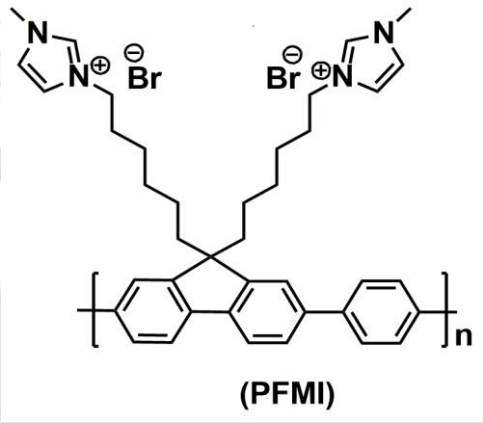

Figure 3. Structure of poly(3,3'-((2-phenyl-9H-fluorene-9,9-diyl)bis(hexane-6,1-diyl))bis(1-methyl-1H-imidazol-3-ium)bromide) (PFMI).

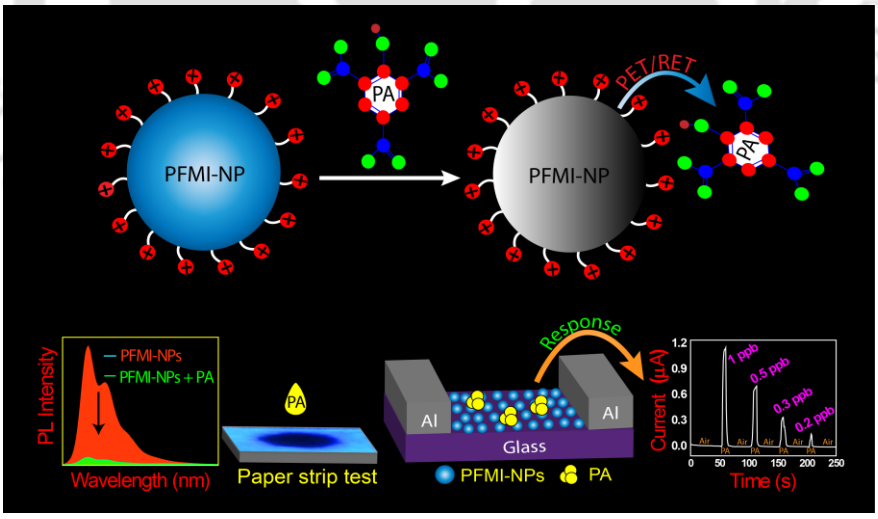

Figure 4. Schematic representation for the detection of picric acid on multiple platforms.

Chapter 3: Conjugated polyelectrolyte based sensitive detection and removal of antibiotics tetracycline from Water

This chapter discusses about the synthesis of new conjugated polyelectrolyte poly[5,5'-(((2-phenyl-9H-fluorene-9,9-diyl)bis(hexane-6,1-diyl))bis(oxy))diisophthalate] sodium (PFPT) (**Figure 5**) *via* palladium catalysed Suzuki cross coupling polymerization method and successfully applied for the rapid, real time and highly sensitive detection of broad spectrum antibiotic tetracycline hydrochloride (Tc) in 100 % aqueous media *via* photo-induced electron transfer. The detection limit of PFPT toward Tc was estimated to be 14.35 nM/6.80 ppb (6.8 ng/ mL) in 100% aqueous medium. High quenching efficiency with a K_{sv} value of 1.57×10^5 M^{-1} was obtained which can be attributed to efficient electron transfer from PFPT to Tc *via* electrostatic/hydrogen bonding interactions. Remarkably, PFPT could also be applied for the trace analysis of Tc in serum samples having recoveries well in the range 92-97% with relative standard deviations (RSD) of 1.01-1.14% confirming reliability of the present method for the analysis of Tc. Additionally, PFPT was blended with the abundant natural polysaccharide chitosan to form CS-PFPT composite films and developed as a biopolymer based membrane for the removal of Tc from water samples with a good adsorption capacity of 3.12 mg g^{-1} thus finding vital application in the treatment of antibiotic infested wastewater (**Figure 6**).

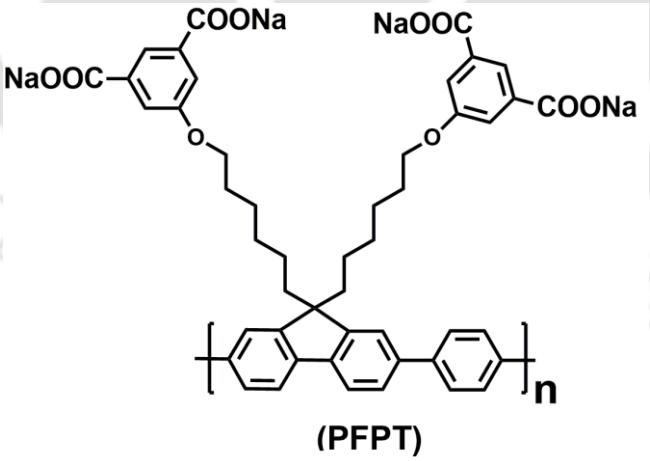

Figure 5. Structure of poly[5,5'-(((2-phenyl-9H-fluorene-9,9-diyl)bis(hexane-6,1-diyl))bis(oxy))diisophthalate] sodium (PFPT).

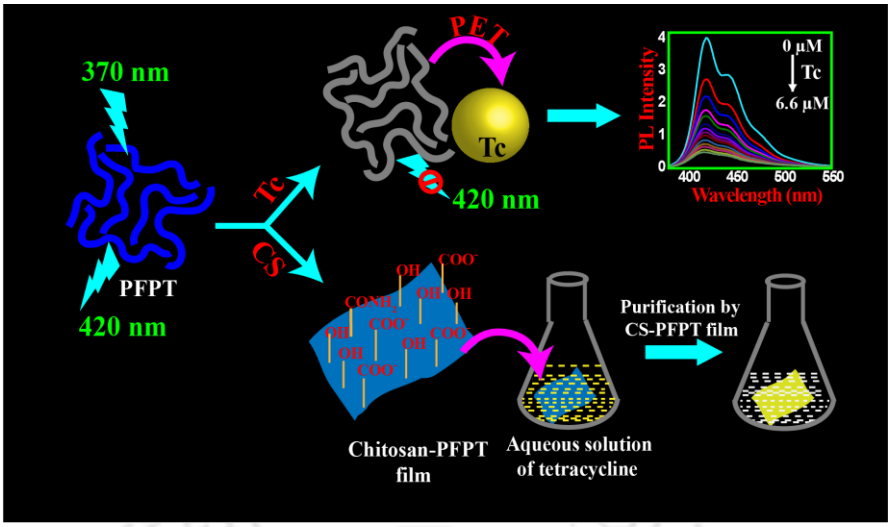

Figure 6. Schematic representation for the detection and removal of tetracycline hydrochloride from water.

Chapter 4: Aggregation induced FRET *via* polymer-surfactant complexation: A new strategy for the detection of spermine

In this chapter we have described the developed of a cationic conjugated polyelectrolyte [9,9-bis(6'-methyl imidazolium bromide)hexyl)fluorene-co-4,7-(2,1,3-benzothiadiazole)] (PFBT-MI) (**Figure 7**) *via* Suzuki cross-coupling polymerization. PFBT-MI displayed emission color change from blue to yellowish green in the presence of most common anionic surfactants SDS and SDBS in 100% aqueous solution and enables naked-eye detection and quantification of these surfactants in real time. The detection of SDS/SDBS at parts per billion levels [SDS - (0.12 μM/34 ppb) and SDBS - (0.13 μM/45 ppb)] is attributed to the inter-molecular FRET due to the aggregation of polymer chains assisted by SDS/SDBS *via* strong electrostatic as well as hydrophobic interactions. Furthermore, ensemble serves as a unique platform for the non-invasive, rapid and sensitive detection of spermine over other relevant amines, which is much lower than the range required for early cancer diagnosis and validates the reliability of the present system for real time practical applications. The PFBT-MI/SDS nanoaggregates thus formed *via* electrostatic as well as hydrophobic interactions has been explored for the sensitive detection of spermine (considered as an excellent biomarker for early cancer diagnosis) with detection limit of 66 ppb (0.33 μM) which is much below the range 1-10 μM pertinent for the early diagnosis of cancer in urinary samples. This, highly sensitive technique would facilitate the direct and non-invasive detection of spermine from urine rapidly and is likely to have great significance in early cancer diagnosis (**Figure 8**).

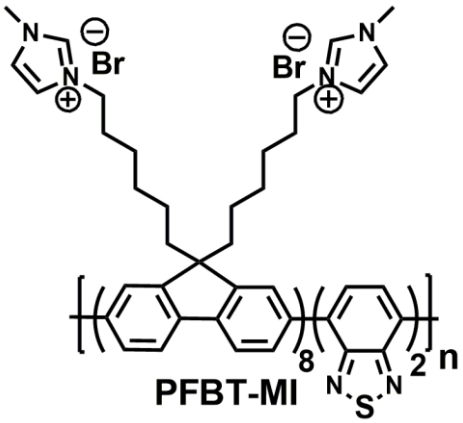

Figure 7. Structure of poly [9,9-bis(6′-methyl imidazolium bromide)hexyl)fluorene-co-4,7-(2,1,3-benzothiadiazole)] (PFBT-MI).

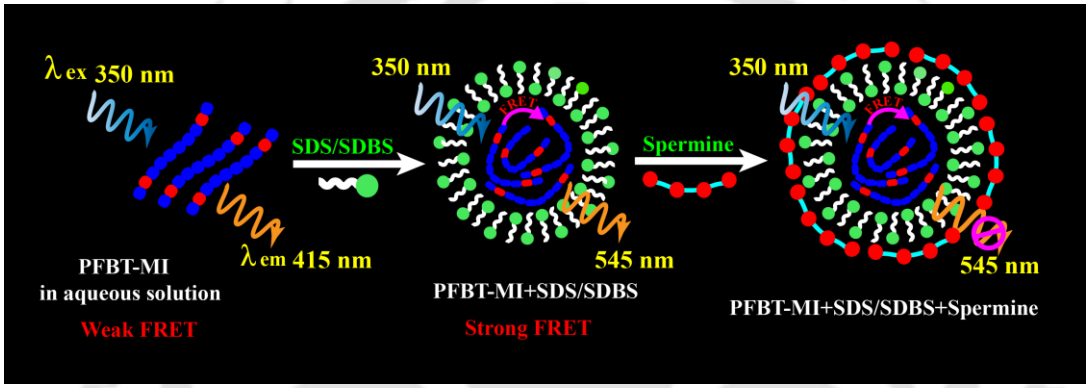

Figure 8. Schematic representation for the detection of anionic surfactants (SDS/SDBS) and spermine in aqueous solution.

Chapter 5: Development of latent fingerprints on various substrates using AIEE active conjugated polyelectrolyte

In this chapter, we have described the development of a simple, sensitive, environmentally friendly and cost-effective approach for the enhanced visualization of LFPs on various substrates including plastic, glass, aluminium foil, metallic substrates, etc. without any additional treatment based on AIEE active conjugated polyelectrolyte PFTPEBT-MI (**Figure 9**) by simply dipping the fingerprint laden substrate into the polymeric solution. The high fluorescence brightness and large Stokes shift contributed to the high-resolution imaging of latent fingerprints without any post-treatment such as fume treatment, surfactants, etc. for latent fingerprint development therefore providing more clear and detailed information (1-3 level), which makes the identification of an individual much easier. Thus, we have effectively applied this method in developing LFPs with high-sensitivity on various smooth surfaces including glass, aluminum foil, steel, coins,

adhesive tape etc. with negligible interference in presence of external abrasions which could hinder in the identification of personal information, thus successfully demonstrated the practicability of our method (**Figure 10**).

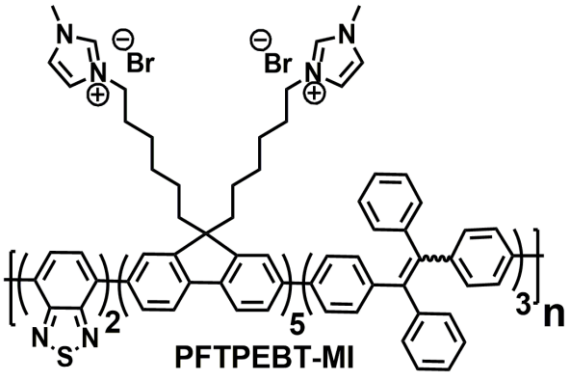

Figure 9. Structure of 3,3'-((2-(4-(1,2-diphenyl-2-(p-tolyl)vinyl)phenyl)-7-(7-methylbenzo[c][1,2,5]thiadiazol-4-yl)-9H-fluorene-9,9-diyl)bis(hexane-6,1-diyl))bis(1-methyl-1H-imidazol-3-ium) bromide (PFTPEBT-MI).

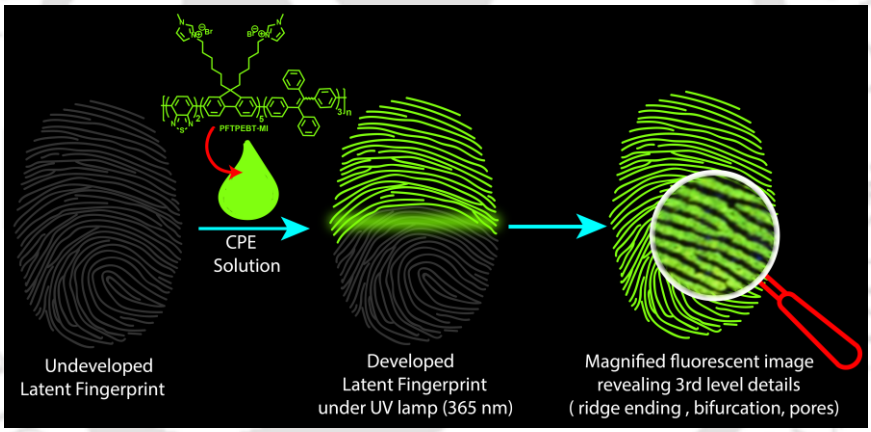

Figure 10. Schematic representation for the detection of latent fingerprints.

Conclusion and thesis overview

In conclusion, various new conjugated polyelectrolyte derivatives of polyfluorene were developed *via* Suzuki cross coupling polymerization reaction followed by post functionalization technique. The as synthesized CPEs were successfully explored for the selective and sensitive detection of various chemical and biological analytes such as potent explosive and environmental contaminant picric acid, corrosive and pollutant anionic surfactants SDS/SDBS, cancer biomarker spermine, antibiotic tetracycline hydrochloride and the detection of latent fingerprints.

Contents

Chapter 1

Introduction

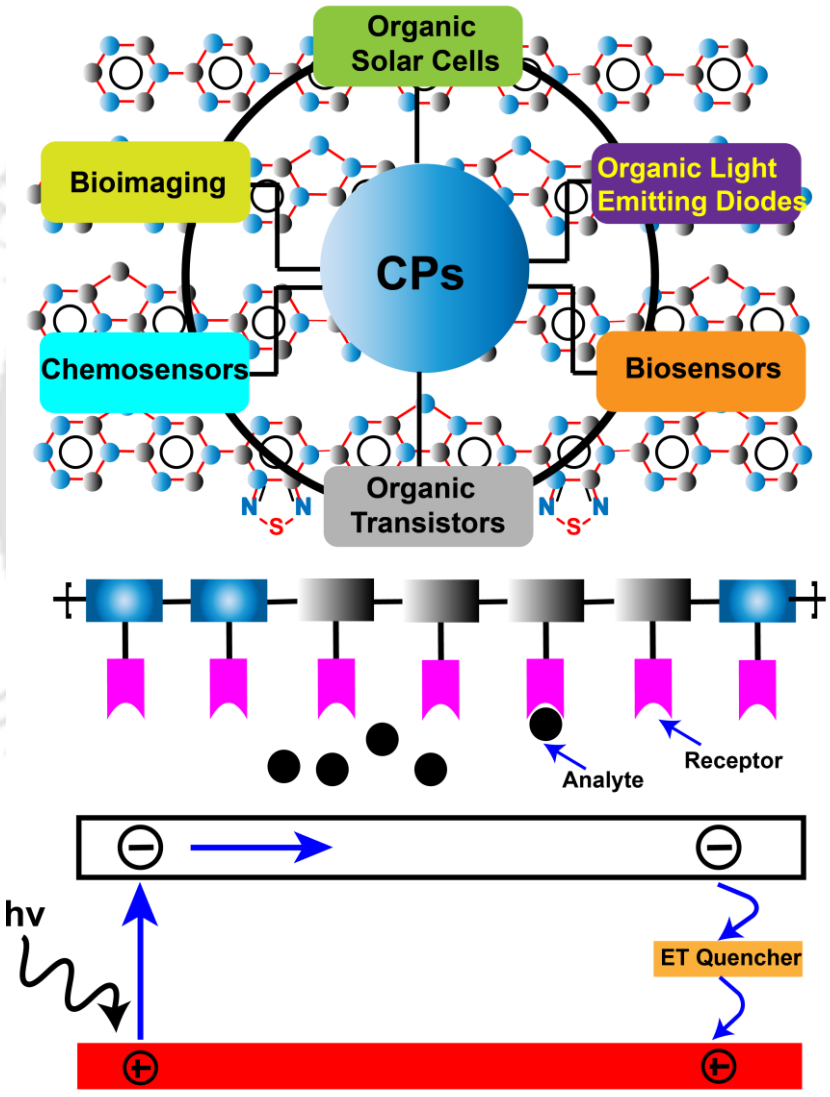

1.1 Introduction

Conjugated polymers (CPs) are organic macromolecules having alternating σ and π bonds along their backbone. The delocalized π-electron cloud over the backbone chain is responsible for the attractive optical and electrochemical properties of CPs. The conducting nature of CP was first discovered and developed by Alan MacDiarmid, Hideki Shirakawa and Alan J. Heeger in 1977 that led them to win the chemistry Nobel Prize in 2000. CPs has attracted significant attention from the last two decades because of their technologically promising future. These CPs have been explored for a variety of applications, including solar cells,[1] light emitting diodes (LEDs),[2,3] field-effect transistors (FETs),[4,5] and chemo- and biosensors.[6,7] CPs can be acquired with variable backbone chains, *viz*. poly (p-phenylene) (PPP), poly (p-phenylene vinylene) (PPV), poly (p-phenylene ethynylene) (PPE), polyfluorene (PF), polythiophene (PT), polypyrrole (PPy), etc. as shown in **Figure 1.1a.**

Conjugated polyelectrolytes (CPEs) are water-soluble conjugated polymers having pendant ionic functionalities such as sulfonate (SO_3^-), carboxylate (CO_2^-), phosphonate (PO_3^{2-}) and quarternary ammonium (NR_3^+) appended with the main conjugated chain that assist them to ionize in high dielectric media and forming stable electrostatic complexes with target analytes.[8-11] These materials combine the optoelectronic properties of neutral conjugated polymers (CPs) as well as electrostatic behaviour of polyelectrolytes, thus, providing an exceptional platform in the field of sensors (chemical and biological)[12-15] because of their capability to transform a binding/unbinding event into a measurable optical or electrochemical response, excellent biocompatibility, low cytotoxicity, strong emission brightness and resistance to photo bleaching. Some examples of CPEs are presented in **Figure 1.1b.**

1.2 Stern-Volmer fluorescence quenching

$$X^* + Q \xrightarrow{kq} X + Q \qquad 1.1$$

$$X + Q \underset{}{\overset{ka}{\rightleftharpoons}} [X, Q] \xrightarrow{hv} [X^*, Q] \longrightarrow X + Q \qquad 1.2$$

$$I_0/I = 1 + k_{sv}[Q] \qquad 1.3$$

From **equations 1.1** and **1.2**, X* is an excited-state fluorophore, Q is a quencher molecule, kq is the bimolecular quenching rate constant, and ka is the association constant for the ground-state complex formation [X, Q].

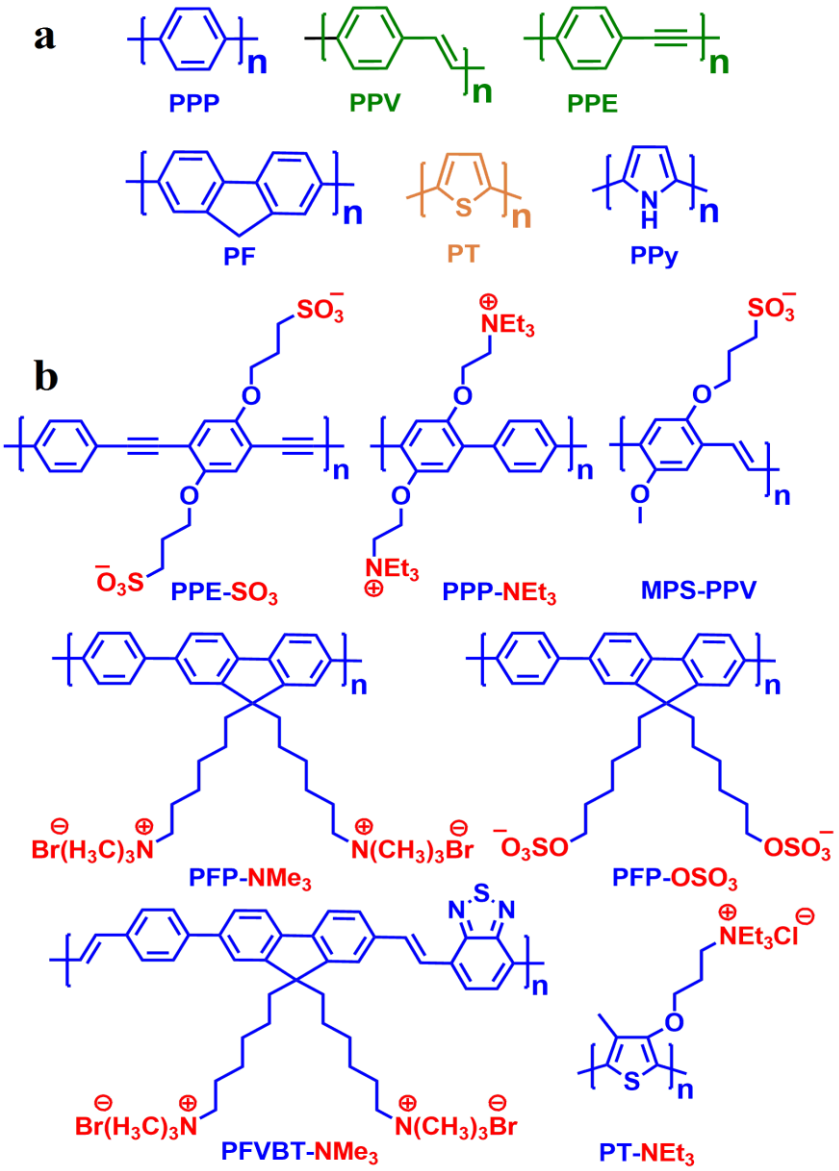

Figure 1.1 Structures of some (a) Common conjugated polymer backbones (b) Selected examples of conjugated polyelectrolytes (CPEs).

Equation **1.3** is known as Stern-Vomer equation, where I_0 is the fluorescence intensity in absence of quencher, I is the fluorescence intensity in presence of quencher, and K_{sv} is the Stern-Volmer quenching constant. Fluorescence quenching can take place by two different mechanisms i.e. dynamic (collisional) quenching and static (complex formation) quenching. Dynamic quenching (**equation 1.1**) occurs when the excited-state fluorophore encounters the quencher molecule which can facilitate non-radiative transitions to the ground state and the fluorescence is quenched. Static quenching takes place by binding of the quencher molecule to the fluorophore. The excited fluorophore generated is immediately and quantitatively quenched (**equation 1.2**). In the case of dynamic

quenching, $K_{sv} = kq\tau_0$, where τ_0 is the fluorescence lifetime of X*. The lifetime of the fluorophore in this case is reduced in the presence of quencher (**Figure 1.2a**). On the other hand, $K_{sv} = Ka$, if quenching is dominated by the static mechanism and its lifetime remains unaffected in presence of quencher (**Figure 1.2b)**. In both static and dynamic quenching, the Stern-Volmer plots of I_0/I versus [Q] should be linear as per **Equation 1.3**. However, in most cases, the Stern-Volmer plots show non linearity (curved graph) which can be explained by various complex processes, such as variation in the association constant with quencher concentration, mixed dynamic and static quenching mechanism, and chromophore aggregation.

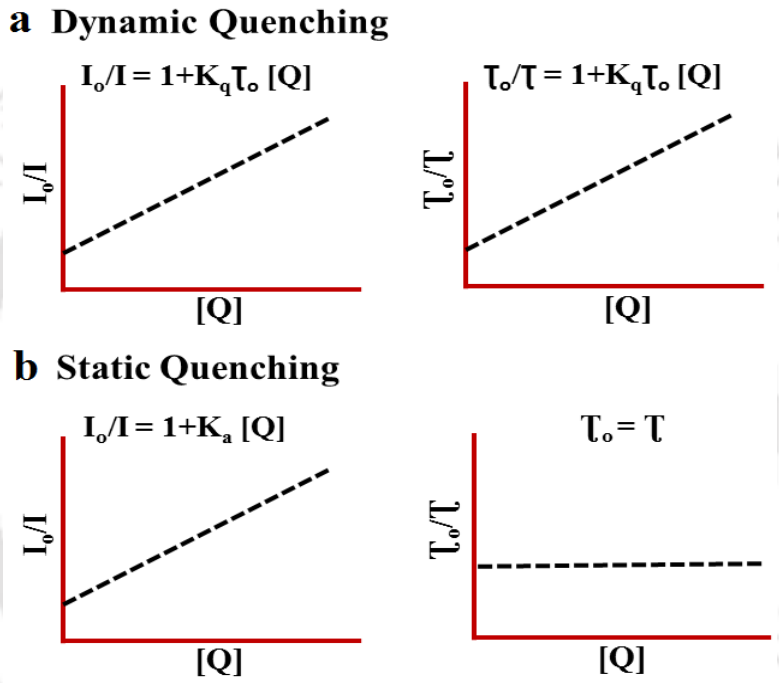

Figure 1.2 Plots showing effect of quencher concentration on fluorescence emission and fluorescence lifetime in case of (a) Dynamic and (b) Static quenching.

1.3 Amplifying signal response in conjugated polymers

One of the interesting property of conjugated polymers is the process of efficient fluorescence quenching at low quencher concentration, which is referred as amplified quenching.[12,16] It was Swager and co-workers in 1995 who for the first time demonstrated this phenomenon[16,17] of super quenching in polymers *via* "molecular-wire effect" which is responsible for its superior sensitivity over small molecule indicators. This signal amplification is an outcome of the ability of the CP to generate exciton (bound electron-hole pair) which migrates efficiently along the conjugated backbone. Because of the efficient charge migration, a single quencher unit bound to the receptor site of the

polymer will quench the fluorescence of almost the entire polymer chain leading to the amplified quenching response to target analyte (**Figure 1.3a**). This incredible feature of CPs validates its widespread application as chemo- and biosensors, since very dilute concentration of the analyte is required. To validate the phenomena of amplified quenching in CPs, fluorescence quenching of a cyclophane-containing poly(phenylene ethynylene) and an oligo(phenylene ethynylene) by methyl viologen (MV^{2+}) was studied (**Figure 1.3b**). MV^{2+} is a known electron transfer quencher agent and can efficiently bind to the cyclophane unit to form a rotaxane complex, thus efficient fluorescence quenching of polymer (about 60 times) was observed compared to the oligomeric compound.

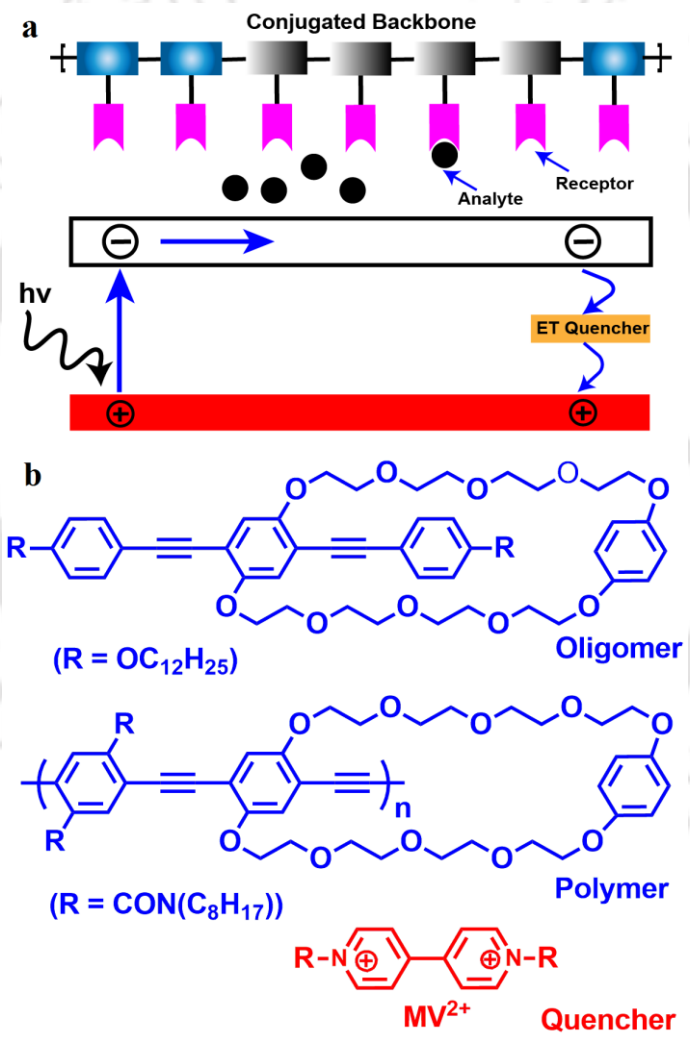

Figure 1.3 (a) Quenching mechanism of molecular wire effect in conjugated polymers (b) Structure of oligomer, polymer and quencher (MV^{2+}) used as fluorescence chemosensor for the first time by Swager and co-workers.

The proposed mechanism of this effect is efficient energy migration along the polymer backbone as discussed above. In 1998 Yang and Swager explored the above phenomena

of signal amplification for the sensitive detection of nitro-explosives 2,4,6-trinitrotoluene (TNT) and 2,4-dinitrotoluene (DNT).[18,19] However, the super quenching effect in CPEs was first described by Whitten and co-workers in the study of the fluorescence quenching of MPS-PPV by MV^{2+} (**Figure 1.4**).[20] The fluorescence of MPS-PPV solution was efficiently quenched by MV^{2+}, with a large K_{sv} value of 10^7 M^{-1}. This amplified quenching was attributed to the strong electrostatic interaction between the negatively charged polymer and MV^{2+} which bring them in close proximity resulting in disruption of exciton diffusion along the polymer backbone which leads to efficient fluorescence quenching.

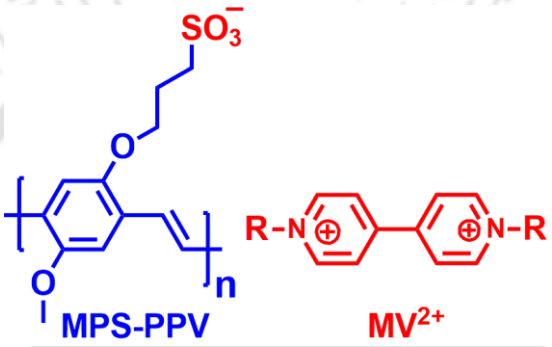

Figure 1.4 Structures of MPS-PPV and quencher (MV^{2+})

1.4 Conjugated polymers used as chemo or biosensors (selected examples)

Over the past few decades, CPs have been extensively used as sensory materials for various chemical and biological species[12,15,21-26] such as metals ions, anions, environmental pollutants, explosive materials, proteins, enzymes, etc. due to their remarkable sensitivity, high photoluminescence quantum yield, large extinction coefficients, photo- and thermal stability, etc. One of the important features of CPs is their capability to transform a binding/unbinding event into a measurable response (electrochemical or optical) which makes them as material of choice for sensing applications.

1.4.1 Detection of explosives

One of the most successful applications of CP sensors is in the detection of electron deficient nitro-aromatic explosives especially 2,4,6-trinitrotoluene (TNT), trinitrobenzene (TNB), Picric acid (PA) which are of great current interest in both national security and environmental protection because they are not only explosives but also recognized as

toxic pollutants.[27] In 1998, *Yang and Swager*[18] used a fluorescence quenching transduction mechanism along with the amplifying nature of CPs to design **P1** (**Figure 1.5**) as a highly sensitive material to detect TNT vapor. An important feature of this design is the rigid pentiptycene group, which prevents the chains of polymer from aggregating and display solution like optical properties in thin films therefore, prevents the quenching interaction that can hinder the exciton migration. Polymer **P1** was able to detect TNT at a concentration of 10 ppb after a few seconds exposure, thus exhibiting extraordinarily high sensitivity because of energy migration through polymer films.

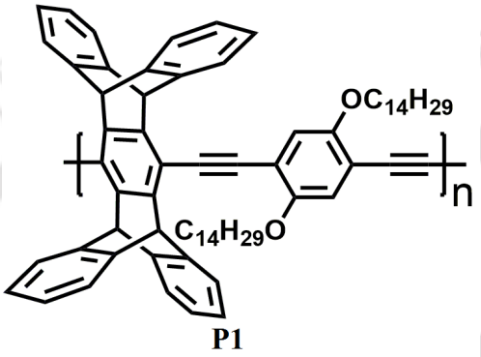

Figure 1.5 Structure of P1.

It has been observed mostly that PA exhibits higher quenching efficiencies than TNT because of its lower LUMO energy level. Therefore, to detect TNT in presence of PA in aqueous solution is challenging. In this regard, *Wang et al.*[28] in 2011, designed donor-acceptor **(P2)** and donor only (**P3** and **P4**) AIE active conjugated polymers (**Figure 1.6**) for the selective detection and discrimination of TNT and PA in aqueous solution. In **P2** the LUMO is mainly localized on acceptor unit of the CP i.e. 2,1,3-benzothiadiazole (BT). Since PA can easily form a negatively charged anion in aqueous solution, an electrostatic repulsive interaction between the BT unit and PA will disrupt the efficient electron transfer from the LUMO of **P2** to PA which will not occur in the case of TNT. Therefore, **P2** can selectively detect TNT instead of PA in aqueous solution. While as in case of polymers **P3** and **P4** having only donor groups behaves similar to most CP sensors i.e. having greater selectivity toward PA rather than TNT. Furthermore, these polymers were spin coated and then exposed to the vapours of TNT and PA. For **P1** film, the K_{sv} of TNT (1.2×10^5 M^{-1}) is almost 100 times more than that of PA (1.8×10^3 M^{-1}) and the limit of detection for TNT is about 23 ppb, while the emission of the **P4** film was selectively quenched by PA with K_{sv} constant of 2.8×10^4 M^{-1} and the detection limit of 2 ppb was observed. The fluorescence quenching response follows the order of DNT >

TNT > PA, which can be explained on the basis of differential vapor pressures of these analytes. Higher quenching for DNT can be attributed to its higher vapour pressure and vice versa in case of PA.

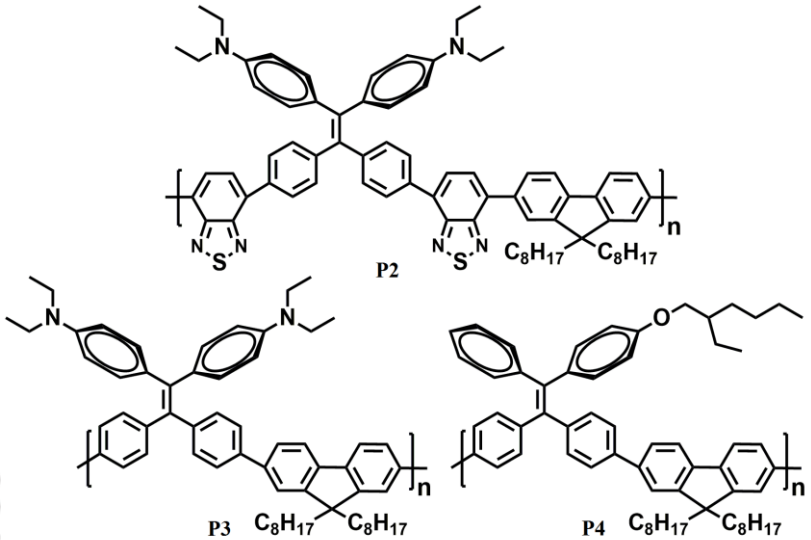

Figure 1.6 Structures of P2, P3, and P4.

In 2014, Scherf *et al.*[29] synthesized two poly(3,6-carbazole) **P5** and **P6** (**Figure 1.7**) with AIE-active tetraphenylethylene (TPE) on their side chains via nickel-catalyzed Yamamoto coupling under microwave heating. The resulting polymers combine the electron deficient behavior of the polycarbazole and the AIE active nature of TPE and displays distinct AIE properties. **P6** shows amplified fluorescence quenching response upon adding trinitrobenzene (TNB) in (1: 9, v/v) THF-water mixtures with a quenching constant of 1.26 $\times 10^6$ M^{-1}.

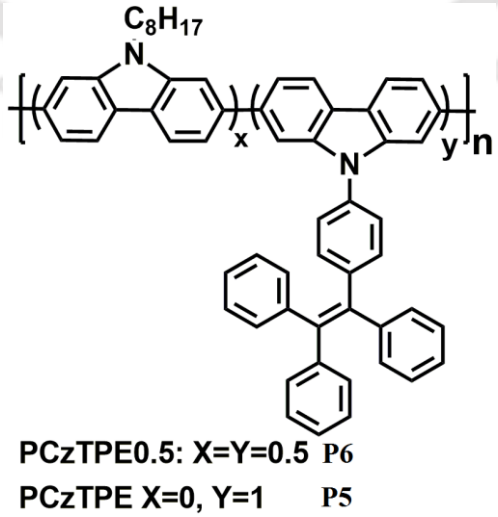

Figure 1.7 Structures of P5 and P6.

This enhanced quenching is ascribed to the increased number of quenching sites due to twisted 3D topology of the polymer in the nanoaggregates that can interact with TNB molecules. The mechanism of quenching was deduced to be excited electron transfer from the LUMO of the polymer to the LUMO of TNB. Furthermore, for practical applications, Whatman filter paper strips were cut and dipcoated into polymer solutions followed by drying in air. Both the polymers show TNB induced fluorescence quenching in solution as well as in vapour phase thus demonstrating the potential in solid state sensors for nitroaromatic explosives.

In 2015, Iyer *et al.*[30] developed a new strategy of introducing an ionic functionality on to the side chain of the polymer as a receptor for the specific interaction of CP with the target analyte. Methyl imidazolium group was introduced into the precursor polymer system to form a cationic polymer **P7 (Figure 1.8)**. Since PA exists as a negative entity in aqueous solution and the receptor attached to the CP is positively charged so there is a strong electrostatic attraction which brings the PA in close vicinity resulting in efficient charge transfer or energy transfer from the conjugated polymer to the analyte and ultimately amplified fluorescence quenching is obtained. Here, in this case highest quenching constant K_{sv} of 1 $\times 10^7$ M^{-1} and a detection limit of 128 ppt was obtained which confirms the method to be highly sensitive towards PA. Furthermore, paper strip and polymer doped chitosan films were used for the contact mode detection of PA which confirms the method to be practicable.

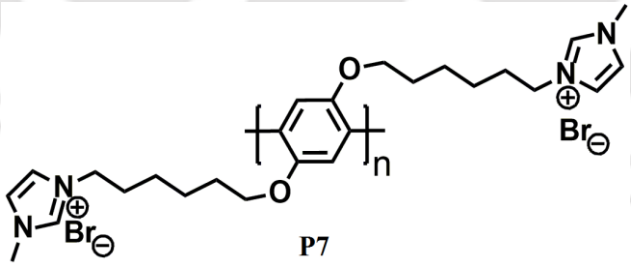

P7

Figure 1.8 Structure of P7

1.4.2 Detection of anions

It is known that selective detection of fluoride anion can be achieved by exploring the unique reactivity of fluoride towards silicon. As shown in **Figure 1.9a** fluoride triggered the removal of silyl from compound **1** which results in the formation of a highly emissive compound **2** (coumarin fluorophore). Swager *et al.*[31] in 2003 designed polymer **P8 (Figure 1.9b)** and applied the above strategy for the amplified detection of fluoride by

exploiting the exciton-transporting property of CPs. As anticipated, fluoride induced formation of coumarin residues along the polymer chain acts as local band gap traps for the migrating excitons and thus gives an enhanced signal response up to 100-fold compared to single molecule-based detection.

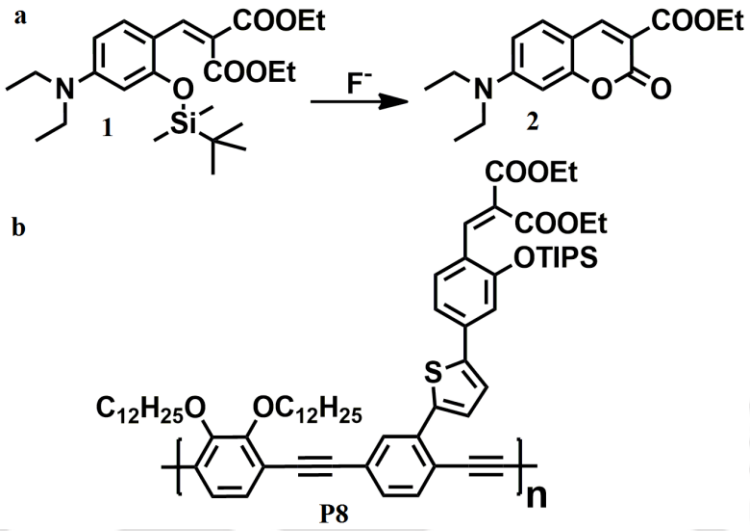

Figure 1.9 (a) Fluoride triggered cleavage of Si-O bond (b) Structure of P8.

In 2010, Schanze *et al.*[32] developed a cationic CPE **P9** (**Figure 1.10**) based on poly (phenyleneethynylene) *via* Sonogashira coupling reaction with polyamine side chains and explored its application in the ratiometric detection of pyrophosphate (PPi) with a detection limit of 340 nM. Polymer **P9** was designed in such a way that it shows red shifts in both emission and absorption spectra upon aggregation.

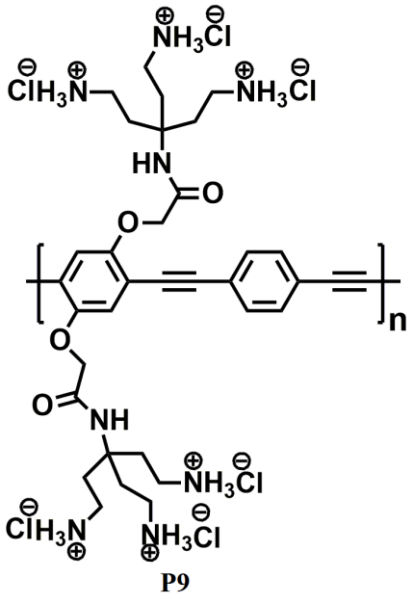

Figure 1.10 Structure of P9.

This phenomenon of colour change by switching from free chain state to the aggregate state was then explored for the naked eye detection of PPi in aqueous solution *via* analyte induced aggregation of CPE. Upon gradual addition of increasing concentration of PPi into the aqueous solution of **P9**, the absorption band at 400 nm decreases and a new absorption band appear at 430 nm. The emission spectra also reveal the clear transition between the two states as the blue emission with well resolved peaks between 433-455 nm decreases in intensity with increasing PPi concentration accompanied by increase in the green emission band at 520 nm. This large red-shift of about 90 nm is due to the efficient intermolecular exciton coupling among the polymer chains which results in lowering of energy in aggregate state.

In 2011, Wang *et al.*[33] developed a new CP **P10** (**Figure 1.11**) based on polyfluorene and dicyano-vinyl as a highly selective and sensitive sensor for cyanide. The design of **P10** is based on the fact that dicyano-vinyl group is a reactive site for cyanide *via* nucleophilic addition reaction which may disrupt the effective conjugation length of the polymer backbone and perturb its optical properties. Moreover, because of the exciton-diffusing property of CPs along its backbone, the nucleophilic adduct thus formed acts as a charge trapping sites which may enhance the fluorescence quenching effect and ultimately results in the higher sensitivity of the CP for cyanide ion with a detection limit of 14 ppb. Furthermore, naked eye detection of cyanide was also observed upon adding cyanide ions into the polymeric solution as the colour changes from yellow green to colourless, while as no colour change could be observed in presence of other common anions.

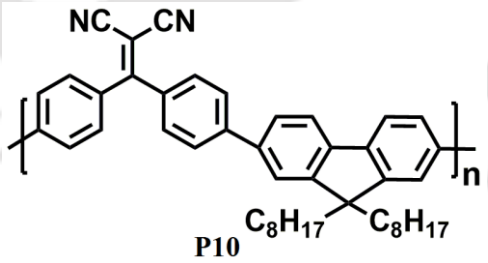

Figure 1.11 Structure of P10.

In 2012, Scherf *et al.*[34] studied the self-assembly complex formation between the cationic CPE **P11 (Figure 1.12)** and two anionic surfactants i.e. sodium octyl sulfate (SOS) and potassium heptadecafluoro-1-octanesulfonate (PFOS) both of which are industrially important. The absorption and emission spectra of **P11** were vividly changed in presence of anionic surfactants due to the formation of self-assembly *via* ionic complex formation.

It was observed that subtle structural differences between these surfactants has helped to understand the effect of head group charge density, chain rigidity, and hydrophobicity on both the complex structure and optical properties using UV/vis absorption, fluorescence and Small-Angle Neutron Scattering (SANS). It was concluded that **P11** is capable of identifying anionic surfactants with distinct subgroups *via* dual mode detection.

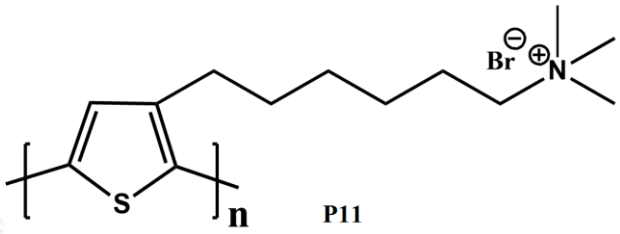

Figure 1.12 Structure of P11.

In 2015, Iyer *et al.*[30] synthesized a new CPE **P7** (**Figure 1.8**) *via* oxidative polymerization which displayed high selectivity and sensitivity towards most common anionic surfactants sodium dodecyl sulphate (SDS) and sodium dodecyl benzenesulfonate (SDBS) under various harsh conditions such as full pH range (1-14), urine, and in brine as well as in sea water. Polymer **P7** is very efficient in detecting and discriminating these moderately dissimilar anionic surfactants under acidic and basic conditions with a detection limit of 31.7 and 17.3 ppb respectively for SDBS and SDS in aqueous solution. Furthermore, **P7** could also remove these hazardous surfactants at very low levels from the water and other biological medium such as urine in the form of gel or precipitate as a result of its differential aggregation behaviour due to inter-polymer cofacial arrangement *via* Columbic attraction.

1.4.3 Detection of biomolecules

In 2004, Bazan *et al.*[35] synthesized a multipurpose cationic CPE **P12** (**Figure 1.13**) *via* Suzuki-coupling copolymerization technique by introducing 5% 2,1,3-benzothiadiazole (BT) units into cationic poly(fluorine-co-phenylene) to obtain two distinct emission colors from a single polymer chain. The cationic polymer **P12** strongly interacts with oppositely charged DNA molecule in aqueous solution, resulting in aggregation of polymer chains. Such inter-polymer interactions lead to increase in the local concentration of benzothiadiazole (BT) units (responsible for FRET) and inter-chain contacts that subsequently improve electronic coupling between the optical partners. This ultimately facilitates the energy transfer process from the fluorine-phenylene (donor) segments to BT (acceptor) units, thus enabling the change in emission color of solution

from blue to green that aided in the determination of DNA concentration. Furthermore, the authors demonstrated that polymer **P12** could also be employed as a three-color DNA assay using a PNA-C* strand. Depending upon the content of solution, three different emission colors could be obtained i.e. (i) blue (in the absence of DNA), (ii) green (in the presence of non-complementary ssDNA) and (iii) red (in the presence of complementary ssDNA). Taking advantage of the signal amplification effect of CPs, fine-tuning of electrostatic and optical events leads to multicolour biosensing assay.

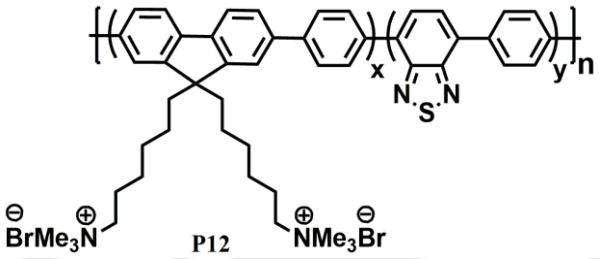

Figure 1.13 Structure of P12.

In 2009, Liu *et al.*[36] designed and synthesized two cationic CPEs **P13** and **P14** which differ only by side chains (**Figure 1.14**). These benzothiadiazole (BT) based CPEs shows low fluorescence emission in aqueous solution while as its fluorescence increases in aggregated state. Taking the advantage of complexation-induced aggregation behaviour, a fluorescence turn-on sensor has been developed for the detection and quantification of heparin. A substantial increase in the fluorescence response of the polymer in presence of heparin as compared to its analog hyaluronic acid (HA) is because of its strong complexation with heparin, thus allowing discrimination of heparin from HA. The advantage of this strategy is that it does not require a prequenching technique and the analyte can be detected directly using this polymer system.

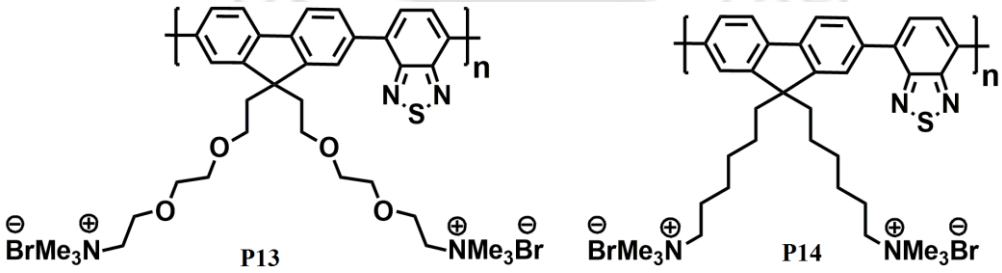

Figure 1.14 Structure of P13 and P14.

In 2009, Liu *et al.*[37] designed a ligand-analyte binding facilitated energy transfer strategy for lysozyme detection using anionic CPE **P15** (**Figure 1.15**) and dye labeled aptamer. When the lysozyme interacts with the dye-labeled aptamer FRET occurs from **P15** to dye

because of the strong electrostatic interactions and green colour formation. In the absence of lysozyme no FRET happens and the colour of the solution is blue. The simplicity, sensitivity and specificity of this method has been explored by using lysozyme and lysozyme aptamer which has not been observed in other methods like electrochemistry, ELISA, aptamer assay based lysozyme assay therefore, this method has been successfully applied in biological media.

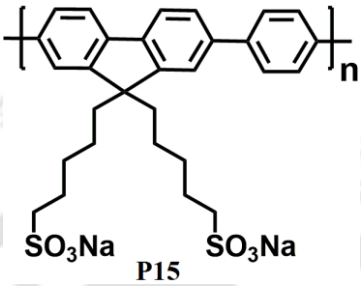

Figure 1.15 Structure of P15.

In 2015, Wang *et al.*[38] designed new water soluble CP **P16** (**Figure 1.16**) with PEG side chain to which carboxylic acid group and boronate-protected fluorescein is covalently attached.

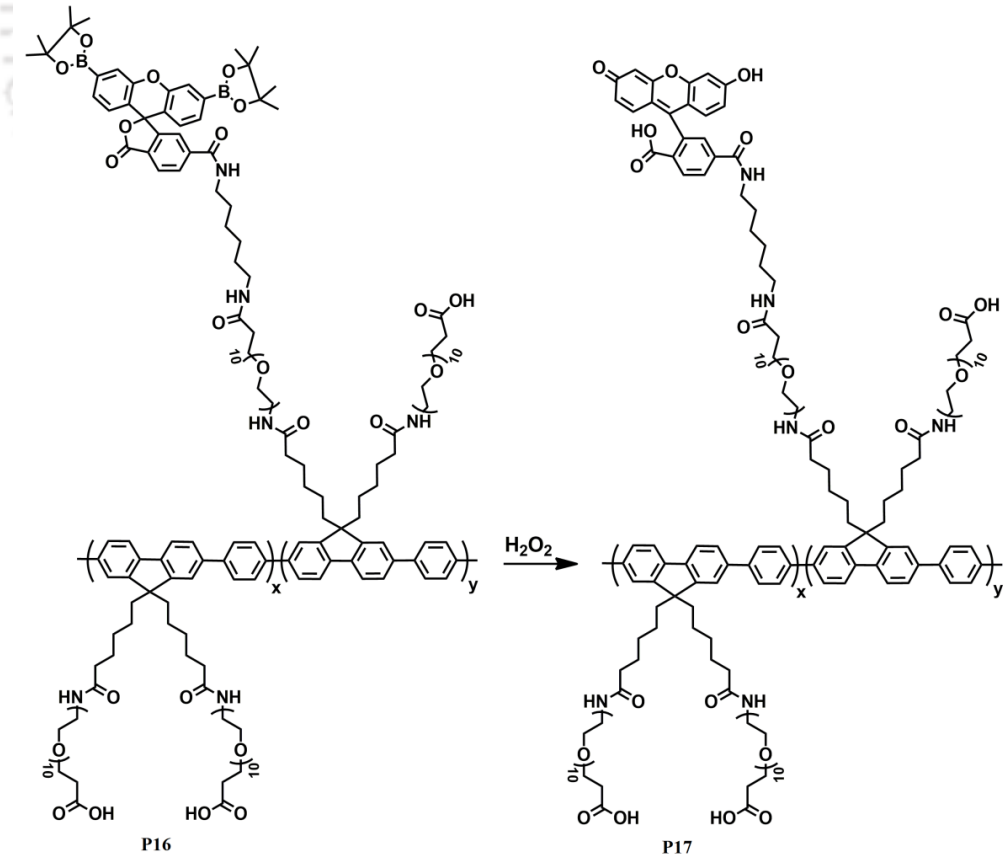

Figure 1.16 Structure of P16 and its conversion into P17 in presence of H_2O_2.

Carboxylic acid functionality and PEG chain not only increases the solubility of the polymer in water but also reduces nonspecific interactions with the cells and allows further modification of CP. Efficient fluorescence resonance energy transfer (FRET) takes place from **P17** backbone to fluorescein unit in the presence of H_2O_2 upon excitation at 380 nm and the colour of polymer solution changes from blue to green. Therefore, the polymer probe shows good ratiometric fluorescence response to H_2O_2 that was generated from choline and acetylcholine (Ach) under AChE/ChOx enzyme-coupled reaction. The present strategy realizes choline and ACh detection in a simple and selective manner and presents high specificity to choline and ACh, respectively.

1.5 Objective and conclusion of the thesis work

The primary focus of the present study was to design and develop conjugated polyelectrolyte (CPE) based fluorescence sensors for the sensitive and selective detection of various target analytes including explosive materials, environmental contaminants, fingerprint residues, cancer biomarkers etc. with an aim to overcome the challenges and problems arising in the existing sensing systems. Among various CPs, polyfluorene (PF) was chosen for sensing studies due to its ease of synthesis, low-cost, high photostability, high quantum yield and excellent film forming ability. All of these properties enable PF to be explored as excellent candidates for optical sensor applications. The key objective and conclusion for each work is described below:

- Picric acid (PA) is a superior explosive material and was extensively used until World War-I due to its potent explosive nature than TNT. Owing to the incredible solubility of PA in water and widespread applications in various industries and forensic investigations, it is likely to contaminate soil and ground water when exposed and is responsible for several health disorders. Therefore, development of superior methods for monitoring the traces of PA in multiple environments remains a challenging task for the researchers due to its low vapour pressure, absence of any specific receptor for PA and interference from other electron deficient nitroexplosives. Chapter II highlighted the synthesis and characterization of conjugated polymer nanoparticles for the selective and sensitive detection of PA on multiple platforms including including aqueous solution, contact mode as well as in vapor phase.
- Tetracycline (Tc) is a versatile broad spectrum bacteriostatic antibiotic, known to inhibit the protein synthesis by binding with the 30s ribosome subunit. Because of its broad spectrum activity, good oral absorption, relatively low toxicity and cost effectiveness, it

has been broadly used in the treatment of bacterial infections in humans, veterinary animals and fish. The misuse or abuse of these antibiotics has led to the elevated levels of resistant antibiotic residues in both surface and ground water, in drinking water as well as in animal products, which has promoted the evolution of multidrug and antibiotic resistant bacteria. Chapter III described the synthesis and characterization of a new anionic conjugated polyelectrolyte and its application in the sensitive detection and removal of broad spectrum antibiotic tetracycline Tc from water.

- Anionic surfactants (SDS/SDBS) form a major source of environmental pollutant due to their widespread use in personal, home/car cleaning agents, industrial and agricultural processes. These surfactants are considered as emerging pollutants. Therefore, their determination at very low levels in the waste water, food preparations, pharmaceuticals, as masking agents in drug-abuse, in biological mediums etc. is highly significant. Chapter IV discussed the synthesis of cationic CPE which has been applied for the detection of widely used anionic surfactants SDS/SDBS in aqueous solution *via* the phenomenon of FRET. Furthermore, the polymer-surfactant assembly thus formed *via* electrostatic as well as hydrophobic interactions has been explored for the non-invasive detection of spermine (considered as an excellent biomarker for early cancer diagnosis) in urine samples.
- Latent fingerprints (LFPs) obtained at the site of crime are considered as important physical evidence in forensic investigation because of the uniqueness in ridge pattern for each individual and thus, can be helpful in cracking a criminal case. Mostly LFPs found are not visible to naked eye under ambient light, hence additional efforts are required for easy visualization. Chapter V discussed the synthesis of a new AIEE active CPE which finds it's practicability in the development of latent fingerprints on various substrates including plastic, glass, aluminium foil, metallic substrates, etc. without any additional treatment.

References

(1) Gunes, S.; Neugebauer, H.; Sariciftci, N. S. *Chem. Rev.* **2007**, *107*, 1324.

(2) Kraft, A.; Grimsdale, A. C.; Holmes, A. B. *Angew. Chem., Int. Ed*. **1998**, *37*, 402.

(3) Montali, A.; Smith, P.; Weder, C. *Synth. Met.* **1998**, *97*, 123.

(4) Torsi, L.; Dodabalapur, A.; Rothberg, L. J.; Fung, A. W. P.; Katz, H. E. *Science* **1996**, *272*, 1462.

(5) Sirringhaus, H. *Adv. Mater.* **2005**, *17*, 2411.

(6) McQuade, D. T.; Pullen, A. E.; Swager, T. M. *Chem. Rev.* **2000**, *100*, 2537.

(7) Thomas, S. W.; Joly, G. D.; Swager, T. M. *Chem. Rev.* **2007**, *107*, 1339.

(8) Jiang, H.; Taranekar, P.; Reynolds, J. R.; Schanze, K. S. *Angew. Chem., Int. Ed*. **2009**, *48*, 4300.

(9) Marques, A. T.; Pinto, S. M. A.; Monteiro, C. J. P.; Melo, J. S. S.; Burrows, H. D.; Scherf, U.; Calvete, M. J. F.; Pereira, M. M. *J. Polym. Sci., Part A: Polym. Chem*. **2012**, *50*, 1408.

(10) Henson, Z. B.; Zhang, Y.; Nguyen, T. Q.; Seo, J. H.; Bazan, G. C. *J. Am. Chem. Soc.* **2013**, *135*, 4163.

(11) Liu, B.; Bazan, G. C. *Chem. Mater*. **2004**, *16*, 4467.

(12) Thomas, S. W.; Joly, G. D.; Swager, T. M. *Chem. Rev*. **2007**, *107*, 1339.

(13) Zhu, C.; Liu, L.; Yang, Q.; Lv, F.; Wang, S. *Chem. Rev*. **2012**, *112*, 4687.

(14) Liang, J.; Li, K.; Liu, B. *Chem. Sci*. **2013**, *4*, 1377.

(15) Rochat, S.; Swager, T. M. *ACS Appl. Mater. Interfaces* **2013**, *5*, 4488.

(16) Zhou, Q.; Swager, T. M. *J. Am. Chem. Soc*. **1995**, *117*, 12593.

(17) Zhou, Q.; Swager, T. M. *J. Am. Chem. Soc*. **1995**, *117*, 7017.

(18) Yang, J.-S.; Swager, T. M. *J. Am. Chem. Soc*. **1998**, *120*, 5321.

(19) Yang, J.-S.; Swager, T. M. *J. Am. Chem. Soc*. **1998**, *120*, 11864.

(20) Chen, L. H.; McBranch, D. W.; Wang, H. L.; Helgeson, R.; Wudl, F.; Whitten, D. G. P *Natl. Acad. Sci. USA* **1999**, *96*, 12287.

(21) McQuade, D. T.; Pullen, A. E.; Swager, T. M. *Chem. Rev*. **2000**, *100*, 2537.

(22) Zhu, C.; Liu, L.; Yang, Q.; Lv, F.; Wang, S. *Chem. Rev*. **2012**, *112*, 4687.

(23) Liang, J.; Li, K.; Liu, B. *Chem. Sci*. **2013**, *4*, 1377.

(24) Kim, H. N.; Guo, Z.; Zhu, W.; Yoon, J.; Tian, H. *Chem. Soc. Rev*. **2011**, *40*, 79.

(25) Lee, K.; Povlich, L. K.; Kim, J. *Analyst* **2010**, *135*, 2179.

(26) Albert, K. J.; Lewis, N. S.; Schauer, C. L.; Sotzing, G. A.; Stitzel, S. E.; Vaid, T. P.; Walt, D. R. *Chem. Rev*. **2000**, *100*, 2595.

(27) Tu, R. Y.; Liu, B. H.; Wang, Z. Y.; Gao, D. M.; Wang, F.; Fang, Q. L.; Zhang, Z. P. *Anal. Chem*. **2008**, *80*, 3458.

(28) Xu, B.; Wu, X.; Li, H.; Tong, H.; Wang, L. *Macromolecules* **2011**, *44*, 5089.

(29) Dong, W.; Fei, T.; Palma-Cando A.; Scherf, U. *Polym. Chem*. **2014**, *5*, 4048.

(30) Hussain, S.; Malik, A. H.; Afroz, M. A.; Iyer, P. K. *Chem. Commun*. **2015**, *51*, 7207.

(31) Kim, T-H.; Swager, T. M. *Angew. Chem., Int. Ed*. **2003**, 42, 4803.

(32) Zhao, X.; Schanze, K. S. *Chem. Commun*. **2010**, *46*, 6075.

(33) Wu, X.; Xu, B.; Tong, H.; Wang, L. *Macromolecules* **2011**, *44*, 4241.

(34) Evans, R. C.; Knaapila, M.; Willis-Fox, N.; Kraft, M.; Terry, A.; Burrows, H. D.; Scherf, U. *Langmuir* **2012**, *28*, 12348.

(35) Liu, B.; Bazan, G.C. *J. Am. Chem. Soc*. **2004**, *126*, 1942.

(36) Pu, K-Y.; Liu, B. *Adv. Funct. Mater*. **2009**, *19*, 277.

(37) Wang, J.; Liu, B. *Chem. Commun*. **2009**, 2284.

(38) Wang, Y.; Li, S.; Feng, L.; Nie, C.; Liu, L.; Lv, F.; Wang, S. *ACS Appl. Mater. Interfaces* **2015**, *7*, 24110.

Chapter 2

Conjugated Polymer Nanoparticles for the Amplified Detection of Nitro-explosive Picric Acid on Multiple Platforms

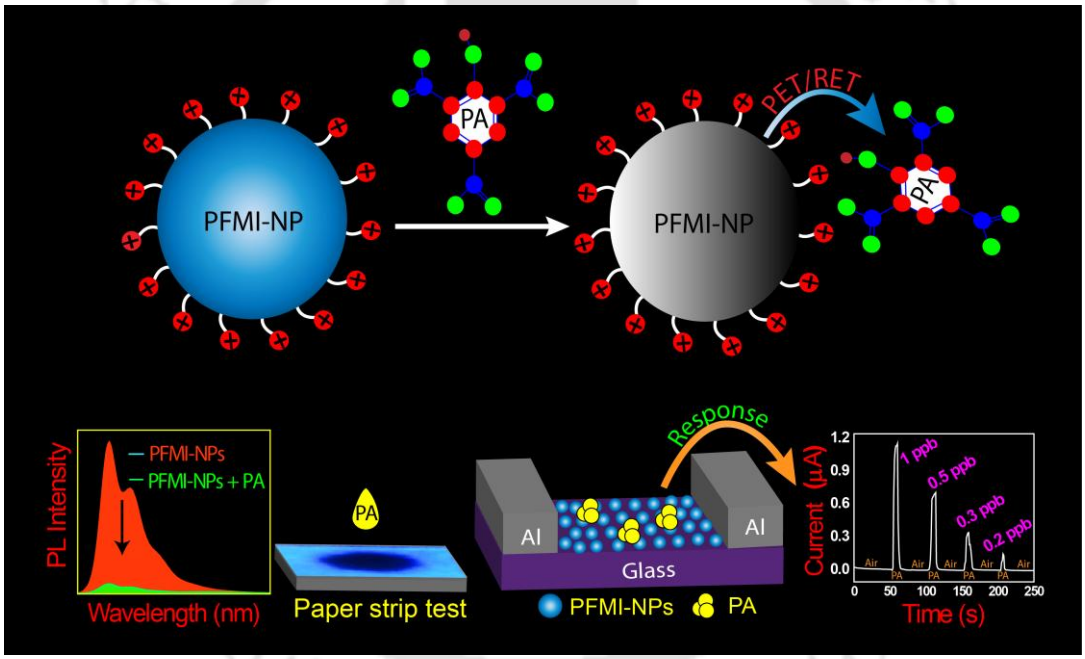

Malik, A. H.; Hussain, S.; Kalita, A.; Iyer, P. K. *ACS Appl. Mater. Interfaces*, **2015**, *7*, 26968–26976.

Abstract

Spontaneously formed conjugated polymer nanoparticles (CPNs) or polymer dots displayed remarkable fluorescence response towards nitroexplosive-picric acid (PA) in multiple environments including 100% aqueous media, solid support using portable paper strips and vapor phase detection *via* two terminal device. This new cationic conjugated polyelectrolyte (CPE) poly(3,3'-((2-phenyl-9H-fluorene-9,9-diyl)bis(hexane-6,1-diyl))bis(1-methyl-1H-imidazol-3-ium)bromide) (PFMI) was synthesized by Suzuki coupling polymerization followed by post functionalization method without employing any hectic purification technique. Highest quenching constant value (K_{sv}) of 1.12×10^8 M^{-1} and a very low detection limit of 30.9 pM/7.07 ppt were obtained exclusively for PA in 100% aqueous environment which is rare and unique for any CPE/CPNs. Contact mode detection of PA was also performed using simple, cost-effective and portable fluorescent paper strips for achieving on-site detection. Furthermore, the two terminal sensor device fabricated with nanoparticles of PFMI (PFMI-NPs) provides an exceptional and unprecedented platform for the vapor mode detection of PA under ambient conditions. The mechanism for the ultra-sensitivity of PFMI-NPs probe to detect PA is attributed to the "molecular-wire effect", electrostatic interaction, photoinduced electron transfer (PET) and/or possible resonance energy transfer (RET).

2.1 Introduction

The development of reliable methods for the rapid and selective detection of ultra-trace amounts of nitro-explosive are of vital concern for national security as well as catastrophic environmental pollution.[1-6] Although, RDX and 2,4,6-trinitrotoluene (TNT) are the most widely used nitroexplosives; picric acid (PA) is another superior explosive material having low safety coefficient, high detonation velocity and extensively used until World War-I due to its potent explosive nature than TNT. Owing to the incredible solubility of PA in water and widespread applications in various industries (leather, pharmaceutical, chemical and dye industries) and forensic investigations, it is likely to contaminate soil and ground water when exposed and is responsible for several health disorders *viz*. sycosis, cancer, anaemia, cause strong irritation to eye/skin and potential destruction of liver, kidney and respiratory organs.[7-10] Hence, there is an urgent need to develop superior methods for monitoring the traces of PA in multiple environments including aqueous solution, contact mode and vapor phase rapidly, in order to avert terrorist threats as well as monitoring environmental pollution.

Though, several analytical techniques have been employed for the detection of nitroaromatics, most of them are expensive, complex, less sensitive, time consuming and suffer from various drawbacks such as portability and on-site detection capability making them inappropriate for practical applications.[5,11-15] Fluorescence signaling is considered as a primary tool for the detection of nitroexplosives due to its simplicity and diverse notable features *viz.* remarkable sensitivity, short response time and potential in both solution as well as solid state. Hence, much attention has been paid in designing fluorometric sensors for explosives based on oligomers/conjugated polymers,[14,16-25] quantum dots,[26] metal-organic frameworks,[27-32] micro/nanoaggregates,[33-38] etc. However, most of the sensors for PA detection have reported problems of limited selectivity, low sensitivity, on-site detection incapability and unviability in 100% aqueous medium as well as incapable vapor phase detection (Surprisingly, there are no efficient methods developed for vapor phase detection of PA). Thus, development of superior probes for monitoring PA with ultra-sensitivity and high selectivity in 100% aqueous medium, solid state on-site as well as in vapor phase is highly desirable and challenging in the present context.

To attain ultra-sensitivity, a few approaches have been made in designing CP based probes for the detection of PA.[14,21,22,39-41] However, low selectivity due to the absence of suitable receptor, interferences by other electron deficient nitro analytes, impracticability

in 100% aqueous media and vapor mode detection persists as a challenge for researchers. Recently, conjugated polymer nanoparticles (CPNs) have emerged as a fascinating class of nanomaterials[42,43] in the field of chemical and biological sensing, imaging and diagnosis due to their numerous advantages *viz*. high quantum efficiency, low cytotoxicity, super-sensitivity, excellent photostability against photobleaching, etc. It is noteworthy to mention that no efficient platforms for the selective detection of PA *via* CPNs, as well as no devices or proficient methods for the vapor phase detection of PA have been ever developed, thereby presenting huge opportunities that are yet to be explored. This motivated us to develop a highly efficient and reliable protocol for monitoring traces of nitroexplosive-picric acid in multiple media and forms [solution (liquid in various solvents), disposable paper film (solid/powder form) as well as devices (vapor/gas)] using CPNs in order to gain ultra-sensitivity and high/unambiguous signal response.

Device based sensors have been proved as promising and excellent candidates for the detection of volatile materials due to their ultra-low cost, high sensitivity, good reproducibility, viability under ambient condition as well as capability to be miniaturized and quantified.[44-47] However, low volatility of the sensing analyte remains a major obstacle for investigators in developing such detection methods. Although, gas sensors have been designed[44,46,48,49] for monitoring trace amounts of explosives such as TNT, DNT etc., an efficient system for the vapor mode detection of PA remains unexplored. Since, PA has very low vapor pressure (7.4×10^{-7} mm Hg at 25 ºC) compared to several other nitroexplosives (including TNT and DNT) therefore, development of a suitable device for vapor phase sensing of PA with high signal response is extremely challenging yet remains highly desirable.

Herein, we report the synthesis and characterization of a new conjugated polymer PFMI using Suzuki coupling method in high yields without employing any tedious purification technique. The pendant cationic imidazolium groups attached on the side chains of the polymer PFMI act as a specific recognition site for PA and also facilitate the solubility of this probe in polar solvents (DMSO, methanol etc.). Spontaneous re-precipitation method was employed to generate nanoparticles (PFMI-NPs) that were well characterized. Detection for PA was achieved at picomolar levels for the first time using CPNs in 100% aqueous media as well as in solid state using portable paper strips that makes the protocol simple, reliable and practical. Furthermore, a two terminal sensor device was fabricated

on glass substrate using PFMI-NPs and conductivity measurements performed with these devices establishes the ability of PFMI-NPs to monitor and quantify trace vapors of PA under ambient conditions which were inaccessible previously due to the extremely low volatility of PA.

2.2 Experimental

2.2.1 Materials and measurements

Nitro-explosive picric acid was purchased from LobaChemie. TNT and RDX were obtained from AccuStandard and used as received. All other nitroaromatics and chemicals were obtained from Sigma Aldrich, Merck and Alfa Aesar. Milli-Q water was used in all sensing experiments. The ^{1}H NMR (600 MHz and 400 MHz) and ^{13}C NMR (150 MHz and 100 MHz) spectra were obtained on Bruker Ascend 600 spectrometer and Varian-AS400 NMR spectrometer, respectively. Photoluminescence spectra were recorded on a Horiba Fluoromax-4 spectrofluorometer using quartz cuvettes of 10 mm path length with a slit width of 2 nm at room temperature. Perkin Elmer Lambda-25 spectrophotometer was used to record absorption spectra. Gel Permeable Chromatography was carried out in THF using polystyrene as standard. Sonication was performed in 500 Watt Sonics Vibra-Cell Ultrasonic Processor. Electrochemistry was performed in CH instruments Model 700D series Electrochemical workstation. Film thickness was recorded by using Dektak 150 Profilometer. Whatman® qualitative filter paper (Grade 1) was use to prepare fluorescent test strips. Edinburgh Life Spec II instrument was employed for performing time resolved fluorescence studies. PFMI-NPs were visualized using Field emission scanning electron microscope (FESEM) (Zeiss sigma microscope) at an accelerating voltage of 2 kV. Transmission electron microscopic (TEM) images were recorded on JEOL 2100 UHR-TEM instrument, operating at 200 KV.

2.2.2 Synthetic procedure

2.2.2a Synthesis of 2, 7-dibromo-9, 9-bis (6-bromohexyl)-9H-fluorene (M1)

In a round bottom flask 2, 7-dibromofluorene (0.50 g, 1.54 mmol) and a catalytic amount of TBAI (0.057 g, 10 mol%) were added as reported.[50] The flask was degassed and 50% aq NaOH was introduced *via* syringe. To remove traces of oxygen from the reaction vessel freeze- pump-thaw cycles were applied three times followed by degasing and purging of argon after each cycle. 1,6-Dibromohexane (2.25 g, 9.25 mmol) was added *via* syringe (degassed) into the reaction vessel and the reaction mixture was heated at 70 °C for 4h. The reaction mixture was cooled to room temperature, extracted with chloroform

and dried over anhydrous sodium sulfate. The solvent was removed under vacuum to get the crude product which was purified by column chromatography to get the product as colorless crystals. (Yield=0.7 g, 70%)

^{1}H NMR (400 MHz, $CDCl_3$ δ ppm): 7.52 (d), 7.43 (t), 3.29 (t), 1.94 (t), 1.67-1.61 (m), 1.23-1.14 (m), 1.10-1.14 (m), 0.59-0.55 (m).

^{13}C NMR (100 MHz, $CDCl_3$, δ ppm): 152.57, 139.27, 130.42, 126.31, 122.32, 55.81, 42.24, 40.29, 33.77, 29.84, 26.64, 23.78.

2.2.2b Synthesis of poly 9, 9-bis (6-bromohexyl)-2-phenyl-9H-fluorene (PF)

A mixture of M (0.200 g, 0.31 mmol), tetrakistriphenylphosphine palladium(0) (0.018 g, 0.015 mmol), benzene-1,4-bisboronic acid (0.053 g, 0.32 mmol), 5 mL of 2 M aq. solution of K_2CO_3 and THF (15 mL) were taken in a Schlenk tube fitted with a condenser. The reaction mixture was degassed thrice by freeze-thaw cycles to remove air from the tube followed by refluxing for 24h under argon atmosphere. The reaction mixture was then cooled, extracted with chloroform/water thrice. The organic layer was evaporated to dryness and purified by repeated precipitation in methanol to get the product as a light yellow colored solid. (Yield=75%, 0.110 g).

^{1}H NMR (600 MHz, $CDCl_3$ δ ppm) : 7.82(b), 7.77(b), 7.69(b), 7.65(b), 7.48(b), 3.29(b), 2.09 (b), 1.68(b), 1.58(b), 1.31(b), 1.25(b), 1.13 (b), 0.79(b).

^{13}C NMR (150 MHz, $CDCl_3$, δ ppm): 151.43, 140.18, 139.69, 128.03, 127.59, 127.04, 126.17, 121.34, 120.21, 55.19, 40.31, 33.97, 32.63, 29.68, 29.08, 27.75, 23.64.

2.2.2c Synthesis of poly (3, 3'-((2-phenyl-9H-fluorene-9, 9-diyl)bis(hexane-6, 1-diyl))bis(1-methyl-1H-imidazol-3-ium) bromide) (PFMI)

The polymer PFMI was prepared according to previously reported procedure.[23] In a 50 mL round-bottom flask, PF (0.100 g, 2.1 mmol) and excess of 1-methylimidazole were taken and kept for reflux under stirring condition at 80 ºC for 24h. The reaction mixture was then decanted into excess chloroform (20 mL) and stirred for 1-2h to get a precipitate. The process was repeated thrice to remove excess of 1-methyl imidazole. The precipitate was then filtered out and dried to obtain dark yellow colored product. (Yield=63%, 0.096 g)

^{1}H NMR (600 MHz, DMSO-d_6, δ ppm): 9.05 (b), 7.92 (b), 7.78 (b), 7.69 (b), 7.68 (b), 7.64 (b), 7.61 (b), 4.02 (b), 3.77 (b), 2.16 (b), 1.56 (b), 1.33 (b), 1.22 (b), 1.09 (b), 0.99 (b) 0.86 (b), 0.59 (b).

^{13}C NMR (150 MHz, DMSO-d_6, δ ppm): 151.18, 139.96, 138.89, 135.94, 128.62, 126.94, 126.22, 125.49, 123.17, 121.79, 120.44, 120.03, 54.95, 48.85, 35.02, 29.25, 28.70, 25.32, 23.40.

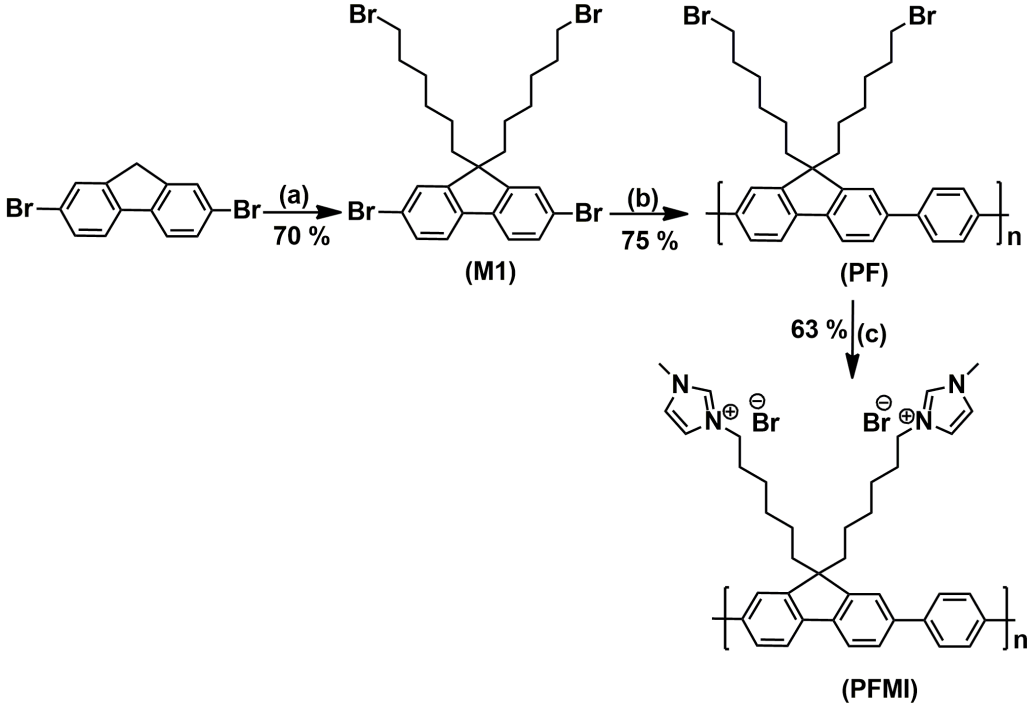

Scheme 2.1 Synthesis of the polymer-PFMI. (a) 1, 6-Dibromohexane, 50% aq. NaOH, TBAI, 70 ºC, 4h. (b) Tetrakis(triphenylphosphine) palladium (0), benzene-1,4-diboronic acid, 2M K_2CO_3 (aq.), THF, reflux, 24h. (c) 1-methyl imidazole, reflux, 24h.

2.2.3 Preparation of PFMI-NPs

The nanoparticles of PFMI were prepared *via* the well-established re-precipitation technique.[51] The procedure involves the preparation of a stock solution of PFMI (10^{-2} M) in methanol followed by filtration through 0.22 μm polytetrafluoroethylene filter. The polymeric solution (200 μL) was then added into 2 mL of Milli-Q water under sonication at 20 kHz/500 watt, 5 min using a microtip probe sonicator. The dispersion was vigorously stirred at 50 °C on a hot plate to evaporate the residual methanol present in the solution. The morphology of nanoparticles was studied by FESEM and TEM.

2.2.4 Preparation of stock solutions for sensing studies

Stock solution of PFMI-NPs and various other nitroaromatic compounds *viz*. picric acid (PA), nitrobenzene (NB), nitromethane (NM), phenol, 4-nitrophenol (4-NP), 2,4-dinitrophenol (2,4-DNP) were prepared in MilliQ water at concentrations of 1×10^{-3} M and 1×10^{-4} M, respectively. Nitroaromatics *viz.* 2,6-dinitrotoluene (2,4-DNT), 2,4-

dinitrotoluene (2,6-DNT), 4-nitrotoluene (4-NT), 1,3-dinitrobenzene (1,3-DNB) were prepared at concentrations of 1×10^{-4} M in HPLC grade THF. Stock solution of RDX and TNT were prepared in 1:1 CH_3CN: MeOH at a concentration of (1×10^{-4} M). The absorption and fluorescence measurements of the PFMI-NPs with various analytes were carried out in 3 mL aqueous solution containing 6.6×10^{-6} M PFMI-NPs in a quartz cuvette (1 cm × 1 cm).

2.2.5 Quantum yield calculations

Photoluminescence quantum yield (Φ_s) of PFMI-NPs were determined using quinine sulphate (Φ_s = 0.54 in 0.1 M H_2SO_4) as standard from the equation shown below.

$$\Phi_s = \Phi_r (A_r F_s / A_s F_r)(\eta_s^2/\eta_r^2)$$

Where, r and s represent reference and sample, Φ denotes the quantum yield, A signifies absorbance, F shows relative integrated fluorescence intensity and η implies the refractive index of the medium.

2.2.6 Calculation for overlap integral value and Förster distance

The extent of energy transfer was determined by calculating the overlap integral values for all the nitroexplosives using the equation[52] shown below.

$$J(\lambda) = \int_0^\infty F_D(\lambda)\, \varepsilon_A(\lambda) \lambda^4 d\lambda$$

where, J(λ) denotes the overlap integral value, F_D (λ) represents corrected fluorescence intensity of PFMI-NPs from λ to Δλ with total intensity normalized to unity, ε_A signifies molar absorptivity of the acceptor at λ in $M^{-1}cm^{-1}$.

Förster distance R_0 was also calculated for the interaction of PFMI-NPs with nitroexplosives using the equation shown below:

$$R_0 = 0.211[(J)Q(\eta^{-4})(k^2)]^{1/6}$$

where, J represents the of extent of spectral overlap between the emission spectrum of donor and absorption spectrum of acceptor, Q denotes the photoluminescence quantum yield of PFMI-NPs (donor), k^2 signifies dipole orientation factor (generally consider as 0.667) and η is the refractive index of the medium.

2.2.7 Method used for detection limit calculation

For the determination of detection limit, various samples of PFMI-NPs (6.6 μM) each containing PA (0.16 nM, 0.33 nM, 0.50 nM, 0.66 nM, 0.83 nM and 1 nM) were prepared separately. The fluorescence spectrum was then recorded for each sample by exciting at 380 nm. A calibration curve was plotted between change in the fluorescence intensity and concentration of picric acid to obtain the regression curve equation. The detection limit (LOD) was then calculated using the below equation.

$$3\sigma/k$$

where σ is the standard deviation (S.D.) for five repeated fluorescence measurements of PFMI-NPs solution in the absence of PA and k denotes the slope of the curve.

2.2.8 Cyclic voltammetry studies

Electrochemical measurements were carried out using three-electrode cell with platinum wire as counter electrode, saturated $Ag/AgNO_3$ electrode as reference electrode and a glassy carbon as working electrode. Tetrabutylammoniumhexafluorophosphate (0.1 M) in acetonitrile was used as supporting electrolyte. The Fc^+/Fc couple was employed as internal reference and all the measurements were performed at room temperature under inert atmosphere. Single oxidation peak was observed for PFMI-NPs. The HOMO level (-6.03eV) was calculated from the onset method [$E_{HOMO} = -(E_{(onset,ox\ vs.\ Fc+/Fc)} + 4.8)$ (eV)]. Band gap (2.95eV) of PFMI-NPs were determined from the onset of UV-visible spectrum to calculate its LUMO level (-3.08eV).

2.2.9 Preparation of fluorescence test strips

Fluorescent test strips were prepared by dipping Whatman filter paper (70 mm diameter) in the solution of PFMI-NPs (10^{-4} M) in methanol followed by drying the solvent in air. The filter paper coated with PFMI-NPs were then cut into desired number of pieces (1 cm × 1 cm) and used for the instant surface sensing purposes.

2.2.10 Device fabrication and electrical measurements

For the fabrication of a two-terminal sensor device, microscopic glass slides were used as substrates. The glass substrates were cleaned in piranha solution ($3:1/H_2SO_4:H_2O_2$) before washing it several times with deionized water. The cleaned substrates were then dried under vacuum at 100 °C. Using masking, 150 nm thick aluminum (Al) electrodes were deposited on to clean glass substrates by thermal evaporation under high vacuum $<10^{-6}$ mbar to make a blank channel with 30 μm length (L) and 1500 μm width (W). From the

stock solution of PFMI-NPs (10^{-3} M) in water, a volume of 10 µL was drop-casted over the channel between electrodes. The solvent was fully dried by heating on a hot plate for 10mins at 50 °C to form a thin film (thickness ~60 nm) across the fabricated Al electrodes. The electrical characteristics of the devices were carried out under ambient condition using a Keithley 4200-SCS semiconductor parameter analyzer.

2.2.11 Vapor phase detection

For vapor phase detection, 50 mg of various nitroaromatics (2,4-DNT, 2,6-DNT, NB, NT and PA) were kept for two days in 20 mL airtight glass vials to ensure complete saturation over the area of headspace. The concentration of vapors in the headspace was calculated using the following equation.

$$\text{Saturation concentration (ppm)} = \text{V.P. (mm Hg)}/760 \text{ mm Hg} \times 10^6$$

where, V.P. denotes vapor pressure[53] of various nitroaromatics.

Each nitroaromatics were then diluted to desired concentration by air and injected into the gas chamber using air tight syringe.

2.3 Result and discussion

2.3.1 Synthesis and characterization of PFMI and PFMI-NPs

The cationic conjugated polymer poly(3,3'-((2-phenyl-9H-fluorene-9,9-diyl)bis(hexane-6,1-diyl))bis(1-methyl-1H- imidazol-3-ium) bromide) (PFMI) was synthesized using Suzuki coupling polymerization method followed by post functionalization technique with 63% yield as shown in **Scheme 2.1** and characterized by NMR shown in (**Figure A2.1-2.6**). The molecular weight (M_w) of precursor polymer PF was found to be 15101 g mol^{-1}, PDI-2.25 (**Figure A2.7).** N-methyl imidazolium groups attached onto the side chains of the polymer act as specific recognition sites for PA and also provide excellent solubility to PFMI in polar solvents such as DMSO and methanol.

The PFMI-NPs were prepared via well-established re-precipitation method[51] (**Figure 2.1a**) and characterized by FESEM and TEM that reveals the presence of spherical shaped nanoparticles with average sizes of ~30 nm (**Figure 2.1b & 2.1c**). The SAED pattern of PFMI-NPs exhibited a broad hollow ring, which is attributed to its amorphous nature (**Figure 2.1d**). The zeta potential of PFMI-NPs at 25 ºC in water was found to be 62.8 mV±1.2.

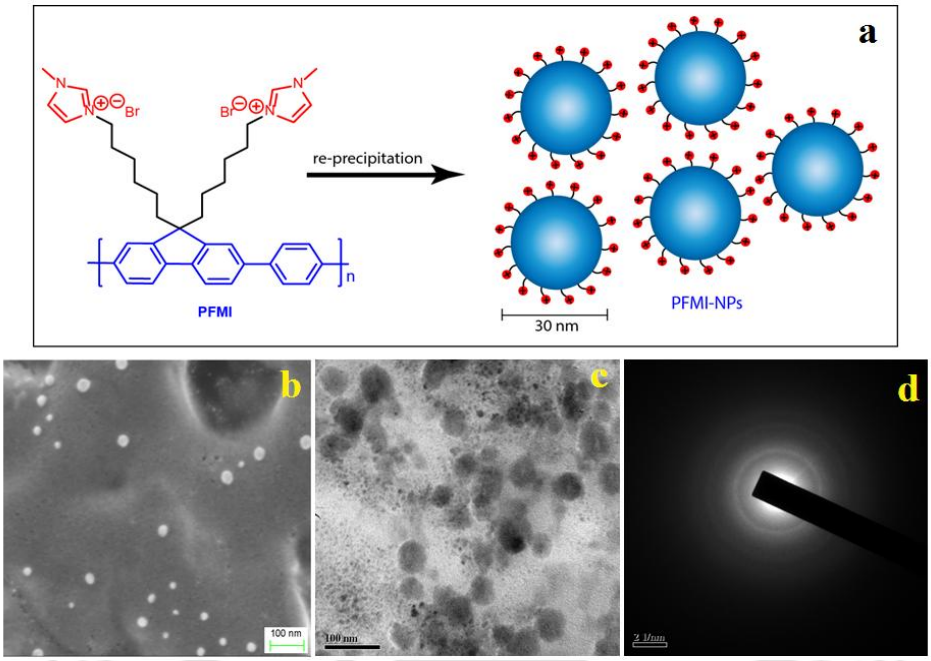

Figure 2.1 (a) Structure of newly synthesized polymer PFMI and its corresponding nanoparticles (b) FESEM and (c) TEM image showing spherical shaped PFMI-NPs with the average sizes of ~30 nm. (d) SAED pattern of PFMI-NPs exhibited a broad hollow ring confirming the amorphous nature of molecules.

2.3.2 Sensing studies in aqueous medium

The sensing studies were performed using both free polymer (PFMI) as well as its nanoparticles (PFMI-NPs). The cationic polymer PFMI displayed absorption maximum at 370 nm with an emission maximum (excitation 370 nm) of 418 nm and vibronic shoulder at 440 nm in water. Compared to free polymer PFMI, the PFMI-NPs exhibit a red shifted absorption peak positioned at 380 nm (**Figure A2.8**) and emission at 420 and 444 nm (excitation 380 nm) respectively, indicating an increase in π-π interaction due to the close association of backbone chains.[54] The photoluminescence quantum yield (Φ_s) of PFMI-NPs was found to be ~46% in aqueous media. PFMI-NPs displayed unprecedented efficiency during sensing experiments compared to free polymer PFMI, established via the high signal response and low detection limit value obtained for PA with PFMI-NPs. Hence, PFMI-NPs were chosen as probes rather than free polymer PFMI for studying sensing behavior towards various nitroexplosives.

To demonstrate the sensing behavior of PFMI-NPs towards nitroexplosives in solution state, fluorometric titration was performed with various common explosive materials *viz*. RDX, TNT, PA, NB, NM, 4-NP, 2,4-DNP 2,4-DNT, 2,6-DNT, 4-NT, 1,3-DNB and

phenol in aqueous media. Interestingly, only PA displayed significant response towards the emission of PFMI-NPs compared to all other analytes. Instant fluorescence quenching of ~25% was observed on adding 33 nM PA solution to PFMI-NPs (6.6 µM) in aqueous media that further reaches to ~94% on total addition of 0.5 µM PA (**Figure 2.2a**). The quenching efficiency was studied *via* Stern-Volmer plot (I_o/I vs [Q] where, 'I_o' denotes fluorescence intensity in the absence of quencher, 'I' represents fluorescence intensity at various concentrations of PA and 'Q' implies concentration of quencher) to acquire the Stern-Volmer constant (K_{sv}). The K_{sv} obtained from the linear fitting of plot was found to be 1.12×10^8 M^{-1}, signifying very high sensitivity of PFMI-NPs for PA (Inset of **Figure 2.2a**).

Interestingly, other nitroexplosives used in the present study did not cause any significant changes on the photophysical properties of PFMI-NPs (**Figure 2.2b & Figure 2A.9**). From the S-V plot of nitroexplosives (**Figure 2.2c**), it was clear that at lower PA concentration, linearity in the curve was obtained which indicates static quenching mechanism. However, at higher concentration the curve deviates and increases exponentially suggesting an amplified signal response *via* the dynamic quenching process. This non-linear nature of S-V plot may also indicate the possibility of self-absorption or an effective energy transfer process in the quenching mechanism.[6,55] However, all other nitroexplosives used in the present study did not display any deviation in the curve and remained linear even at higher concentration, confirming the absence of energy transfer mechanism. The limit of detection (LOD) value calculated for PA on the basis of the standard method reported[23] was observed to be 30.99 pM/7.07 ppt (**Figure 2.3**). To the best of our knowledge, such high K_{sv} and incredibly low LOD value is being reported for the first time using CPNs in 100% aqueous media and is superior among all the previous detection methods for PA (**Table A2.1**).

2.3.3 Demonstrating selectivity in competitive environment

The specific recognition of PA is an exciting and appealing area of research. However, owing to the similar electron deficient nature of all the nitroexplosives, the specific recognition of PA remains a challenging task for researchers. To validate the selectivity of PFMI-NPs system, its fluorescence quenching by PA was performed in the presence of different nitroexplosives. It is noteworthy to mention that PFMI-NPs showed remarkable response towards PA even in the presence of various common interfering nitro analytes **(Figure 2.2d & Figure A2.10a-A2.10i**). Similar experiments were also performed in the

presence of various common metal ions (Cr^{3+}, Ni^{2+}, Zn^{2+},Al^{3+}, Co^{2+}, Pb^{2+}, Cd^{2+}, Mn^{2+}, Cu^{2+}, Ag^{+}, Ca^{2+}, La^{2+} and Fe^{3+}) as well as anions (BH_4^- , NO_3^-, N_3^-, S^{2-}, BF_4^-, $H_2PO_4^-$, HPO_4^{2-}, PO_4^{3-} and AcO^-) usually found in natural water. Interestingly, PFMI-NPs showed exceptional response exclusively towards PA even in the presence of these most common interfering analytes (**Figure A2.10j & A2.10k**) validating the applicability of this system for the investigation of natural water samples.

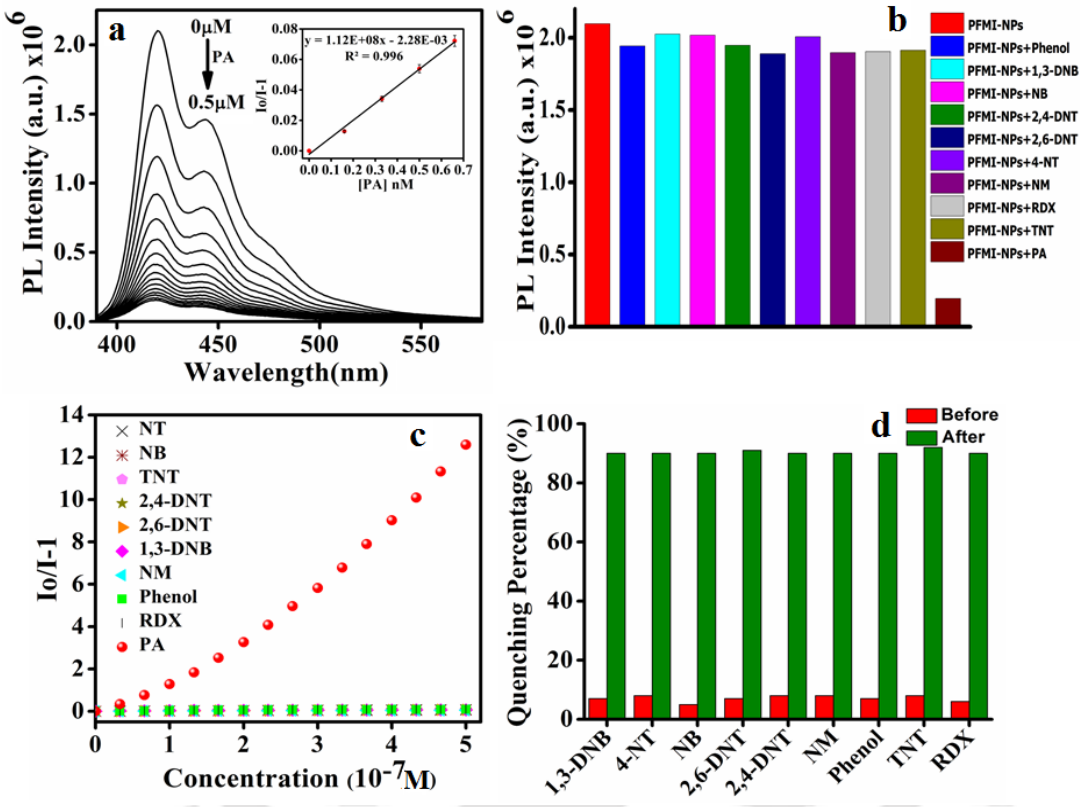

Figure 2.2 (a) Emission spectra of PFMI-NPs (6.6 μM) with variable concentration of PA in aqueous media. Inset: Stern-Volmer plot at lower PA concentration. (b) Bar diagram showing the effect of various nitroexplosives (0.5 μM) on the emission of PFMI-NPs (6.6 μM). (c) Stern-Volmer plots obtained for different nitroexplosives used in the study. (d) Percentage quenching of PFMI-NPs (6.6 μM) obtained for various nitroexplosives (0.5 μM) before and after addition of PA (0.5 μM) in aqueous media.

To elucidate the effect of ionic strength on PA sensing by PFMI-NPs, fluorescence quenching experiment was performed in the solutions of different salt concentration (0, 0.1, 0.2, 0.4, 0.6, 0.8 and 1M NaCl). It was observed that increasing the ionic strength reduces the quenching efficiency due to the weak Columbic interaction between the oppositely charged PFMI-NPs and PA molecules (**Figure 2.4**). Yet, the quenching efficiency of ~50% was observed in the presence of 1M NaCl which confirms that PFMI-

NPs system can detect PA even at relatively high electrolyte concentrations in the aqueous media.

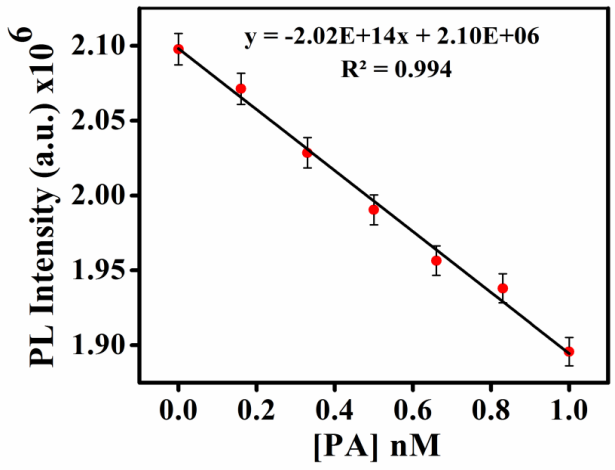

Figure 2.3 Fluorescence intensity of PFMI-NPs in aqueous medium as a function of PA concentration.

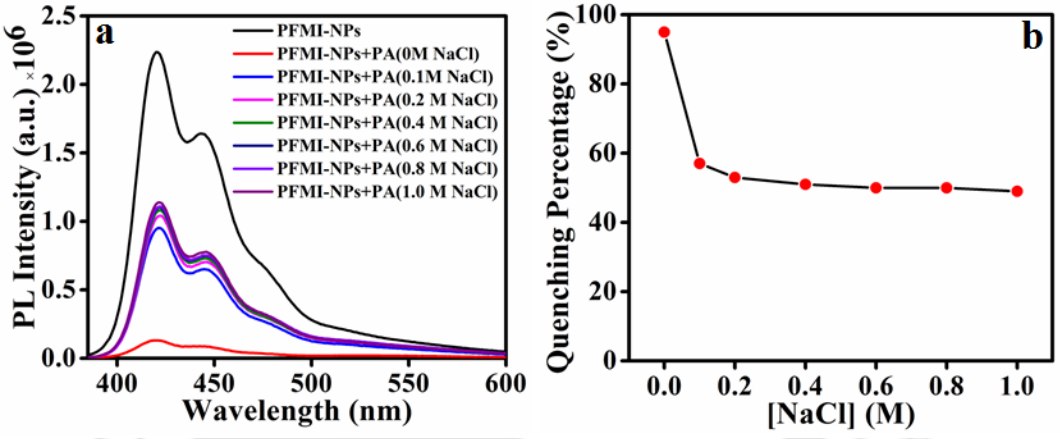

Figure 2.4 (a) PL spectra depicting the change in emission of PFMI-NPs (6.6 µM) after adding PA (0.5 µM) in the solution containing various concentrations of salt. (b) The effect of ionic strength on the quenching efficiency of PFMI-NPs by PA.

2.3.4 Sensing mechanism

The origin of the remarkable selectivity and the exceptional quenching efficiency by PA can be explained via the electrostatic interaction between PA and PFMI-NPs. Since PA consists of strong acidic phenolic –OH group with the ability to deprotonate in aqueous medium, positively charged PFMI-NPs have strong tendency to interact with the resulting picrate ions through Columbic interaction. This interaction may further facilitate the electron and/or energy transfer process. To investigate the possibility of electron transfer process in the quenching mechanism, higher occupied molecular orbital (HOMO) level

and lower unoccupied molecular orbital (LUMO) level of PFMI-NPs was obtained *via* cyclic voltammetry studies (**Figure 2.5a**). There is a possibility of excited state electron transfer from LUMO of PFMI-NPs (-3.08eV) to the LUMO of PA (-3.89eV) resulting in the quenching process **(Figure 2.5b**). Although, PA (-3.89eV) has lowest LUMO level compared to DNT (-3.5eV), NT (-3.2eV), TNT (-3.7eV) etc.,[30] the quenching does not follow the order. Thus, it can be concluded that electron transfer may not be the only mechanism involved in the quenching process. Non-linear nature of S-V plot and the outstanding response of PFMI-NPs towards PA suggests that an additional energy transfer process may also be associated with the quenching process.

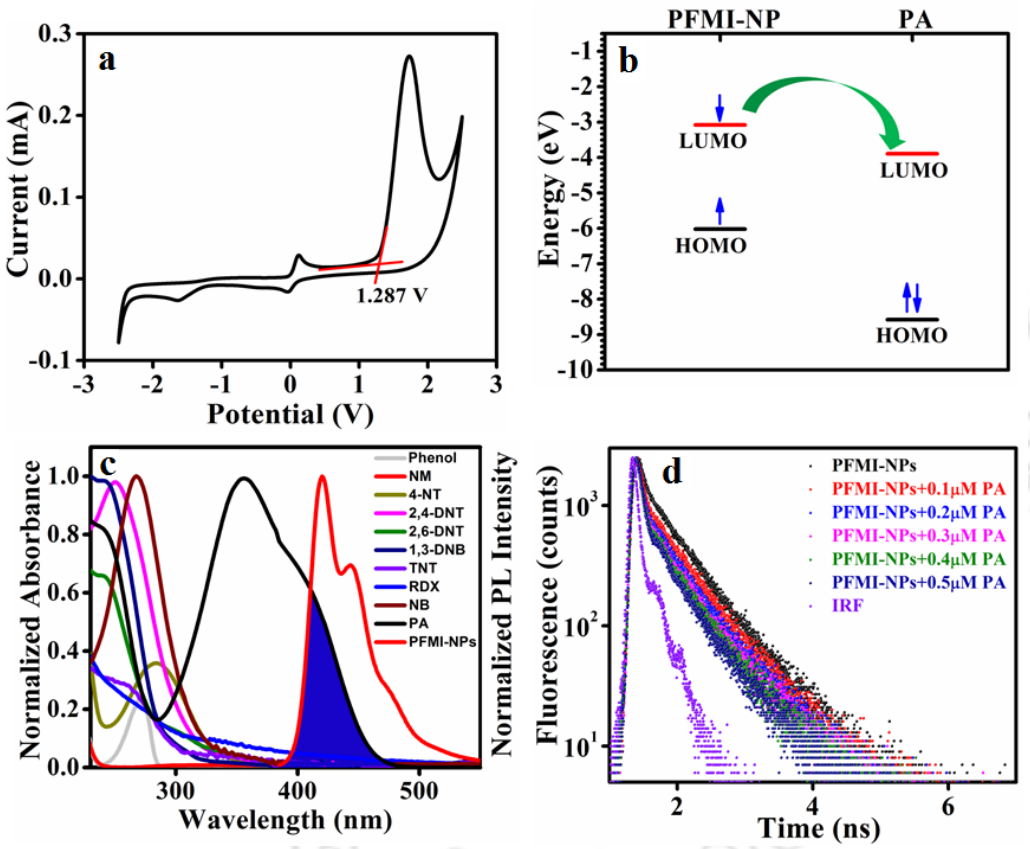

Figure 2.5 (a) Cyclic voltammogram of PFMI-NPs film obtained on glassy carbon electrode with a scan rate of 50 mV/s. (b) Pictorial representation of excited state electron transfer from LUMO of PFMI-NPs to the LUMO of PA. (c) Spectral overlap between emission spectrum of PFMI-NPs and absorption spectra of nitroexplosives used in the study. (d) Time-resolved decay curves of PFMI-NPs in absence and presence of different concentrations of PA.

To elucidate this presumption, a plot was obtained between normalized emission spectrum of PFMI-NPs and absorption spectrum of all nitroexplosives. It is evident

(**Figure 2.5c**) that there is a significant overlap between the emission spectrum of PFMI-NPs and absorption spectrum of PA unlike other nitroexplosives. Hence, there is a strong possibility of resonance energy transfer (RET) from the flourophore PFMI-NPs (donor) to the non-emissive PA (acceptor), which can enhance the quenching efficiency as well as sensitivity. The overlap integral value (J_λ) was calculated for all the nitroexplosives to ascertain the extent of energy transfer. It was observed that J_λ value for PA (1.59×10^{14} $M^{-1}cm^{-1}nm^4$) was significantly higher compared to other explosives by ~100 times (**Table 2.1**). The value of Förster distance R_0 (33.32 Å) for PFMI-NPs and PA interaction also falls well in the range 10-100 Å that is appropriate for RET. To confirm the nature of quenching and the occurrence of RET from PFMI-NPs to PA, time correlated single-photon-counting (TCSPC) experiments were performed. The lifetime of PFMI-NPs was measured at 420 nm in the absence and presence of variable concentrations of PA using pulse excitation 375 nm (**Figure 2.5d**).

Table 2.1 Overlap integral J (λ) values calculated for various nitroexplosives used in the study.

Nitro aromatic analytes	J (λ) values (M^{-1} cm^{-1} nm^4)
PA	1.59×10^{14}
TNT	4.17×10^{10}
RDX	3.00×10^{11}
NM	2.18×10^{12}
NB	2.33×10^{11}
4-NT	4.90×10^{11}
2,6-DNT	4.86×10^{11}
2,4-DNT	2.22×10^{11}
Phenol	1.97×10^{11}
1,3-DNB	1.89×10^{12}

Meanwhile, the lifetime of PFMI-NPs was determined to be 0.241 ns that reduces dramatically and shortened to 0.05 ns at 0.5 µM PA. This significant reduction in the

lifetime strongly supports the possibility of energy transfer from PFMI-NPs to PA and indicates a dynamic quenching mechanism.

To further clarify the interaction between PA and PFMI-NPs, a control experiment was performed using model compounds i.e. 2,4-DNP and 4-NP having properties somewhat similar to PA. The photophysical properties of PFMI-NPs showed similar response to these analytes but with the quenching order as PA>2,4-DNP>4-NP (**Figure 2.6**). It is notable that the quenching pattern followed the order of acidity by these analytes. Since, PA consists of three electron deficient $–NO_2$ groups that boost its ability to dissociate in aqueous medium, a more favorable electrostatic interaction between PA and PFMI-NPs is expected compared to the 2,4-DNP or 4-NP which subsequently enhanced the quenching efficiency. This interaction may further facilitate the PET and/or energy transfer process to deliver the remarkable response of PFMI-NPs selectively towards PA. Other nitroexplosives that do not possess any –OH groups were ineffectual towards quenching process even though their LUMO level lies below the LUMO level of PFMI-NPs. Furthermore, triflic acid (TFA), a stronger acid compared to PA did not affect the emission of PFMI-NPs (**Figure 2.7**), indicating that acid itself cannot quench the fluorescence of PFMI-NPs and electron and/or energy transfer is the main factor behind the quenching process.

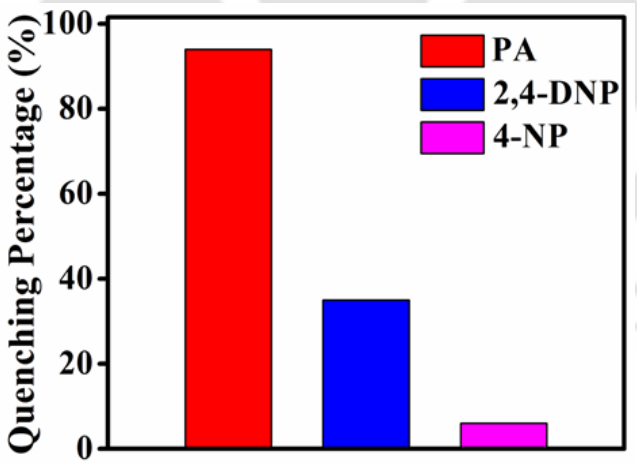

Figure 2.6 Comparative fluorescence quenching by PA, 2, 4-DNP and 4-NP in aqueous media. Concentration of PFMI-NPs and other analytes were 6.6 µM and 0.5 µM, respectively.

Hence, on the above basis, it was concluded that the extraordinary selectivity and excellent sensitivity of PFMI-NPs for PA in aqueous media is accountable for the favorable excited state electron transfer process, efficient energy transfer process and

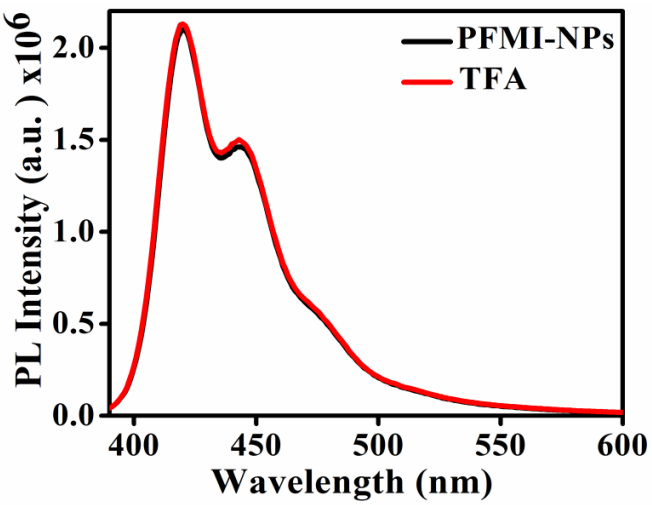

Figure 2.7 Change in photoluminescence spectra of PFMI-NPs (6.6 µM) before and after the addition of TFA (3 µM) in aqueous medium.

the well-established[56] "molecular-wire effect" of these polymers. This simple, yet rare method comprising of conjugated polymer nanoparticles provides an exceptional and unique platform for the highly selective and super amplified detection of nitroexplosive PA in 100% aqueous media.

2.3.5 Contact mode detection

Lesser volatile explosive materials like PA can contaminate the subjects, containers etc. by leaving trace residues during manufacturing of fireworks, transportation and handling. Hence, detection of such explosives at actual site is highly significant for forensic investigations. To realize portability and low cost on-site detection capability, fluorescent test strips were prepared by dipping the Whatman filter paper (70 mm diameter) in the solution of PFMI-NPs (10^{-4} M) in methanol followed by drying the solvent in air. The filter paper coated with PFMI-NPs were then cut into desired number of pieces (1 cm × 1 cm) and used for the instant surface sensing purposes by applying 10 µL of various concentration of PA solution. A solvent spot was also applied as a blank. Noticeable dark spots were observed under UV-light (365 nm excitation) that varies with the concentration of PA (**Figure 2.8**). The detection limit of 22.9fg/cm^2 was obtained for PA which is among the best reported value and confirms the method as simple, portable and most efficient for on-site detection.

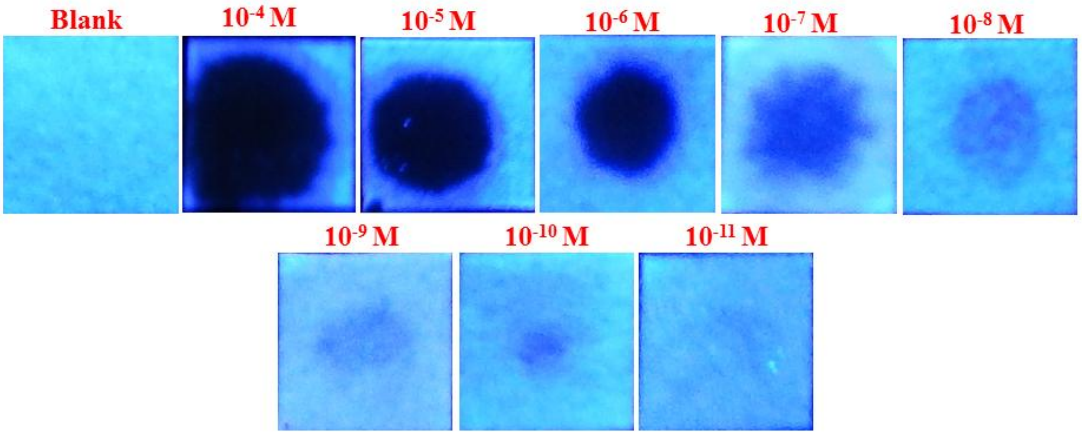

Figure 2.8 Color of fluorescent test strips under UV-light after the addition 10 µL of various concentrations of PA. Dark spots of different strength were observed that varied with concentration of PA (10^{-4}-10^{-10} M).

2.3.6 Vapour phase detection

The two terminal sensor devices fabricated with PFMI-NPs were kept in an air-tight chamber and connected to Keithley 4200 SCS semiconductor parameter analyzer to perform I-V characterization by sweeping the voltage from -10 V to +10 V. The channel and interface between PFMI-NPs film and bare aluminum surface were visualized under optical microscope (**Figure A2.11**). I-V curve thus obtained demonstrated a good conducting nature of PFMI-NPs thin film (**Figure 2.9a**). The exposure of device to air did not cause any change in the output current, confirming its stability under ambient condition. The vapors of nitroaromatics were injected into the testing chamber with the help of an airtight syringe (**Figure 2.9b**). Four successive on/off cycles were effectively attained that correspond to four different PA concentrations ranging from 0.2 ppb to 1 ppb, respectively (**Figure 2.9c**) confirming the unprecedented sensitivity of PA present even in very minute quantities. Notably, increasing the PA concentration leads to increased output current which subsequently enhances the sensitivity. Although the vapor pressure of PA is much lower than other nitroaromatics, yet it displayed significant increment in the current intensity confirming remarkable sensitivity of PFMI-NPs based device exclusively for PA. To study the selectivity of the device, similar sensing experiments were performed by introducing various other nitroaromatic vapors. As revealed in **Figure 2.9d**, vapors of other nitroexplosives showed negligible responses to the current intensity even at much higher concentration (100 times more) than PA and the current intensity increases rapidly only when PA vapors were delivered into the testing chamber. Interestingly, the device also displayed high signal response (6s) and fast

recovery (5s) for PA detection (**Figure 2.10**). Furthermore, to check the reproducibility of the device, certain concentrations (0.3 ppb) of PA vapors were exposed repeatedly into the test chamber after certain interval of time (**Figure 2.11**). After each exposure, nearly similar increment in current intensity was observed confirming the viability of device for practical application. The robustness and reproducibility of the device response to the PA vapors was tested over several weeks and found consistent.

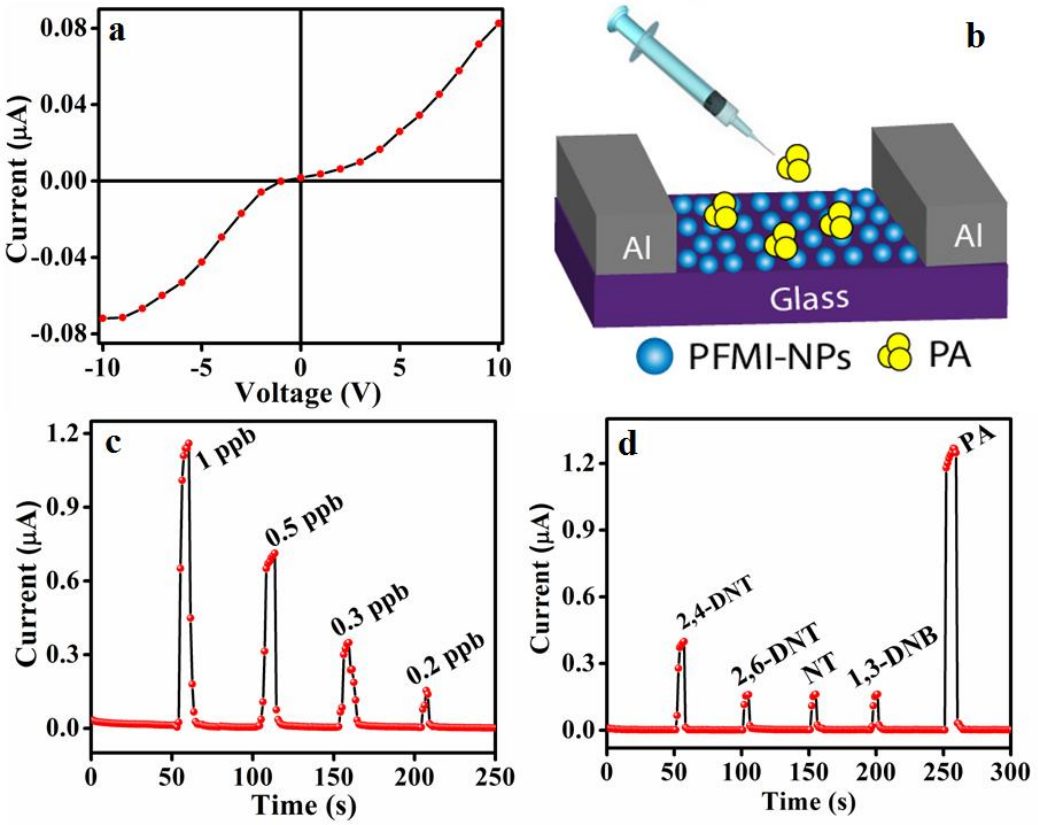

Figure 2.9 (a) I-V characteristics of PFMI-NPs under ambient conditions. (b) Schematic representation of two terminal sensor device (c) Change in output current of the device with increasing concentration of PA at an applied voltage of 10 V. (d) Selectivity studies of PFMI-NPs with various nitroaromatics (100 ppb) and PA (1 ppb).

PA being an electron-withdrawing molecule, could dope the p-channel semiconductors[44] (PFMI-NPs) and induce increase in the output current as the device is exposed to PA vapors. The unprecedented selectivity of PFMI-NPs towards PA is assigned primarily to the specific receptor site for PA present on the side chains of PFMI. Thus, these outcomes established a highly prospective route for the development of a rapid, low cost, reliable and easily processible device for vapor mode sensing of PA which remains an unexplored area.

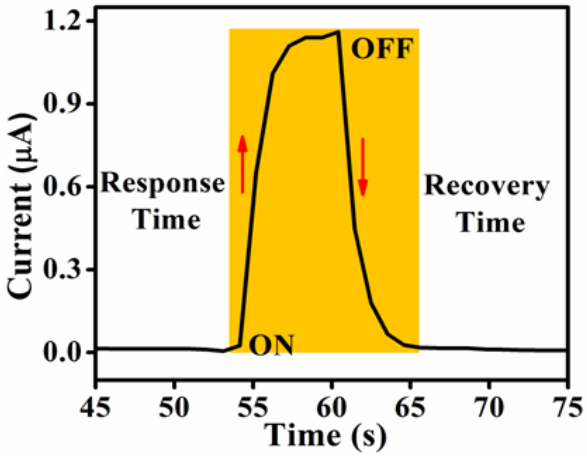

Figure 2.10 The response and recovery time of sensor device exposed to 1 ppb of PA.

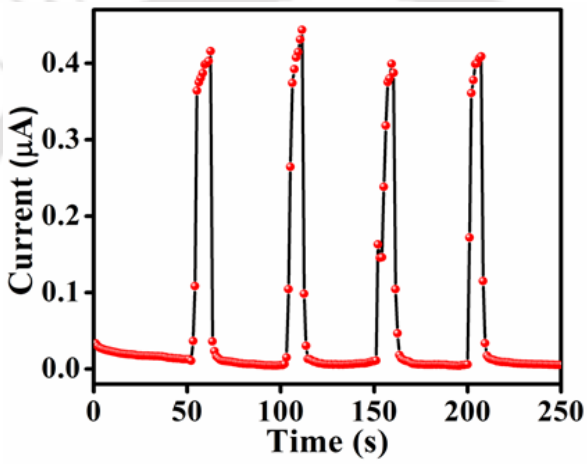

Figure 2.11 The response of the device on repeatedly exposing PA (0.3 ppb) vapours after certain time intervals.

2.4 Conclusion

In conclusion, a rapid and highly sensitive platform is developed for the selective detection of nitroexposive picric acid in multiple environments (100% water, disposable film and as devices) using newly synthesized conjugated polymer nanoparticles PFMI-NPs. Ultra-sensitivity of PFMI-NPs for PA is attributed to the "molecular-wire effect", electrostatic interaction, photoinduced electron transfer (PET) and/or possible resonance energy transfer (RET). PFMI-NPs performed PA detection even in the presence of several other interfering nitroexplosives and most common analytes usually found in natural water that makes the protocol reliable and suitable for real sample analysis. Contact mode detection using simple fluorescent strips confirms the technique to be widely applicable for instant on-site detection of PA. Furthermore, vapor mode sensing of PA was achieved for the first time using solution-casted conjugated polymer nanoparticles fabricated as

two terminal portable devices on glass substrates that displayed remarkable response exclusively for PA presenting a highly reliable method with rapid on-site detection ability.

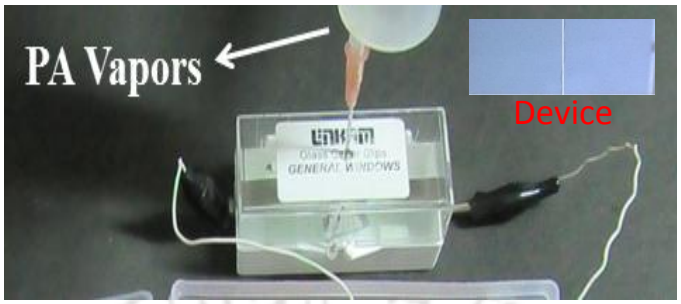

Digital image of the sensing chamber. Inset: image of the two terminal device.

References

(1) Ma, R.-M.; Ota, S.; Li, Y.; Yang, S.; Zhang, X. *Nat. Nanotechnol.* **2014**, *9*, 600.

(2) Rose, A.; Zhu, Z.; Madigan, C. F.; Swager, T. M.; Bulovic, V. *Nature* **2005** *434*, 876.

(3) Shanmugaraju, S.; Mukherjee, P. S. *Chem.–Eur. J.* **2015**, *21*, 6656.

(4) Hu, Z.; Deibert, B. J.; Li, J. *Chem. Soc. Rev.* **2014**, *43*, 5815.

(5) Germain, M. E.; Knapp, M. J. *Chem. Soc. Rev.* **2009**, *38*, 2543.

(6) Salinas, Y.; Martínez-Máñez, R.; Marcos, M. D.; Sancenón, F.; Costero, A. M.; Parra, M.; Gil, S. *Chem. Soc. Rev.* **2012**, *41*, 1261.

(7) Ashbrook, P. C.; Houts, T. A. *ACS Div. Chem. Health Safety* **2003**, *10*, 27.

(8) Akhavan, J. *Chemistry of Explosives, Royal Society of Chemistry*, 2nd ed., **2004**.

(9) *Innovative Treatment Technologies: Annual Status Report, U.S. Environmental Protection Agency*: Washington, D.C., 8th ed., **1996**.

(10) Wollin, K.-M.; Dieter, H. H. *Arch. Environ. Contam. Toxicol.* **2005**, *49*, 18.

(11) Dasary, S. S. R.; Senapati, D.; Singh, A. K.; Anjaneyulu, Y.; Yu, H.; Ray, P. C. *ACS Appl. Mater. Interfaces* **2010**, *2*, 3455.

(12) Enkin, N.; Sharon, E.; Golub, E.; Willner, I. *Nano Lett.* **2014**, *14*, 4918.

(13) Díaz Aguilar, A.; Forzani, E. S.; Leright, M.; Tsow, F.; Cagan, A.; Iglesias, R. A; Nagahara, L. A; Amlani, I.; Tsui, R.; Tao, N. J. *Nano Lett.* **2010**, *10*, 380.

(14) Toal, S. J.; Trogler, W. C.. *J. Mater. Chem.* **2006**, *16*, 2871.

(15) Palma-Cando, A.; Scherf, U. *ACS Appl. Mater. Interfaces* **2015**, *7*, 11127.

(16) Dong, W.; Fei, T.; Palma-Cando, A.; Scherf, U. *Polym. Chem.* **2014**, *5*, 4048.

(17) Sohn, H.; Sailor, M. J.; Magde, D.; Trogler, W. C. *J. Am. Chem. Soc.* **2003**, *125*, 3821.

(18) Kartha, K. K.; Babu, S. S.; Srinivasan, S.; Ajayaghosh, A. *J. Am. Chem. Soc.* **2012**, *134*, 4834.

(19) Xu, B.; Wu, X.; Li, H.; Tong, H.; Wang, L. *Macromolecules* **2011**, *44*, 5089.

(20) Martinez, H. P.; Grant, C. D.; Reynolds, J. G.; Trogler, W. C. *J. Mater. Chem.* **2012**, *22*, 2908.

(21) Wei, W.; Lu, R.; Tang, S.; Liu, X. *J. Mater. Chem. A* **2015**, *3*, 4604.

(22) Sang, N.; Zhan, C.; Cao, D. *J. Mater. Chem. A* **2015**, *3*, 92.

(23) Hussain, S.; Malik, A. H.; Afroz, M. A.; Iyer, P. K. *Chem. Commun.* **2015**, *51*, 7207.

(24) Li, X.-G.; Liao, Y; Huang, M.-R.; Strong, V.; Kaner, R. B. *Chem. Sci.* **2013**, *4*, 1970.

(25) Thomas III, S. W.; Amara, J. P.; Bjorka, R. E.; Swager, T. M. *Chem. Commun.* **2005**, 4572.

(26) Lin, L.; Rong, M.; Lu, S.; Song, X.; Zhong, Y. Yan, J.; Wang, Y.; Chen, X. *Nanoscale* **2015**, *7*, 1872.

(27) Nagarkar, S. S.; Joarder, B.; Chaudhari, A. K.; Mukherjee, S.; Ghosh, S. K. *Angew. Chem. Int. Ed. Engl.* **2013**, *52*, 2881.

(28) Lan, A.; Li, K.; Wu, H.; Olson, D. H.; Emge, T. J.; Ki, W.; Hong, M.; Li, J. *Angew. Chem. Int. Ed. Engl.* **2009**, *48*, 2334.

(29) Gong, Y.-N.; Jiang, L.; Lu, T.-B. *Chem. Commun.* **2013**, *49*, 11113.

(30) Xu, H.; Liu, F.; Cui, Y.; Chen, B.; Qian, G. *Chem. Commun.* **2011**, *47*, 3153.

(31) Gole, B.; Bar, A. K.; Mukherjee, P. S. *Chem. Commun.* **2011**, *47*, 12137.

(32) Béreau, V.; Duhayon, C.; Sutter, J.-P. *Chem. Commun.*, **2014**, *50*, 12061.

(33) Bhalla, V.; Gupta, A.; Kumar, M.; Rao, D. S. S.; Prasad, S. K. *ACS Appl. Mater. Interfaces* **2013**, *5*, 672.

(34) Bhalla, V.; Gupta, A.; Kumar, M. *Org. Lett.* **2012**, *14*, 3112.

(35) Vij, V.; Bhalla, V.; Kumar, M. *ACS Appl. Mater. Interfaces* **2013**, *5*, 5373.

(36) Hou, X.-G.; Wu, Y.; Cao, H.-T.; Sun, H.-Z.; Li, H.-B.; Shan, G.-G.; Su, Z.-M. *Chem. Commun.* **2014**, *50*, 6031.

(37) Feng, H.-T.; Zheng, Y.-S. *Chem.–Eur. J.* **2014**, *20*, 195.

(38) Shiraishi, K.; Sanji, T.; Tanaka, M. *ACS Appl. Mater. Interfaces* **2009**, *7*, 1379.

(39) Wang, Q.; Chen, M.; Yao, B.; Wang, J.; Mei, J.; Sun, J. Z.; Qin, A.; Tang, B. Z. *Macromol. Rapid Commun.* **2013**, *34*, 796.

(40) Ghosh, K. R.; Saha, S. K.; Wang, Z. Y. *Polym. Chem.* **2014**, *5*, 5638.

(41) Hu, R.; Maldonado, J. L.; Rodriguez, M.; Deng, C.; Jim, C. K. W.; Lam, J. W. Y.; Yuen, M. M. F.; Ramos-Ortiz, G.; Tang, B. Z. *J. Mater. Chem.* **2012**, *22*, 232.

(42) Feng, L.; Zhu, C.; Yuan, H.; Liu, L.; Lv, F.; Wang, S. *Chem. Soc. Rev.* **2013**, *42*, 6620.

(43) Li, K.; Liu, B. *Chem. Soc. Rev.* **2014**, *43*, 6570.

(44) Huang, J.; Dawidczyk, T. J.; Jung, B. J.; Sun, J.; Mason, a. F.; Katz, H. E. *J. Mater. Chem.* **2010**, *20*, 2644.

(45) Zang, Y.; Zhang, F.; Huang, D.; Di, C.; Meng, Q.; Gao, X.; Zhu, D. *Adv. Mater.* **2014**, *26*, 2862.

(46) Engel, Y.; Elnathan, R.; Pevzner, A.; Davidi, G.; Flaxer, E.; Patolsky, F. *Angew. Chem. Int. Ed. Engl.* **2010**, *49*, 6830.

(47) Squillaci, M. A; Ferlauto, L.; Zagranyarski, Y.; Milita, S.; Müllen, K.; Samorì, P. *Adv. Mater.* **2015**, *27*, 3170.

(48) Kong, H.; Jung, B. J.; Sinha, J.; Katz, H. E. *Chem. Mater.* **2012**, *24*, 2621.

(49) Kong, H.; Sinha, J.; Sun, J.; Katz, H. E. *Adv. Funct. Mater.* **2013**, *23*, 91.

(50) Saikia, G.; Iyer, P. K. *J. Org. Chem.* **2010**, *75*, 2714.

(51) Pecher, J.; Mecking, S *Chem. Rev.* **2010**, *110*, 6260.

(52) Lakowicz, J. R. *Principles of Florescence spectroscopy*, 3rd ed; Springer: Singapore, **2010**; pp 443.

(53) Robert G. E.; Melanie, J. W.; David A. A.; Jay, W. G.; Peter J. H. *Trends Anal. Chem.* **2013**, *42*, 35.

(54) Wang, H.; Li, Y.; Chen, Y.; Li, L.; Fang, T.; Tang, Z. *J. Mater. Chem. C* **2015**, *3*, 5136.

(55) Zhao, D.; Swager, T. M. *Macromolecules* **2005**, *38*, 9377.

(56) Zhou, Q.; Swager, T. M. *J. Am. Chem. Soc.* **1995**, *117*, 12593.

Appendix

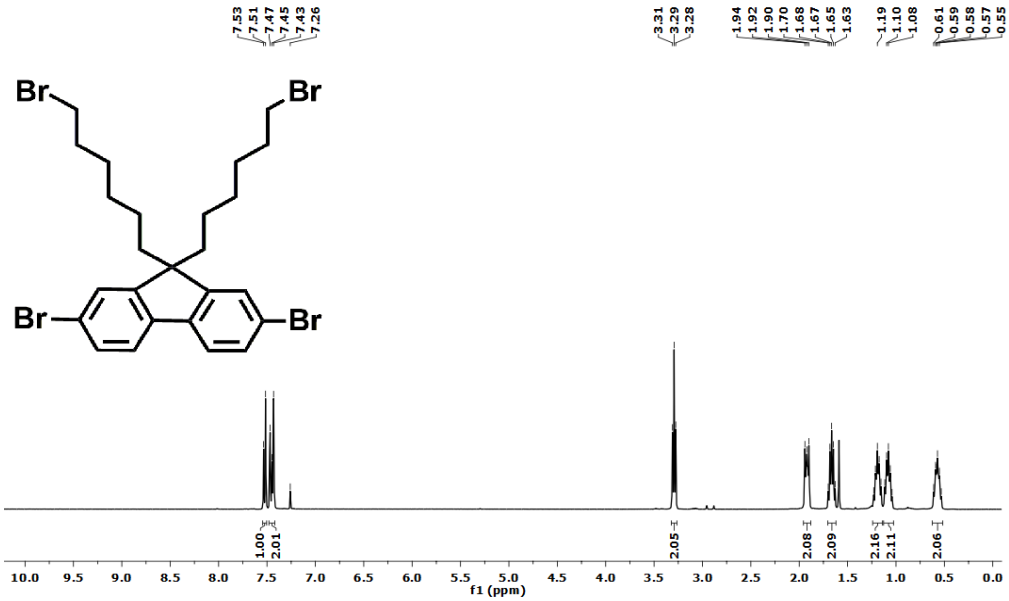

Figure A2.1 ^{1}H NMR spectra of M1.

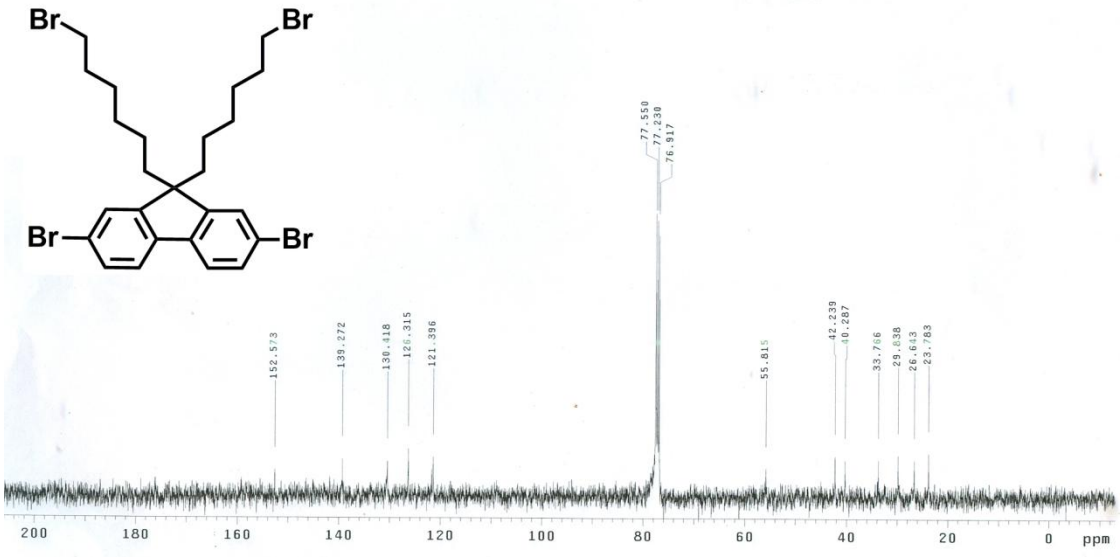

Figure A2.2 ^{13}C NMR spectra of M1.

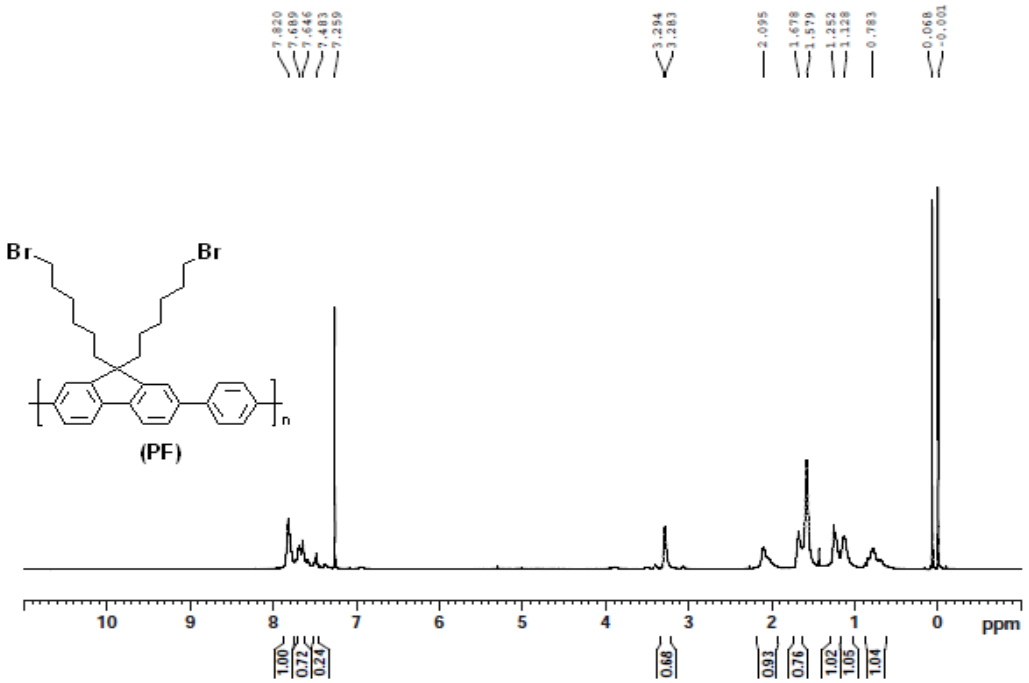

Figure A2.3 ^{1}H NMR spectra of PF.

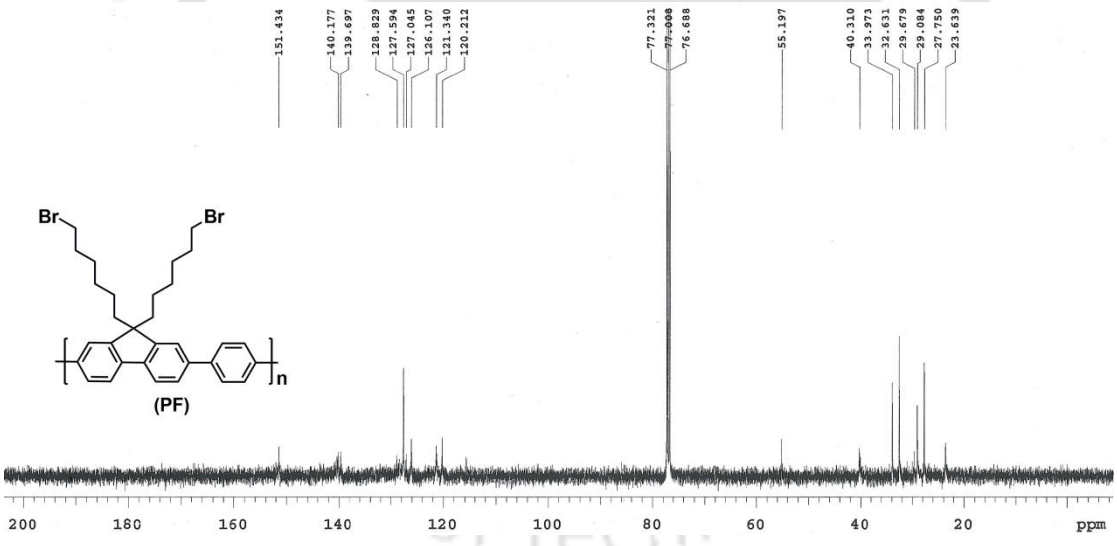

Figure A2.4 ^{13}C NMR spectra of PF.

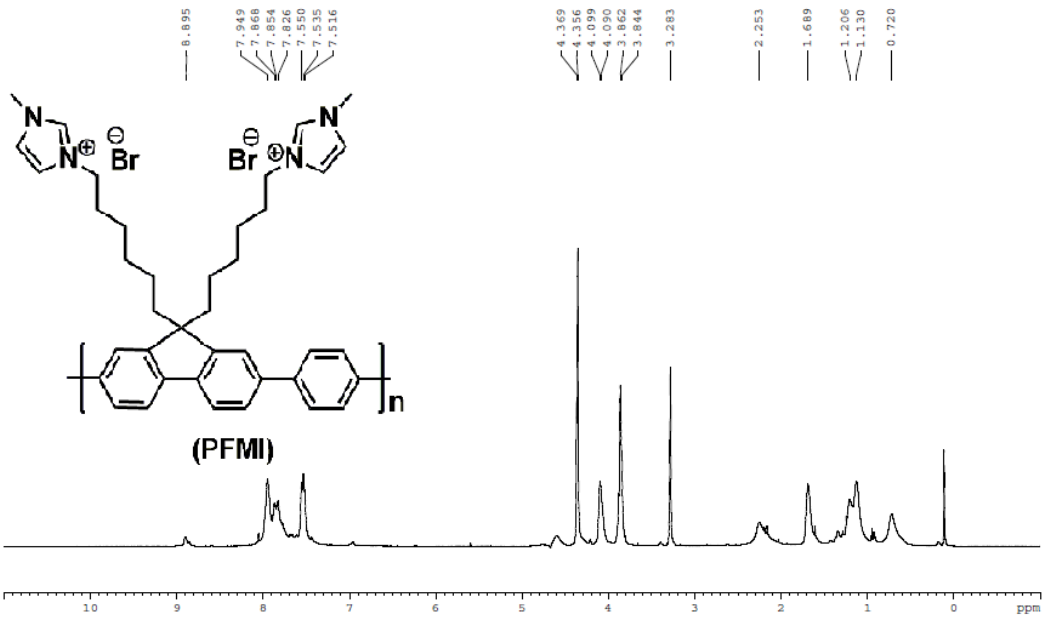

Figure A2.5 ^{1}H NMR spectra of polymer PFMI.

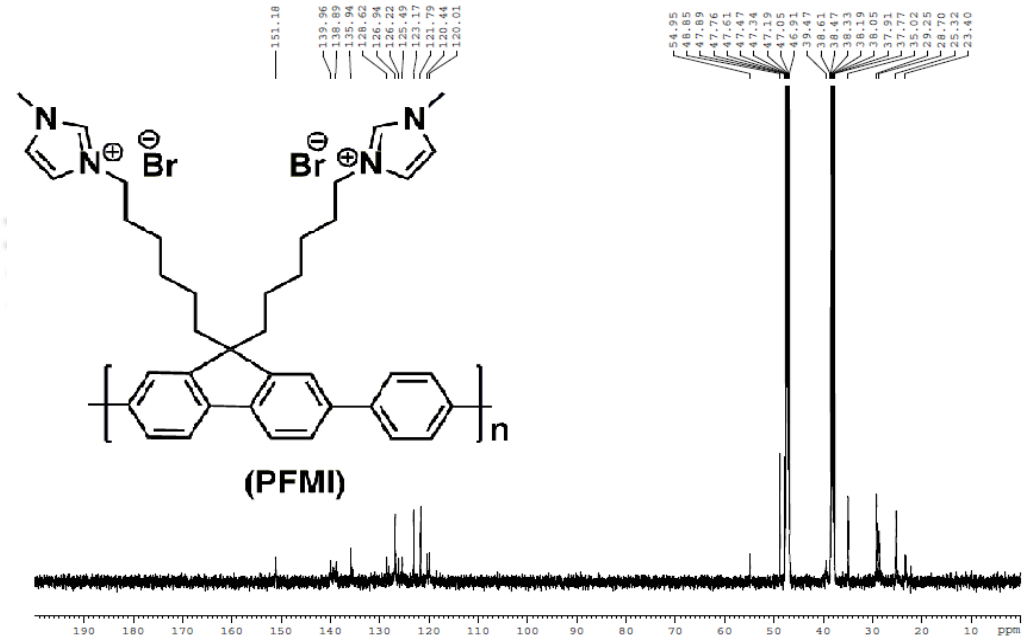

Figure A2.6 ^{13}C NMR spectra of polymer PFMI.

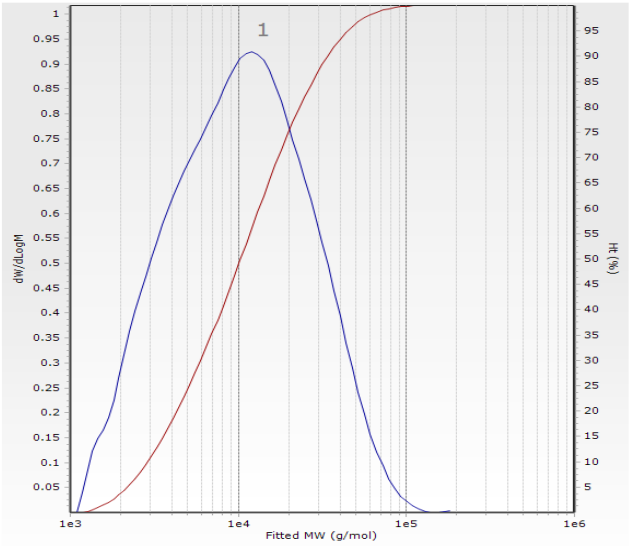

Molecular Weight Averages

Peak	Mp	Mn	Mw	Mz	Mz+1	Mv	PD
Peak 1	12028	6705	15101	29329	45934	27095	2.252

Figure A2.7 GPC chromatogram of polymer PF.

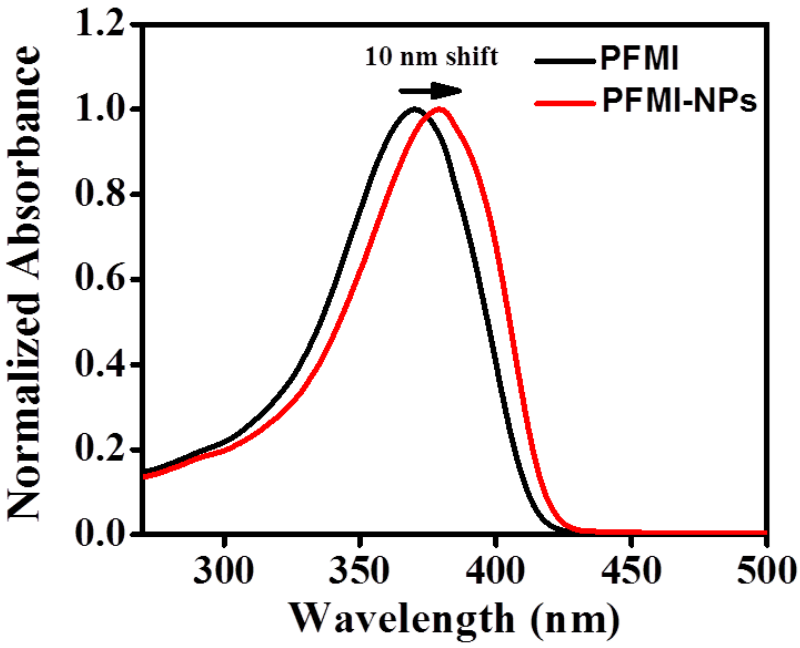

Figure A2.8 Comparison of absorption maxima of PFMI and PFMI-NPs in solution.

Table A2.1 A comparative study of recently reported probes for PA with our results.

Publication	Material used	Stern-Volmer Constant (M^{-1})	Detection Limit (LOD)	Medium Used
Current Manuscript	***Conjugated polymer nanoparticles***	***1.12 × 10^8***	***3.09 × 10^-11 M (7.07 ppt)***	***Water***
Chem. Commun., **2014**, *50*, 6031-6034	Metal complex	5.2×10^4	-	Water/Acetone (v/v=9:1)
ACS Appl. Mater. Interfaces, **2014**, *6*, 10722-10728	Graphene oxide (GO)	1.3×10^5	125 ppb	Buffer
Chem. Eur. J. **2014**, 20, 195-201	Tetraphenylethelene Nanosphere	3.0×10^4	5×10^{-9} M	Water/THF (v/v=9:1)
Chem. Comm., ***2014***, *50*, 12061-12064	Bimetallic Schiff-base Al^{3+} complexes	3.58×10^3 1.81×10^3	5.5×10^{-5} M 1.68×10^{-4} M	MeOH/DMSO
Chem. Mater., **2014**, *26*, 4221-4229	Derivative of graphene	8.9×10^5	300 ppb	Water/THF (v/v=9:1)
Chem. Eur. J., **2014**, *20*, 12215-12222	Derivative of α-cyanostilbene	3.3×10^5	2.8×10^{-7} M	Water/THF (v/v=7:3)
Chem. Commun., **2014**, *50*, 15788-15791	Cage compound	2.2×10^5	6.4 ppb	DCM
J. Mater. Chem. A, **2014**, *2*, 15560-15565	PDA microtube	1.3×10^4	$(4.8 \times 10^{-7}$M) 0.11 ppm	Water
Polym. Chem., **2014**, *5*, 5628-5637	Poly(acrylate) derivative	9.72×10^4 6.98×10^4 4.27×10^4	2.5 ppm	Water/THF (v/v=9:1)
J. Mater. Chem. A, **2014**, *2*, 13983-13989	Polymeric ionic liquid	4.15×10^4 2.03×10^4	-	DMSO
Macromolecules **2014**, *47*, 4908-4919	Conjugated polymers	2.7×10^5	1μM	Water/THF (v/v=9:1)
J. Mater. Chem. A, **2015**, *3*, 92-96	Conjugated polymer	2.6×10^5 8.3×10^4	~1 ppm	Methanol
Chem. Eur. J. **2015,** *DOI: 10.1002/chem.201500727*	Polyfunctional lewis acid	1.6×10^7	18 ppb	DMF
ACS Appl. Mater. Interfaces, ***2015,*** *DOI: 10.1021/acsami.5b01102*	Curcumin derivatives	-	1.35×10^{-8} M 1.35×10^{-8} M	Water
J. Org. Chem., **2015**, *80*, 4064-4075	Triphenylamine derivative	5.72×10^6 2.90×10^5	~5 ppb	DMA, $CHCl_3$

Chem. Commun., **2015**, *51*, 7207–7210	Conjugated polyelectrolyte	1×10^7	5.61×10^{-10} M 128 ppt	Water
Chem. Commun., **2015**,*51*, 8300-8303	MOFs	2.40×10^4 2.46×10^4	-	DMA

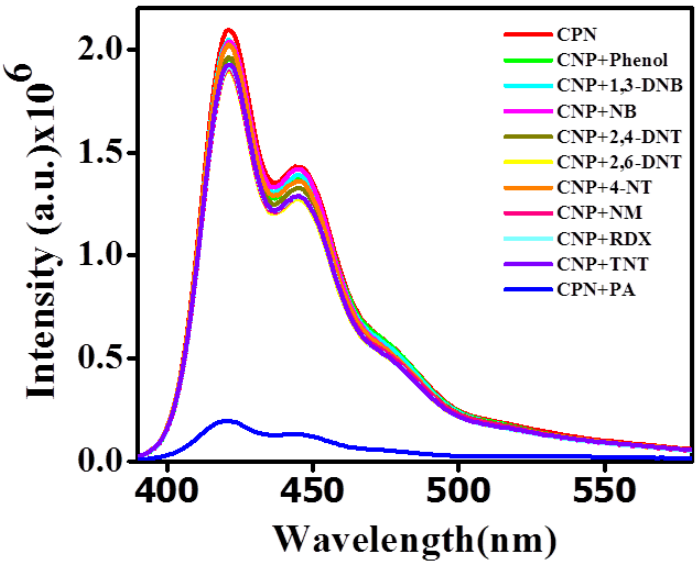

Figure A2.9 Change in emission spectra of PFMI-NPs (6.6 µM) on the addition of PA (0.5 µM) in the presence of various nitroexplosives (0.5 µM).

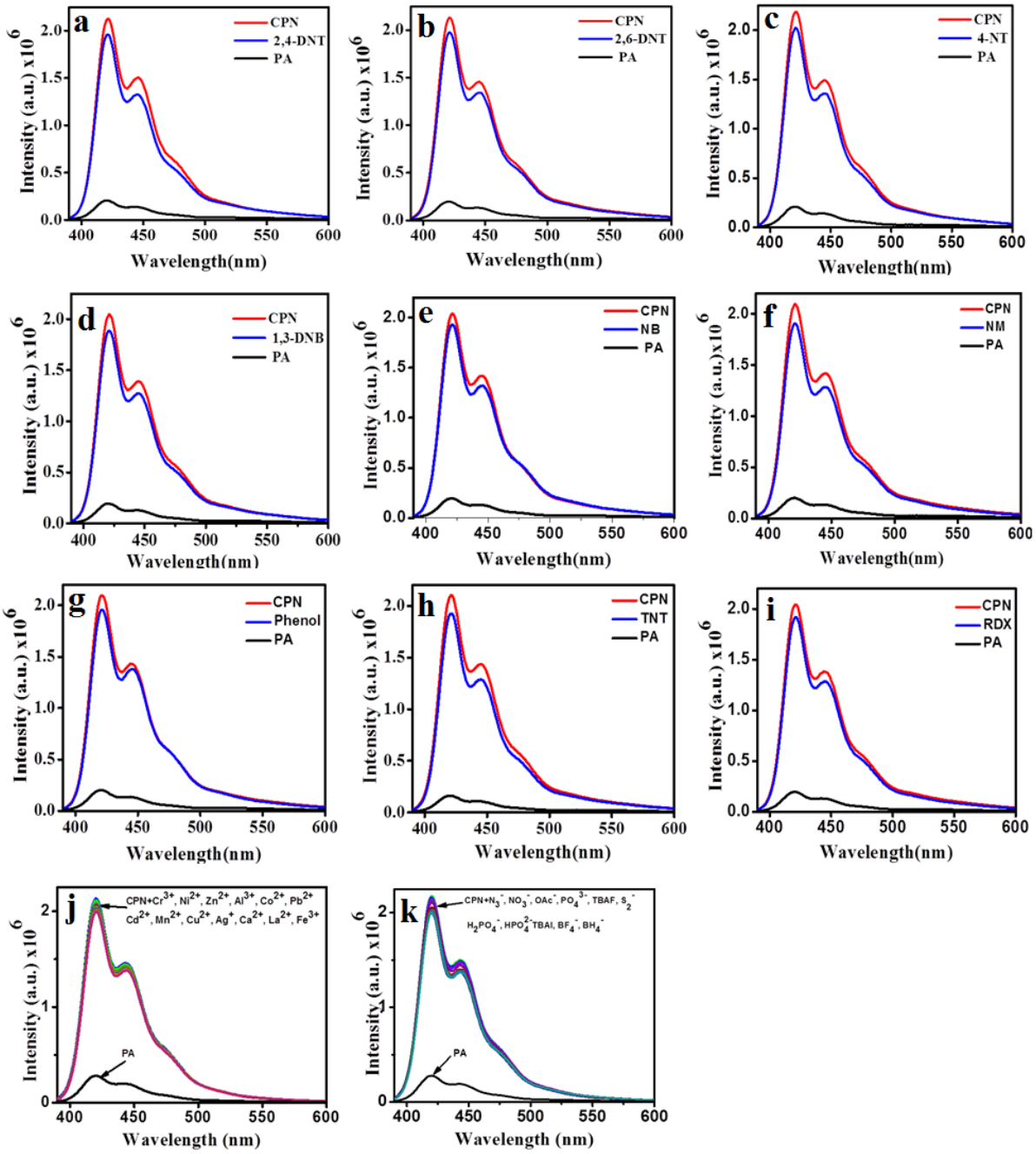

Figure A2.10 Change in photoluminescence spectra of PFMI-NPs (6.6 µM) with (a) 2,4-DNT, (b) 2,6-DNT, (c) 4-NT, (d) 1,3-DNB, (e) NB, (f) NM, (g) Phenol, (h) TNT, (i) RDX (0.5 µM) and (j) various metal ions (1.66 µM) and (k) common anions (1.66 µM) followed by addition of PA (0.5 µM) in aqueous medium.

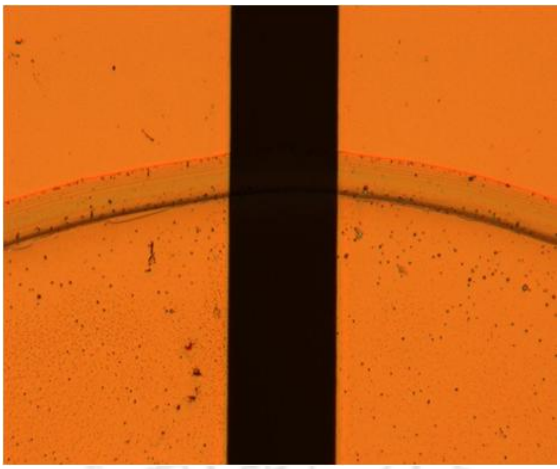

Figure A2.11 Optical microscope image of device showing channel and interface between PFMI-NPs film and bare aluminium surface.

Chapter 3

Conjugated Polyelectrolyte Based Sensitive Detection and Removal of Antibiotics Tetracycline from Water

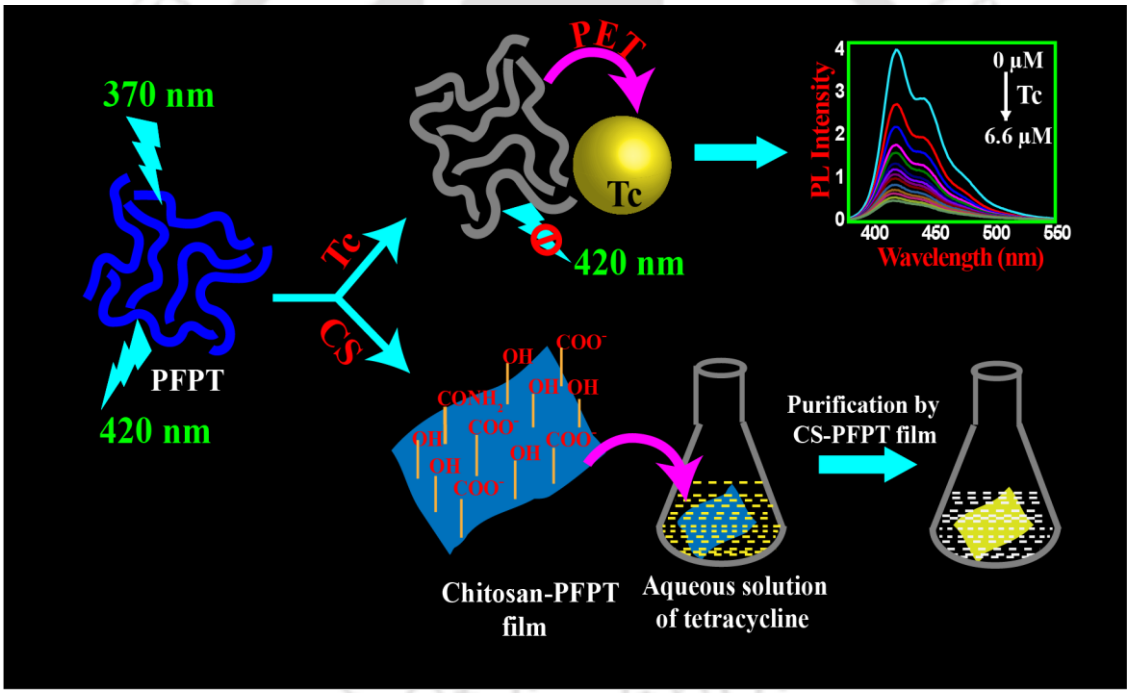

Malik, A. H.; Iyer, P. K. *ACS Appl. Mater. Interfaces* **2017**, *9*, 4433–4439.

Abstract

A new conjugated polyelectrolyte poly[5,5'-(((2-phenyl-9H-fluorene-9,9-diyl)bis(hexane-6,1-diyl))bis(oxy))diisophthalate] sodium (PFPT) was synthesized *via* Palladium catalysed Suzuki cross coupling polymerization method and successfully applied for the rapid, real time and highly sensitive detection of antibiotics tetracycline (Tc) in 100% aqueous media *via* photo-induced electron transfer with detection limit in ppb level. Remarkably, PFPT could also be applied for the trace analysis of Tc in serum samples having recoveries well in the range 92-97% with relative standard deviations (RSD) of 1.01-1.14% confirming reliability of the present method for the analysis of Tc. Additionally, PFPT was blended with the abundant natural polysaccharide chitosan to form CS-PFPT composite films and developed as a biopolymer based membrane for the removal of Tc from water samples with a good adsorption capacity of 3.12 mg g^{-1} thus finding vital application in the treatment of antibiotic infested wastewater.

3.1 Introduction

Tetracycline (Tc), an aromatic polyketide product of the biosynthetic pathway, is a versatile broad spectrum bacteriostatic antibiotic, known to inhibit the protein synthesis by binding with the 30s ribosome subunit.[1] Tc is active against pathogenic microorganisms such as Streptococcus, Pneumococcus, Staphylococcus, Gonococcus, Dysentery bacillis, Mycoplasma, Pertussis, Cholera, Rickettsia, and Chlamydia. Because of its broad spectrum activity, good oral absorption, relatively low toxicity and cost effectiveness[2] it has been broadly used in the treatment of bacterial infections in humans, veterinary animals and fish. It is estimated that ~5000 metric tons of Tc antibiotics are consumed annually.[3] The misuse or abuse of these antibiotics has led to the elevated levels of antibiotic residues in both surface and ground water, in drinking water as well as in animal products,[4-6] which has promoted the evolution of multidrug and antibiotic resistant bacteria. Furthermore, Tc resistance in bacteria are also predicted to be ribosomal-mechanism dependent that can not only disrupt the decoding of genetic information but also hinder the initiation of protein synthesis.[7]

This merited the development of methods for the detection of Tc that included high performance liquid chromatography (HPLC),[8] capillary electrophoresis (CE),[9] mass spectrometry (MS),[10] microbiological analysis (MA),[11] Raman spectroscopy (RS),[12] and ion mobility spectrometry (IMS).[13] However, most of these methods are either time consuming or require expensive and sophisticated instruments, yet present lower sensitivity and selectivity than required. Furthermore, meagre or no attention has been paid for the removal of antibiotic contaminants from the environment. Therefore, development of a reliable and cost effective method for the rapid and sensitive detection as well as removal of Tc residues is utmost important to human health and to prevent the unrestrained spread of antibiotic resistant bacteria.

Fluorescence based methods are considered as superior among various detection techniques because of its easy operation, high sensitivity and rapid signal response time. In recent years, various research groups have reported fluorescent sensors for the detection of tetracycline-based on either inner filter effect (IFE) and/or charge transfer using carbon dots,[14,15] silica based quantum dots[16] etc. However, most of these systems suffer from the issue of complex synthesis, low sensitivity and low signal response time etc. Additionally, hitherto all efforts have been directed to design systems which can perform only a single function at any given time i.e. either detection[14-16] or removal. This

necessitates urgent attention and presents a unique opportunity to develop materials and methods for the detection as well as the removal of Tc from water and other competing environment that would prevent the ever spreading menace of antibiotic-resistant bacteria.

Conjugated polyelectrolytes (CPEs) encompass a unique family of materials that consist of delocalized electronic backbone and ionic side groups appended with the main conjugated chain. CPEs have emerged as novel and promising materials in the subject of sensing because of their high quantum yields, excellent transport properties, viability in biological systems, amplified rapid signal response *via* "molecular wire effect"[17-32] which has ultimately resulted in high sensitivity towards chemical and biological analytes.

Herein, we have synthesised a new CPE, poly[5,5'-(((2-phenyl-9H-fluorene-9,9-diyl)bis(hexane-6,1-diyl))bis(oxy))diisophthalate] sodium (PFPT) *via* palladium catalysed Suzuki cross-coupling polymerization in good yields. The anionic functionality attached on to the side chains of the polymer were designed not only to facilitate its solubility in polar solvents such as water, DMSO, methanol etc. but also to serve in the electrostatic/hydrogen bonding interaction among PFPT and Tc and assist their proximate interaction for the occurrence of efficient electron transfer. Thus, PFPT has been explored for the selective and amplified detection of antibiotic Tc in presence of various inorganic ions and biomolecules that are likely to compete and interfere in their detection process. Furthermore, PFPT was blended in the low cost polysaccharide "chitosan hydrogel" to form a fluorescent composite biomembrane which has been explored for the rapid and highly efficient removal of Tc from water *via* the phenomenon of adsorption. Rapid detection of Tc was achieved at picomolar levels for the first time using PFPT in 100% aqueous medium. To the best of our knowledge this PFPT conjugated polyelectrolyte based method is the first practical report that is capable of performing the dual application of detection as well as removal of antibiotics (Tc) from water at room temperature rapidly with unprecedented efficiency.

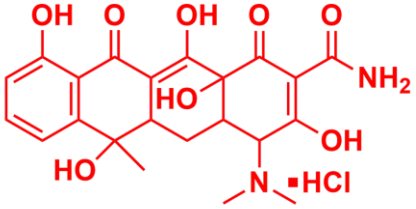

Tetracycline Hydrochloride

3.2 Experimental

3.2.1 Materials and measurements

All chemicals, including Tetracycline hydrochloride (Tc), kanamycin, streptomycin, ampicillin, neomycin, and chitosan were purchased from Sigma Aldrich. Milli-Q water was used in all sensing experiments. The ^{1}H NMR (600 MHz and 400 MHz) and ^{13}C NMR (150 MHz and 100 MHz) spectra were recorded on either Bruker Ascend 600 spectrometer or Varian-AS400 NMR spectrometer, respectively. Fluorescence measurements were performed on a Horiba Fluoromax-4 spectrofluorometer at a slit width of 2 nm using quartz cuvette of 10 mm path length at room temperature. Absorbance measurements were performed using Perkin Elmer Lambda-25 spectrophotometer. Gel Permeable Chromatography was carried out with THF solvent using polystyrene standard to calculate the molecular weight of the newly synthesized conjugated polymers (PF). Electrochemistry was performed on a CH instruments Model 700D series Electrochemical work-station. Time resolved fluorescence studies were performed on an Edinburgh Life Spec II instrument. Fetal bovine serum RM9955 was purchased from Himedia. Fluorescence microscopic images were recorded on an Olympus BX51y micro-scope. FESEM images were recorded on a Sigma Carl ZEISS scanning electron microscope.

3.2.2 Synthetic procedure

3.2.2a Synthesis of M and PF

Synthesis of monomer M and polymer PF was carried out using a previously established procedure shown in chapter 2.

3.2.2b Synthesis of poly [tetramethyl 5, 5'-(((2-phenyl-9H-fluorene-9, 9-diyl)bis(hexane-6,1-diyl))bis(oxy))diisophthalate] (PFPTE)

PF (0.100 g, 0.18 mmol) and dimethyl-5-hydroxyisophthalate (0.296 g, 1.4 mmol) were taken in a 25 mL RB flask and dissolved in anhydrous DMF (3 mL) followed by addition of K_2CO_3 (10 eq.). The reaction mixture was stirred overnight at 80 °C. After cooling to room temperature, the reaction mixture was filtered to remove residual solid K_2CO_3. The filtrate was poured into chloroform and washed with dil. HCl and brine solution. The separated organic layer was dried over anhydrous sodium sulfate and evaporated to obtain the PFPTE as light yellow powder (0.109g, 75% yields).

^{1}H NMR (400MHz, $CDCl_3$, δ ppm) 8.20 (b), 7.76 (b), 7.66 (b), 3.89 (b), 2.07 (b), 1.62 (b), 1.17 (b), 0.88 (b).

FTIR: IR (KBr, cm^{-1}): 3439, 2932, 2859, 1722, 1595, 1464, 1431, 1337, 1317, 1243, 1112, 1043, 809, 760.

3.2.2c Synthesis of poly [5, 5'-(((2-phenyl-9H-fluorene-9,9-diyl)bis(hexane-6,1-diyl))bis(oxy))diisophthalate] sodium (PFPT)

The final conjugated polyelectrolyte PFPT was obtained *via* the alkali induced saponification method. PFPTE (0.05 g) was taken in a 25 mL RB flask, dissolved in minimum amount of THF and a solution of NaOH (0.3 g) in 3 mL water was added. The mixture was heated overnight at 50 °C. After cooling to room temperature, THF was removed and the mixture was dialyzed against water for 3 days to remove excess alkali and lower molecular weight polymer using a membrane with a molecular weight cut-off of 3.5 kDa. The solution was then freeze-dried to get PFPT as a light brown fibrous solid (0.082 g, 80%).

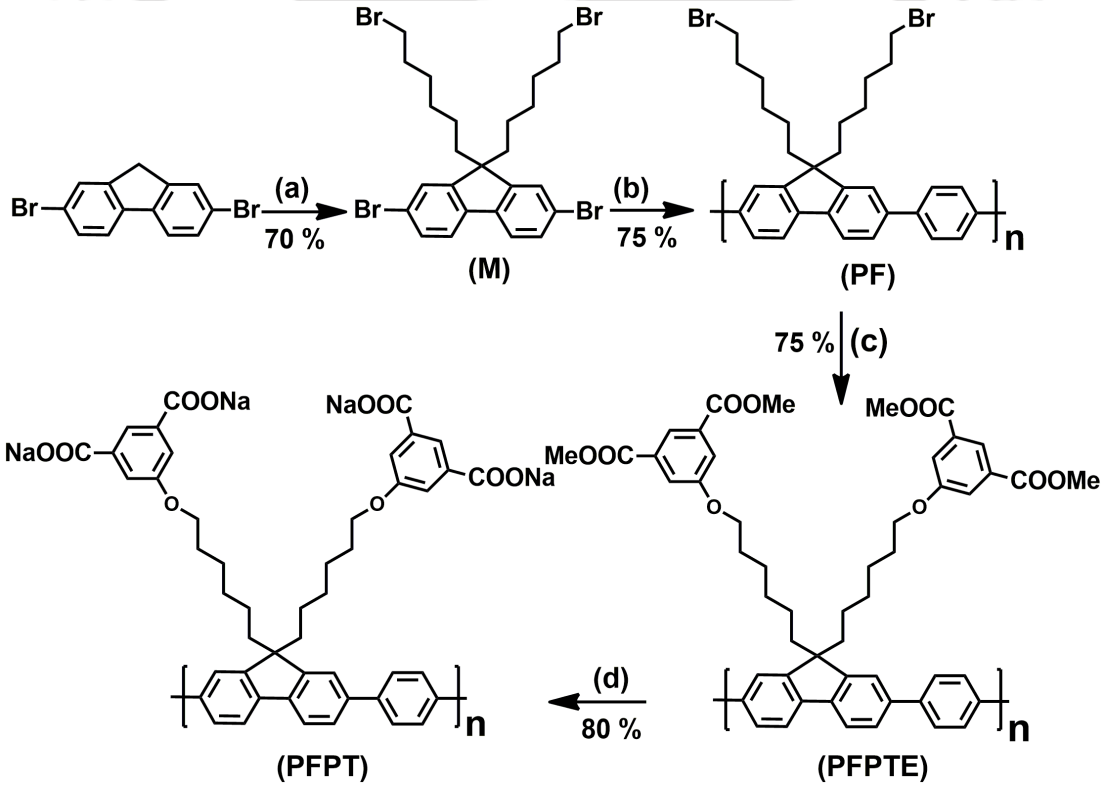

Scheme 3.1 Synthesis of the polymer-PFPT. (a) 1, 6-Dibromohexane, 50% aq. NaOH, TBAI, 70 ºC, 4h. (b) Tetrakis(triphenylphosphine) palladium(0), benzene-1,4-diboronic acid, 2M K_2CO_3 (aq.), THF, reflux, 24h. (c) dimethyl-5-hydroxyisophthalate, DMF(dry), 80 °C, overnight (d) 30% aq. NaOH, THF, 50 °C, 6h.

^{1}H NMR (400 MHz, CD_3OD, δ ppm) 8.14 (b), 7.86 (b), 7.72 (b), 7.52 (b), 3.92 (b), 2.26 (b), 1.61 (b), 1.30 (b), 1.22 (b), 0.76 (b).

FTIR: IR (KBr, cm^{-1}): 3464, 2932, 2854, 1636, 1562, 1456, 1411, 1366, 1259, 1129, 1043, 814, 785.

3.2.3 Preparation of stock solutions for sensing studies

Stock solution of PFPT and all other analytes including Tc were prepared in Milli-Q water at concentrations of 1 mM respectively. The absorption and fluorescence measurements of the PFPT with various analytes were carried out in 3 mL solution (HEPES 10 mM, pH 7.4) containing 6.6 µM PFPT in a quartz cuvette (1 cm × 1 cm).

3.2.4 Quantum yield calculations

Fluorescence quantum yield (Φ_s) of PFPT were determined by single-point measurement using quinine sulphate (Φ_s = 0.54 in 0.1 M H_2SO_4) as standard from the below equation.

$$\Phi_s = \Phi_r (A_r F_s / A_s F_r) (\eta_s^2 / \eta_r^2)$$

Where, r and s signify the reference and sample, Φ denotes the quantum yield, A indicates absorbance, F denotes relative integrated fluorescence intensity and η implies the refractive index of the medium.

3.2.5 Method used for the detection limit calculation

For detection limit calculation, various samples of PFPT (6.6 µM) each containing Tc (0.16 µM, 0.33 µM, 0.66 µM, 1.00 µM, 1.3 µM, 1.6 µM and 2 µM) were prepared separately. The fluorescence spectrum was then recorded for each sample by exciting at 370 nm in HEPES buffer (10 mM, pH 7.4). A calibration curve was plotted between change in the fluorescence intensity and concentration of Tc to obtain the regression curve equation. The detection limit (LOD) was then calculated using the equation 3σ/k, where σ is the standard deviation (S.D.) for five repeated fluorescence measurements of PFPT solution in the absence of Tc and k denotes the slope of the curve.

3.2.6 Cyclic voltammetry studies

Electrochemical measurements were carried out using an electrochemical workstation at a scan rate 50 mVs^{-1} under argon atmosphere. It consisted of three-electrode cell with counter electrode as platinum wire, saturated $Ag/AgNO_3$ electrode acts as a reference electrode and glassy carbon as a working electrode. Tetrabutylammoniumhexafluorophosphate ($TBAPF_6$) (0.1 M) in acetonitrile was used as

the supporting electrolyte. The Fc^{+}/Fc couple was employed as internal reference. PFPT was drop casted on glassy carbon and dried before taking the measurement. Single oxidation peak was observed for PFPT. The HOMO level (-5.95 eV) was calculated from the onset method [$E_{HOMO} = -(E_{(onset,ox\ vs.\ Fc+/Fc)} + 4.8)$ (eV)]. Band gap (3.35 eV) of PFPT were determined from the onset of UV-visible spectrum to calculate its LUMO level (-2.60 eV). To obtain the CV of tetracycline, it was dissolved in aqueous solution contained in the cell chamber were platinum was used as working electrode with platinum wire and Ag/AgCl counter and reference electrodes calibrated against ferrocene. KCl (0.1 M) was used as a supporting electrolyte in PBS buffer (pH 7, 1 mM) and KCl (1 M) as reference electrolyte.

3.2.7 Determination of Tc in serum samples

The stock solutions of Tc (0.1 mM) were prepared in serum sample (diluted 5 times with water). Different concentrations of Tc were prepared separately by spiking them with stock solutions of Tc and then introduced into the cuvette containing PFPT (6.6 µM) in HEPES (10 mM pH 7.4) and fluorescence spectra recorded at an excitation of 370 nm. All measurements were repeated thrice and compared with the calibration curves to obtain the results.

3.2.8 Removal of Tc from water

For the removal of Tc from contaminated water samples, transparent fluorescent biomembrane films were prepared by doping different percentage of PFPT with commercially available chitosan (CS). In a 50 mL beaker containing chitosan (100 mg) and PFPT (5, 10, 15, and 20 wt % taken separately) a 10 mL mixture of 0.1 M acetic acid and glycerol in 3:2 ratios was added followed by continuous stirring for about 2 h at room temperature to ensure complete dissolution of chitosan *vis-à-vis* homogenous distribution of PFPT in the viscous liquid. After adding 5 mL of 5% NaOH drop wise into the liquid, a hydrogel material separated out. This material was repeatedly washed with Milli-Q to ensure complete removal of excess base and residual polymer PFPT. This hydrogel was spread on pre-cleaned glass slide and dried for 2h at 50 ºC in a vacuum oven. A transparent free-standing film was obtained with a thickness of 0.02 mm that could be easily peeled off using forceps and cut into desired size (1 cm ×1 cm). Adsorption studies were performed at 298 K by immersing one such film in a beaker, spiked with known concentration of Tc for a fixed time interval. The solution was then analyzed using UV-visible studies to determine the Tc concentration based on the calibration plot obtained

from the solutions of known Tc concentrations. Similarly, a blank film (without PFPT) was also prepared and adsorption studies were checked by the same procedure. The amount of Tc adsorbed (q_t) with time t was calculated using following equation [34]

$$q_t = (C_o - C_t)V/m$$

Where, C_o was the initial concentration, C_t was the concentration at time t; V (mL) is the volume of solution; and m (g) is the mass of Chitosan-PFPT film.

3.3 Result and discussion

3.3.1 Synthesis and characterization of PFPT

The anionic conjugated polyelectrolyte poly[5,5'-(((2-phenyl-9H-fluorene-9,9-diyl)bis(hexane-6,1-diyl))bis(oxy))diisophthalate] sodium (PFPT) was prepared *via* Pd-catalyzed Suzuki coupling polymerization method followed by post functionalization technique with 80% yield (**Scheme 1**). The product at each step was well characterized by NMR and FTIR studies (**Figure A3.1-A3.3**). The molecular weight (M_w) of precursor polymer PF was found to be 18726 g mol^{-1}, PDI-2.09 in THF using polystyrene as standard (**Figure A3.4**). 5-Hydroxyisophthalate groups were attached onto the side chains of the polymer that facilitated its solubility in polar solvents such as water, DMSO, methanol etc. as well as assisting in bringing PFPT and Tc in close vicinity *via* electrostatic/hydrogen bonding interactions between the carboxylate groups strapped onto the polymer chains and the multiple functionalities present on the tetracycline molecules. Such interactions help in the strong association between the fluorophore and the quencher molecules which eventually resulted in efficient electron transfer as in this case from PFPT polymer to tetracycline. Due to the presence of carboxylate groups onto the side chain of the polymer it is liable to be affected by pH change. Therefore, we studied the effect of pH on the emission (420 nm) of PFPT and it was observed that in acidic pH the fluorescence emission of PFPT diminished to some extent due to the aggregation but upon increasing the pH from 6-14 the emission intensity was almost constant as shown in **Figure 3.1**. The quantum yield (ϕs) of PFPT was found to be 62% in water upon excitation at 370 nm. The anionic polymer PFPT displayed absorption maximum at 360 nm with an emission maximum (excitation 370 nm) of 420 nm and vibronic shoulder at 444 and 477 nm in HEPES buffer, pH 7.4, 10 mM. The PFPT showed deep blue luminescence in dilute aqueous solutions under the illumination of UV light that could be visualized without doubt by naked eye.

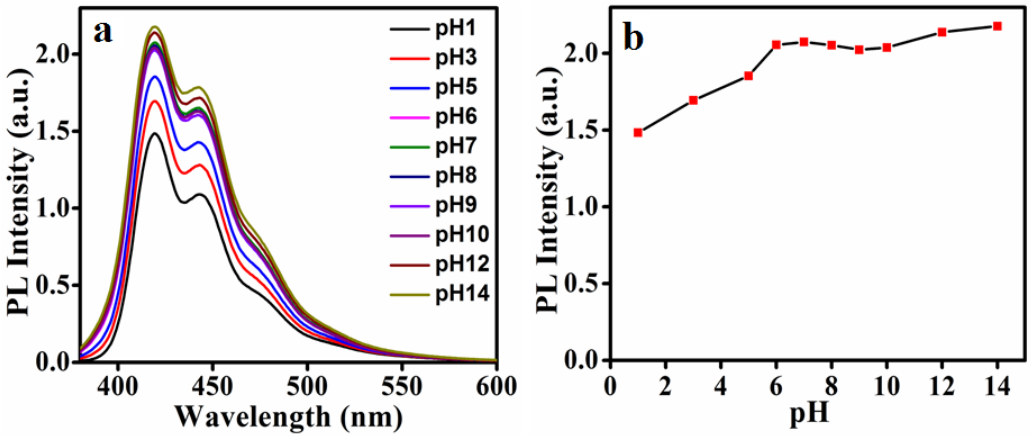

Figure 3.1 (a) Fluorescence emission spectra of PFPT in presence of acid and base (pH 1-14). (b) and its corresponding plot showing the variation of emission intensity (420 nm) with pH.

3.3.2 Sensing and selectivity studies

To explore the ability of PFPT in detecting trace quantities of Tc, the sensing experiments were performed in 100% aqueous media (HEPES buffer 10 mM, pH 7.4). Fluorescence quenching experiments were performed in a cuvette by gradually adding Tc into the PFPT solution (6.6 µM) (HEPES 10 mM, pH 7.4). Instant quenching of ~32% was observed on adding 0.3 µM of Tc into the solution of PFPT (6.6 µM) which finally reached 88% on adding a total of 6.6 µM of Tc (**Figure 3.2a**) while other competing analytes showed insignificant effect on the fluorescence quenching of PFPT. The blue emission of PFPT disappeared in the presence of Tc which was confirmed by illuminating UV light (lamp excitation-325 nm) (**Inset of Figure 3.2a**). Furthermore, selectivity of PFPT towards Tc was examined by checking the changes in the fluorescence of PFPT in the presence other antibiotics such as neomycin, ampicillin, kanamycin, streptomycin. From **Figure 3.2b** it is clear that only Tc quenches the PFPT fluorescence significantly while other antibiotics do not show any significant quenching. The fluorescence quenching efficiency of PFPT in presence of Tc can be studied by Stern-Volmer plot (I_0/I vs [Q] where, 'I_0' and 'I' signifies fluorescence intensity of PFPT in the absence and presence of Tc respectively, [Q] denotes concentration of Tc added to obtain the Stern-Volmer constant K_{sv} (M^{-1}). The K_{sv} value obtained from the linear fitting was found to be 1.57×10^5 M^{-1}, with a correlation coefficient of 0.99 in the range 1.6 nM- 2 µM (**Figure 3.2c)**. Based on the K_{sv} value and standard deviation for five repeated measurements, the limit of detection (LOD) for Tc was found to be 14.35 nM/6.80 ppb (**Figure 3.2d**).

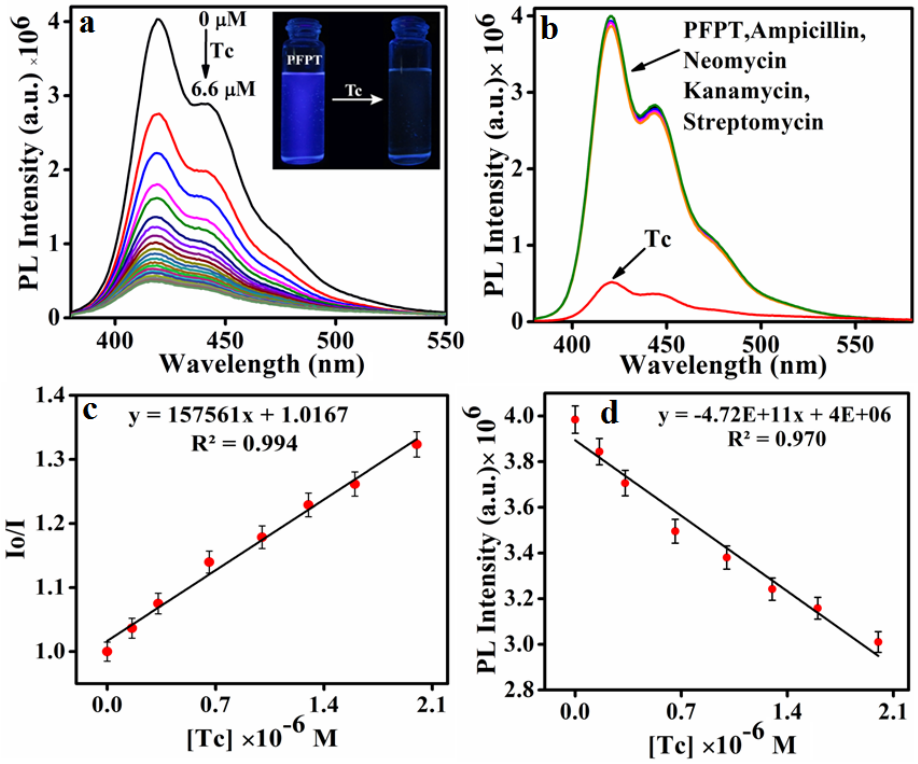

Figure 3.2 (a) Fluorescence spectra of PFPT (6.6 µ M) with increasing concentration of Tc (6.6 µM) in aqueous media (HEPES 10 mM, pH 7.4). Inset: Color change of PFPT under UV lamp excited at 365 nm before and after adding Tc. (b) Effect of Tc (6.6 µ M) and various other antibiotics (6.6 µ M) on the emission spectra of PFPT (6.6 µ M) (c) K_{sv} plot of PFPT upon addition of Tc in aqueous media. (d) Detection limit plot: Fluorescence intensity of PFPT in aqueous medium (HEPES 10 mM, 7.4) as a function of Tc concentration.

Such high K_{sv} and incredibly low detection limit was being observed for the first time using CPEs in 100% aqueous media. Furthermore, the selectivity of PFPT towards Tc was examined by checking the changes in the fluorescence of PFPT in the presence of other likely interfering/competing ions including anions (F^-, Cl^-, Br^-, I^-, BF_4^-, PF_6, $H_2PO_4^-$, HPO_4^{2-}, PO_4^{3-}, HSO_4^-, HCO_3^-, CO_3^{2-}, NO_3^-, N_3^- and CN^-), metals (Mn^{2+}, Cd^{2+}, Zn^{2+}, Yb^{3+}, Eu^{3+}, Pb^{2+}, $Hg^{2+}$and Cr^{3+}), biomolecules (Ala, Asp, Gly, Arg, Ser, Val, Phe, Gln, Glu, Asn, Trp, Tyr, Ribose, Fructose, Glucose, Citrate, Pyrophosphate, ADP, and ATP) (**Figure 3.3**). Among all these analytes only Tc specifically quenched the fluorescence of PFPT which is desirable for real-time practical applications.

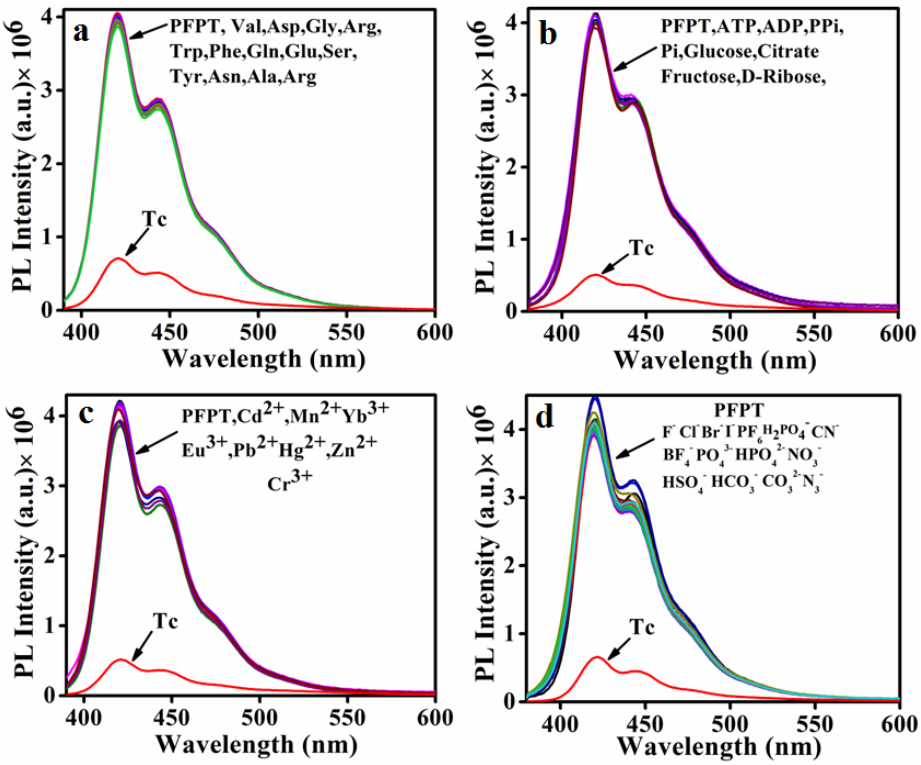

Figure 3.3 Emission spectra depicting the quenching of PFPT fluorescence in presence of Tc and various other competing analytes such as (a) amino acids (6.6 µM) (b) biological molecules (c) cations and (d) anions in HEPES buffer (10 mM, pH 7.4).

3.3.3 Mechanism of sensing

To investigate the reason behind the highly selective fluorescence quenching of PFPT by Tc, the change in the absorbance and emission profile were studied carefully. A spectral overlap between the absorption spectrum of Tc with the excitation and emission band of PFPT was observed, suggesting that the quenching of PFPT fluorescence can take place *via* FRET, IFE and PET process. From **Figure 3.4a**, it was observed that Tc possesses a broad absorption band ranging from 250-440 nm whereas the PFPT has emission and excitation bands centered at 420 (ex 370 nm) and 285 nm respectively, suggesting the possibility of FRET. Since the fluorescence lifetime of PFPT remained unchanged (**Figure 3.4b**) both in the presence (0.750 ns) and absence (0.736 ns) of Tc under a pulsed excitation of 336 nm (λem 420 nm), decay curve was fitted bi-exponentially as shown in **Table 3.1**. The above result discards the involvement of FRET in the process of quenching. Furthermore, a correction for self-absorption[14,35] was done using below equation and the correction factor of the inner filter effect (IFE) at different concentrations of Tc was calculated as shown in **Table 3.2.**

$$I_{corr} = I_{obs} \times 10^{(Aexc + Aem)/2}$$

where, I_{obs} is the maximum fluorescence intensity measured and I_{corr} is the corrected fluorescence intensity after removing the IFE from I_{obs}; A_{ex} and A_{em} are the absorbance of PFPT after the addition of Tc at 370 and 420 nm, respectively. The correction factor (CF) of the IFE (I_{cor}/I_{obsd}) at different concentrations of Tc could be calculated from **Table 3.2.** After subtracting IFE from the quenched fluorescence, it was observed that only 5% of the contribution comes from IFE as shown in **Figure 3.5a**. As a consequence, IFE could not be considered as the major factor in the fluorescence quenching which undoubtedly implies that some other mechanism exists. In PET, electrons are excited from Highest Occupied Molecular Orbital (HOMO) of the PFPT to its Lowest Unoccupied Molecular Orbital (LUMO) and then transferred to the LUMO of Tc. To validate this, cyclic voltammetry (CV) studies were carried out to calculate the HOMO and LUMO energy levels of PFPT (**Figure A3.5a**). Since the polymer PFPT is electron rich, only oxidation peak was observed in the CV, from which the HOMO level was calculated to be -5.95 eV. From the onset of UV-Vis absorption spectra, optical band gap calculated was -3.35 eV and the LUMO level was found to be -2.6 eV. The HOMO (-7.55 eV) and LUMO (-4.53 eV) of tetracycline were also obtained from CV (**Figure A3.5b**) and onset UV-Vis studies. These results confirm that the mechanism operative for the selective quenching of PFPT fluorescence by Tc is the photo induced electron transfer from the LUMO (-2.6 eV) of polymer to the LUMO (-4.53 eV) of the quencher Tc as represented in **Figure 3.5b**.

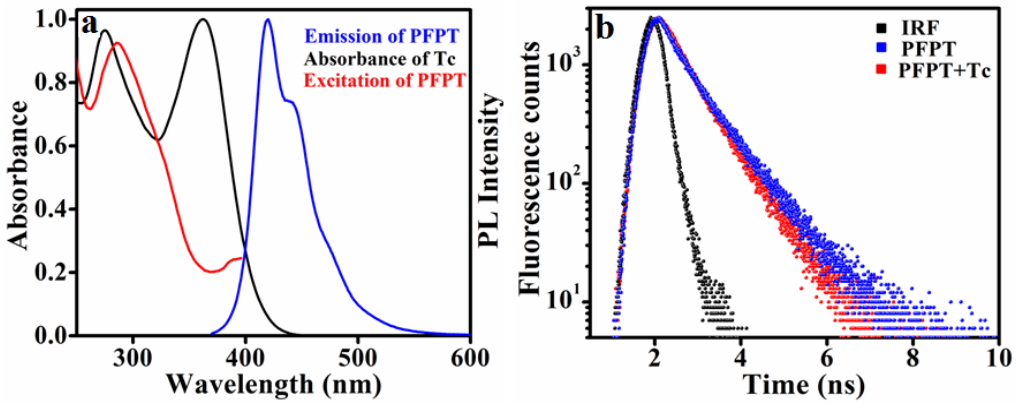

Figure 3.4 (a) Emission/excitation spectra of PFPT and absorption spectrum of Tc in aqueous medium (HEPES buffer 10 mM, pH 7.4). (b) Lifetime decay profile of PFPT (6.6 μM) in presence and absence of Tc (6.6 μM).

Table 3.1 Fluorescence lifetime decay of each component of PFPT in presence and absence of Tc with their fractions and fitting parameters.

Sample	τ_1 (ns)	%	τ_2 (ns)	%	χ^2	τ_{avg} (ns)
PFPT	0.351	36.85	0.800	63.15	1.010	0.736
PFPT –Tc	0.367	40.16	0.940	59.84	1.042	0.750

Table 3.2 Inner filter effect (IFE) of tetracycline on the fluorescence emission of PFPT.

Tc (μM)	A_{ex}	A_{em}	CF (I_{corr}/I_{obs})	I_{corr}	I_{obs}
0	0.236	0.076	1.27	4029810	5120172
1.6	0.305	0.144	1.67	1352260	2264958
3.3	0.314	0.145	1.69	859296	1455937
5.0	0.328	0.146	1.72	622274	1073944
6.6	0.338	0.148	1.74	482980	845140

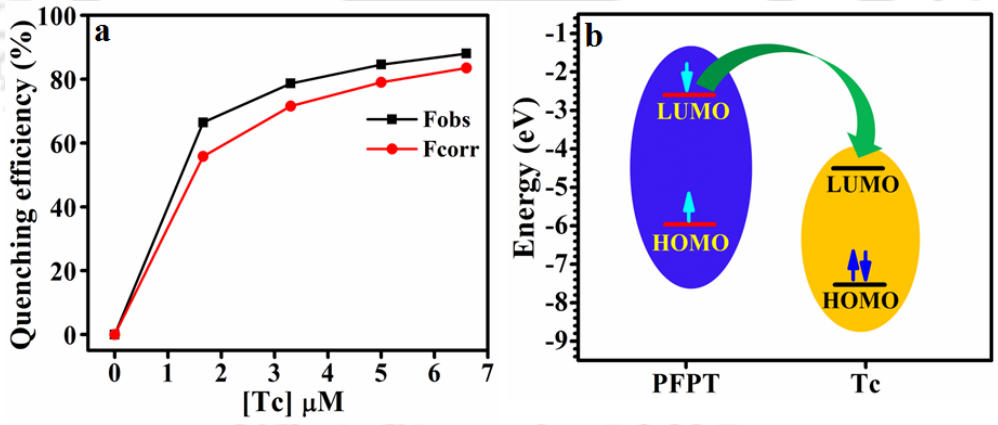

Figure 3.5 (a) Quenching efficiency (E% =1-F/F_0), (where F_0 and F are the fluorescence intensities of PFPT in the absence and presence of Tc, respectively) of corrected (red curve) and observed (black curve) measurements for PFPT after each addition of different concentrations of Tc. (b) Schematic representation of electron transfer from the LUMO of PFPT into the LUMO of Tc.

3.3.4 Application of PFPT in determining Tc in serum samples

To explore the practicability of the PFPT system for the detection of Tc, the studies were extended to serum samples. Serum is an ideal sample to explore the biological

applications of a probe because it provides a competitive and arduous environment due to the presence of a number of components such as proteins, high concentration salts, etc. which can interfere directly in the analysis of a particular analyte during the detection process. For any detection method to be practically reliable there should not be any effect of serum on the emission properties of PFPT. It was observed that unspiked serum samples do not affect the fluorescence emission of PFPT. Further, a series of serum samples containing spiked Tc with different concentrations were prepared and analyzed by the established method. The recoveries have been obtained well in the range 92-97% (from the calibration plot **Figure A3.6**) with relative standard deviations (RSD) of 1.01-1.14% (**Table 3.3**). The above results substantiate that PFPT based method for the determination of Tc had excellent accuracy and precision even in the presence of complicated biological samples. Hence, the PFPT based probe provides a rapid, sensitive and reliable approach for the quantification of tetracycline rapidly and can be readily applied for the real time recognition of Tc in the field of drug analysis and food control.

Table 3.3 Detection of Tc in serum samples.

Serum Samples	Tc added (10^{-8}M)	Tc found (10^{-8} M)[a]	Recovery (%)	RSD (%)
S1	13	12	92	1.14
S2	33	30	90	1.01
S3	46	45	97	1.13

3.3.5 Removal of antibiotics from water

In addition to detection, the removal of antibiotic Tc from wastewater is utmost important in waste water treatment and to prevent the spread of antibiotic-resistant bacteria that pose a serious threat to antibiotic efficacy, which has been a global public health menace for the past several years. It has been reported earlier that CP composites can be used as a good adsorbent for the removal of organic components from water.[36] However, relevant studies on antibiotic are scarce up to now. Motivated by the remarkable ability of PFPT for sensing Tc in trace quantities (ppb levels) and the need to discover a rapid process to separate this class of antibiotics i.e. tetracycline from water on an urgent basis, the PFPT polymer films were prepared with abundantly available biopolymer chitosan (CS). CS acts as a structural component supporting functional polymers and is an ultimate substrate due to its good film-forming ability, ease of modification, ready availablity and

environmental biocompatibility.[37] CS has excellent ability to adsorb a variety of chemical compounds *via* electrostatic attraction/hydrogen bonding because of the presence of multiple amine and hydroxyl functional groups. PFPT being negatively charged due to the presence of carboxylate functionalities interacts strongly with the positively charged CS (due to the dispersion in acidic medium) to form uniform fluorescent membrane of thickness (0.02 mm) as is evident from the fluorescence images shown in **Figure 3.6a**. Furthermore, shifting of FTIR bands clearly indicate electrostatic/hydrogen bonding interaction between PFPT and CS and its successful incorporation into the matrix of CS **(Figure 3.6b)**. The morphology of CS-PFPT films before and after adsorption of tetracycline is shown in **Figure 3.6c & 3.6d** respectively. The adsorption of Tc in CS-PFPT composite membrane was ascertained with the help of UV-Vis spectroscopy at different time intervals. It was observed that the composite film with 15% PFPT exhibited highest change in absorption spectra as shown in **Figure A3.7**. It is evident from the comparative UV studies (**Figure 3.7a**) that the decrease in the concentration of Tc is fast in case of solution dipped with CS-15% PFPT film

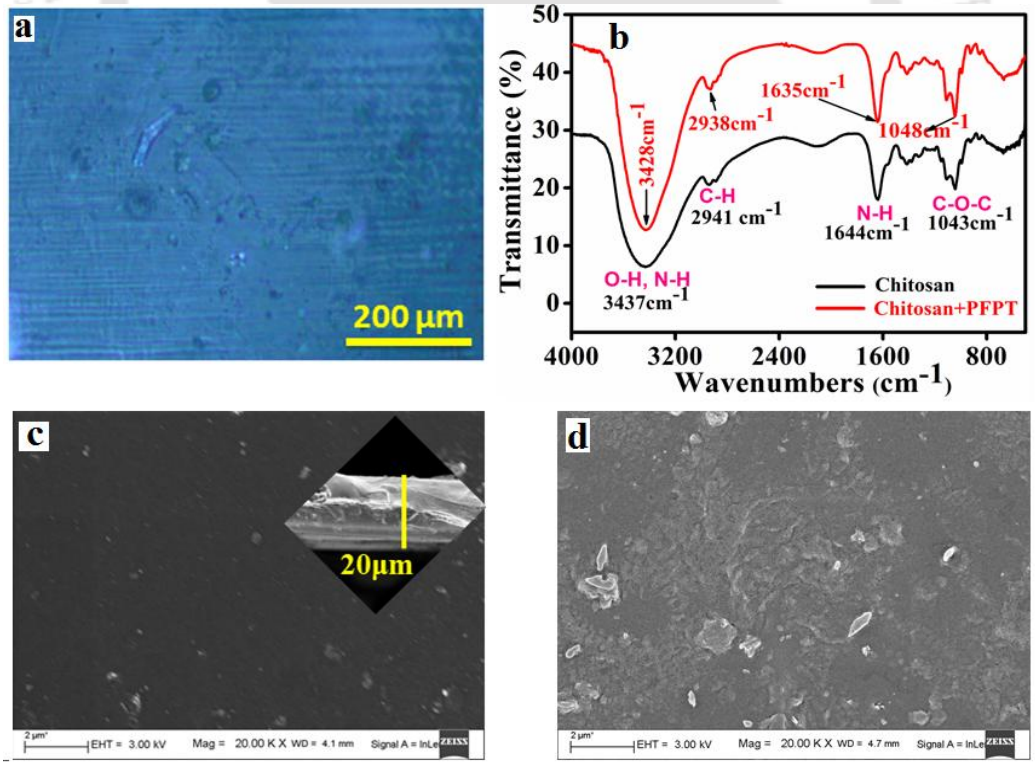

Figure 3.6 (a) Fluorescence microscopic image of Chitosan-PFPT composite film. (b) Comparative FTIR spectra of PFPT-Chitosan composite and blank chitosan film. FESEM images depicting the morphology of CS-PFPT composite film (c) before inset: film thickness (0.02 mm) and (d) after adsorption of tetracycline.

as compared to the blank film (CS only) with time that confirmed the fast adsorption response of CS-PFPT composite and reaches a plateau after 3h.

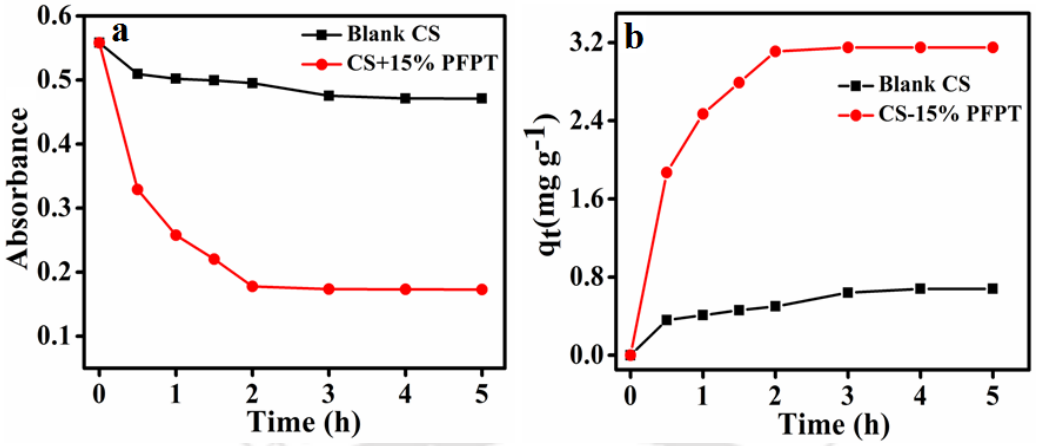

Figure 3.7 (a) Comparative UV-vis study for the adsorption of Tc by blank CS and CS-15% PFPT film with time. (b) Time dependent adsorption studies of CS and CS-15% PFPT films at 298 K.

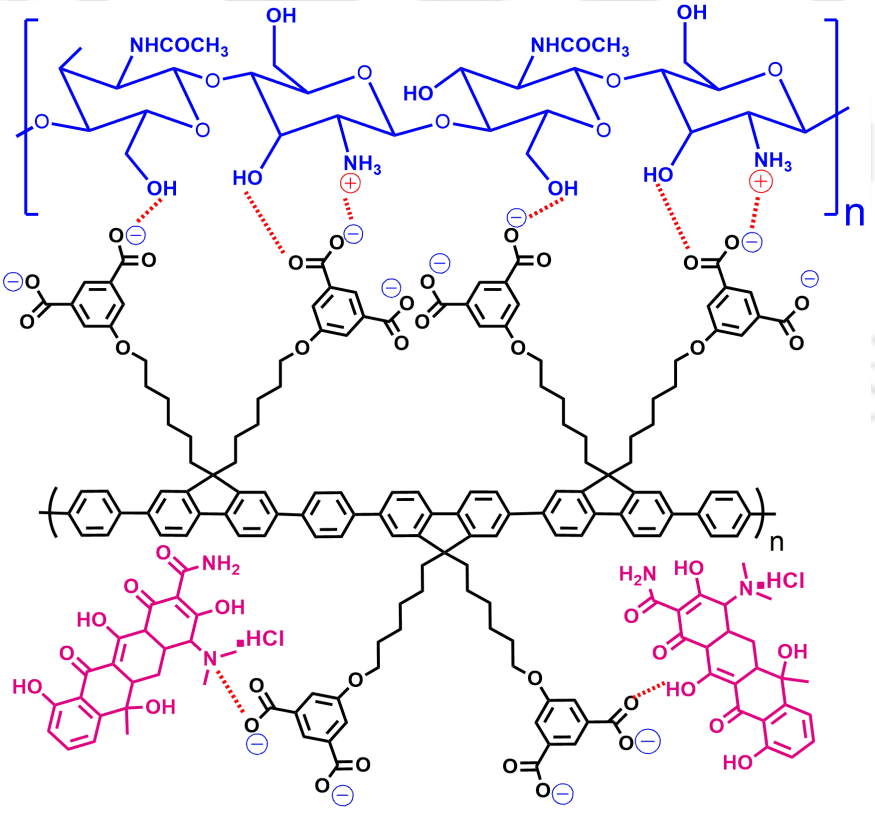

Figure 3.8 Schematic representation of proposed mechanism governing the adsorption of tetracycline by PFPT-Chitosan composite film *via* electrostatic interactions/hydrogen bonding for the removal of Tc from water.

From the standard calibration curve obtained for various concentrations of Tc (**Figure A3.8**), the adsorption capacity of CS-15% PFPT and CS (blank) films obtained were 3.12 mg g^{-1} and 0.68 mg g^{-1} respectively as depicted in **Figure 3.7b**. Furthermore, the percentage of Tc removal from the aqueous solution containing 4.45 mg of Tc was found to be 70% and 15% for PFPT loaded chitosan film and blank films respectively. The higher adsorption performance of CS-PFPT membrane rather than blank could be ascribed to the strong interaction with the adsorbate because of the increase in the number of carboxylate functionalities. The carboxylate groups of CS-PFPT film interacts strongly with multiple functional groups of tetracycline such as –OH, $^{+}NR_3$, -$CONH_2$ etc. *via* electrostatic/hydrogen bonding interactions which resulted in the adsorption of Tc on the surface of the composite film as shown schematically in **Figure 3.8.**

3.4 Conclusion

In conclusion, the design and development of new anionic water soluble conjugated polymer PFPT for the selective and sensitive detection as well as removal of a broad spectrum antibiotic tetracycline from water has been reported. The detection limit of PFPT toward Tc is estimated to be 14.35 nM/6.80 ppb (6.8 ng/mL) in 100% aqueous medium. High quenching efficiency with a K_{sv} value of 1.57 $\times 10^5$ M^{-1} was obtained which can be attributed to efficient electron transfer from PFPT to Tc *via* electrostatic/hydrogen bonding interactions. Chitosan-PFPT composite membrane shows good adsorption capacity (3.12 mg g^{-1}) towards Tc (with excellent removal ability of 70%), thus providing a new and handy strategy for the exclusion of Tc from water that can find immediate application in the treatment of wastewater.

References

(1) Spahn, C.M.T.; Prescott, C.D. *J. Mol. Med.* **1996**, *74*, 423.

(2) Schnappinger, D.; Hillen, W. *Arch. Microbiol.* **1996**, *165*, 359.

(3) Behal, V.; Hunter, I.S. Genetics and Biochemistry of Antibiotic Production, Butterworth-Heinemann, Boston, **1995**, pp. 359-385.

(4) Wasch, K. D.; Okerman, L.; Croubels, S.; Brabander, H. D.; Hoof, J. V.; Backer, P. D. *Analyst* **1998**, *123*, 2737.

(5) Croubels, S.; Peteghem, C. V.; Baeyens, W. *Analyst* **1994,** *119*, 2713.

(6) Jeon, M.; Paeng, I. R. *Anal. Chim. Acta*. **2008**, *626*, 180.

(7) Pioletti, M.; Schlünzen, F.; Harms, J.; Zarivach, R.; Glühmann, M.; Avila, H.; Bashan, A.; Bartels, H.; Auerbach, T.; Jacobi, C.; Hartsch, T.; Yonath, A.; Franceschi, F. *EMBO J.* **2001**, *20*, 1829.

(8) Ng, K.; Linder, S.W. *J. Chromatogr. Sci.* **2003**, *41*, 460.

(9) Vinas, P.; Balsalobre, N.; Erroz, C.L.; Cordoba. M.H. *J. Chromatogr. A* **2004**, *1022,* 125.

(10) Granelli, K.; Elgerud, C.; Lundstrom, A.; Ohlsson, A.; Sjoberg. P. *Anal. Chim. Acta*. **2009**, *637*, 87.

(11) Myllyniemi, A. L.; Nuotio, L.; Lindfors, E.; Rannikko, R.; Niemi, A.; Backman, C. *Analyst* **2001**, *126*, 641.

(12) Chen, J. L.; Hsieh, K. H. *Electrophoresis* **2010**, *31*, 3937.

(13) Tabrizchi, M.; Ilbeigi, V. *J. Hazard. Mater*. **2010**, *176*, 692.

(14) Lin, M.; Zou, H. Y.; Yang, T.; Liu, Z. X.; Liu, H.; Huang, C. Z. *Nanoscale* **2016**, *8*, 2999.

(15) Hou, J.; Yan, J.; Zhao, Q.; Li, Y.; Ding, H.; Ding, L. *Nanoscale* **2013**, *5*, 9558. (16) Zhang, L.; Chen, L. *ACS Appl. Mater. Interfaces* **2016**, *8*, 16248.

(17) Sohn, H.; Calhoun, R. M.; Sailor, M. J.; Trogler, W. C. *Angew. Chem. Int. Ed. Engl*. **2001**, *40*, 2104.

(18) Zhu, C.; Liu, L.; Yang, Q.; Lv, F.; Wang, S. *Chem. Rev.* **2012**, *112*, 4687.

(19) Kim, H. N.; Guo, Z.; Zhu, W.; Yoon, J.; Tian, H. *Chem. Soc. Rev*. **2011**, *40*, 79.

(20) Thomas III, S. W.; Joly, G. D.; Swager, T. M. *Chem. Rev*. **2007**, *107*, 1339.

(21) McQuade, D. T.; Pullen, A. E.; Swager, T. M. *Chem. Rev*. **2000**, *100*, 2537.

(22) Rochat, S; Swager, T. M. *ACS Appl. Mater. Interfaces* **2013**, *5*, 4488.

(23) Liang, J.; Lia, K.; Liu, B. *Chem. Sci*. **2013**, *4*, 1377.

(24) Gutacker, A.; Lin, C.Y.; Ying, L.; Nguyen, T.Q.; Scherf, U.; Bazan, G. C. *Macromolecules* **2012**, *45*, 4441.

(25) Feng, X.; Lv, F.; Liu, L.; Tang, H.; Xing, C.; Yang, Q.; Wang, S. *ACS Appl. Mater. Interfaces* **2010**, *2*, 2429.

(26) Malik, A. H.; Hussain, S.; Kalita, A.; Iyer, P. K. *ACS Appl. Mater. Interfaces* **2015**, *7*, 26968.

(27) Hussain, S.; Malik, A. H.; Afroz, M. A.; Iyer, P. K. *Chem. Commun*. **2015**, *51*, 7207.

(28) Hussain, S.; Malik, A. H.; Iyer, P. K. *ACS Appl. Mater. Interfaces* **2015***, 7*, 3189.

(29) Malik, A. H.; Hussain, S. Iyer, P. K. *Anal. Chem*. **2016**, *88*, 7358.

(30) Hussain, S.; Malik, A. H.; Iyer, P. K. *J. Mater. Chem. B* **2016**, *4*, 4439.

(31) Malik, A. H.; Hussain, S.; Tanwar, A. S.; Layek, S.; Trivedi, V.; Iyer, P. K. *Analyst* **2015**, *140*, 4388.

(32) Tanwar, A. S.; Hussain, S.; Malik, A. H.; Afroz, M. A.; Iyer, P. K. *ACS Sens.* **2016**, *1*, 1070.

(33) Saikia, G.; Iyer, P. K. *J. Org. Chem*. **2010**, *75*, 2714.

(34) Zhu, H.; Yang, X.; Cranston, E. D.; Zhu, S. *Adv. Mater.* **2016**, *28*, 7652.

(35) Sahu, S.; Sil, T. B.; Das, M.; Krishnamoorthy, G. *Analyst* **2015**, *140*, 6114.

(36) Huang, Y.; Li, J.; Chen, X.; Wang, X. *RSC Adv*. **2014**, *4*, 62160.

(37) Shahabuddin, S.; Sarih, N. M.; Ismail, F. H.; Shahid, M. M.; Huang, N. M. *RSC Adv*. **2015**, *5*, 83857.

Appendix

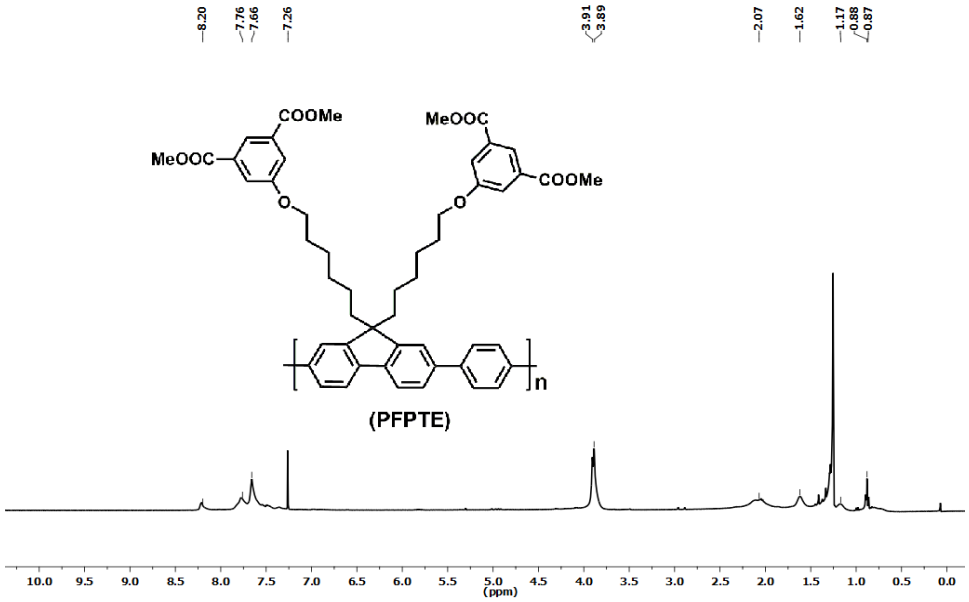

Figure A3.1 ^{1}H NMR spectra of PFPTE.

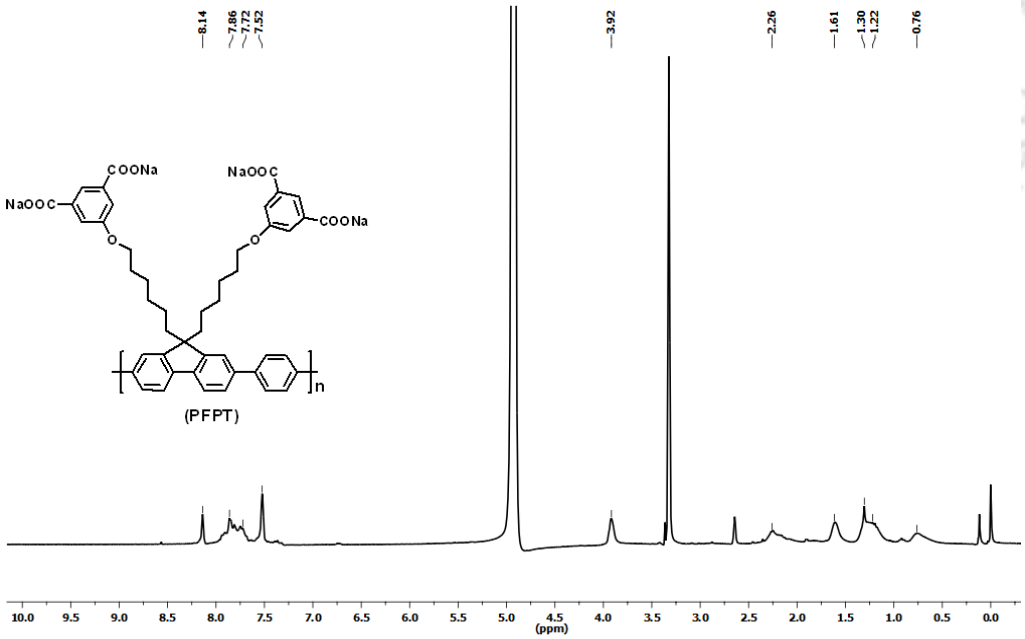

Figure A3.2 ^{1}H NMR spectra of PFPT.

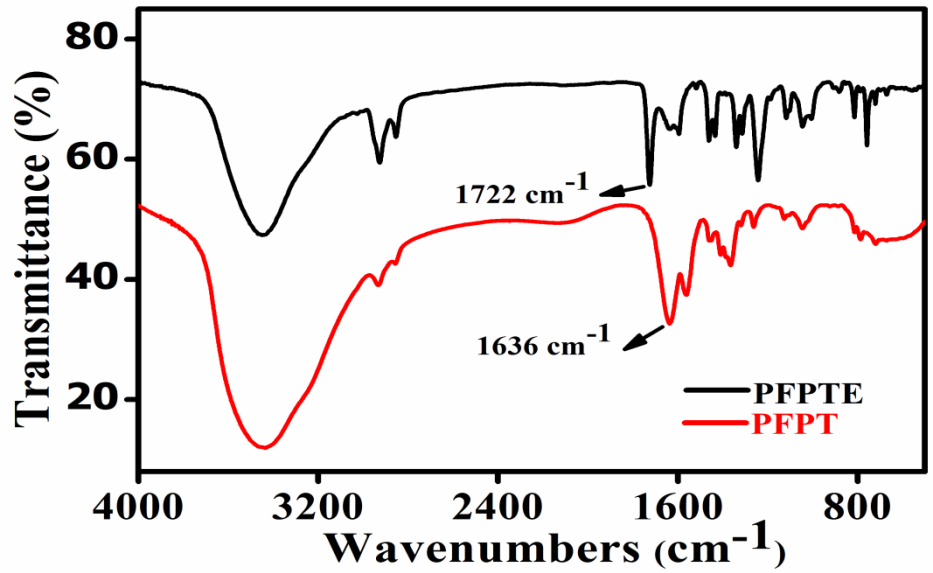

Figure A3.3 Comparison of FT-IR spectra of PFPTE and PFPT.

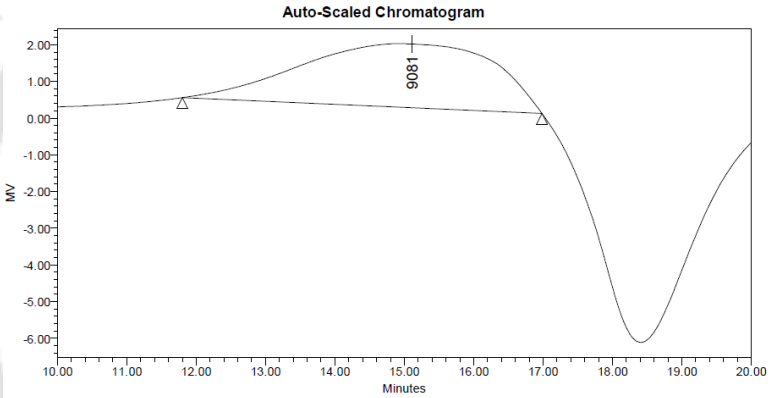

GPC Results

	SampleName	Mn	Mw	MP	Mz	Mz+1	Polydispersity
1	PF-C6-Br(P61-2)	8946	18726	9081	33400	44652	2.093162

Figure A3.4 GPC chromatogram of polymer PF.

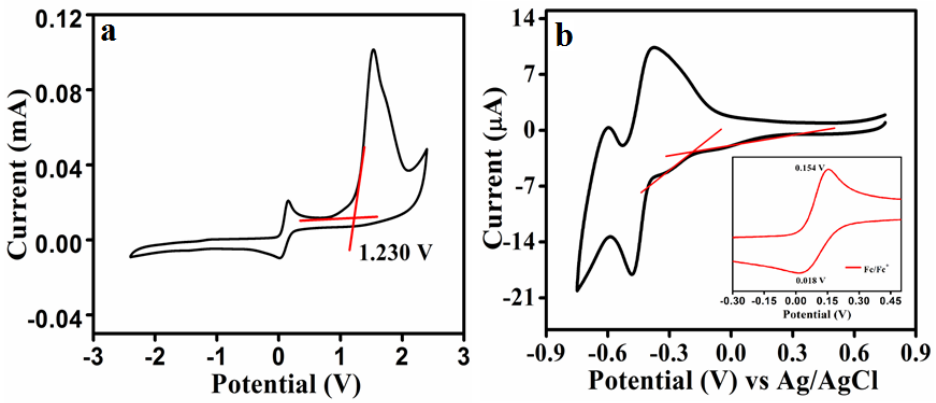

Figure A3.5 Cyclic voltammogram of (a) PFPT film obtained on glassy carbon electrode and (b) tetracycline obtained on platinum electrode (inset: CV of ferrocene) with a scan rate of 50 mV/s.

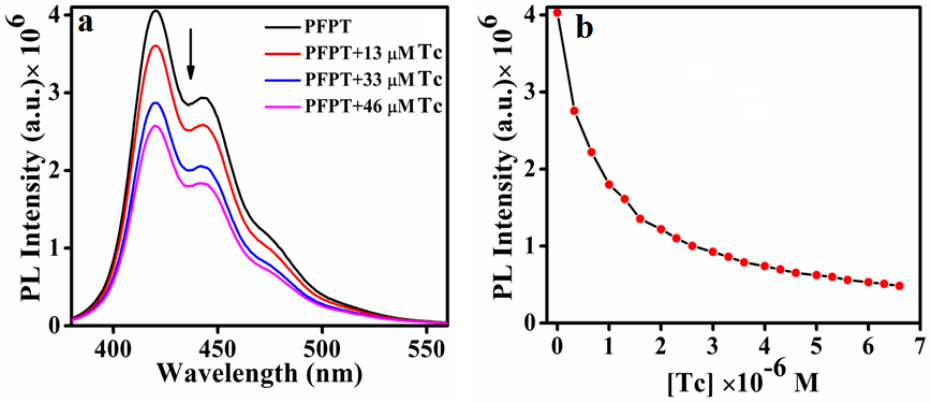

Figure A3.6 (a) Fluorescence emission spectra of PFPT upon addition of serum samples spiked with known concentrations of Tc. (b) Calibration plot obtained for the estimation of Tc.

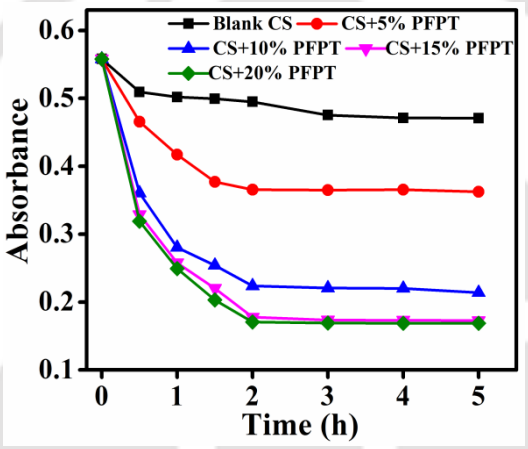

Figure A3.7 Absorbance plot depicting the effect of varying percentage of PFPT concentration in CS films on the adsorption of Tc.

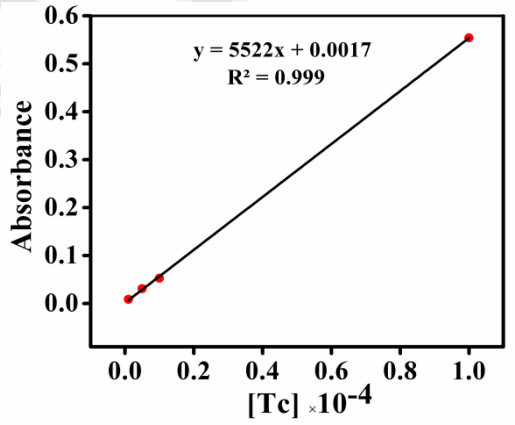

Figure A3.8 Calibration plot obtained for the estimation of Tc.

Chapter 4

Aggregation Induced FRET via Polymer-Surfactant Complexation: A New Strategy for the Detection of Spermine

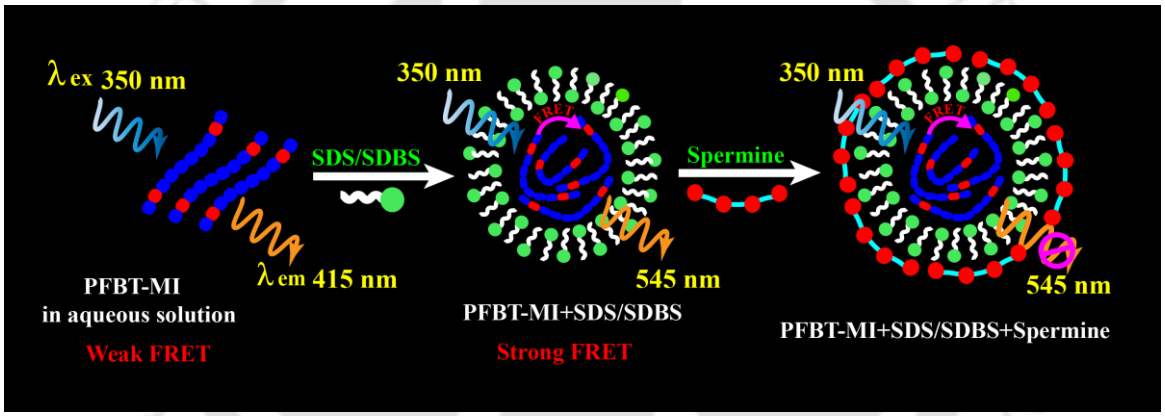

Malik, A. H.; Hussain, S.; Iyer, P. K. *Anal. Chem.*, **2016**, *88*, 7358–7364.

Abstract

A new water-soluble cationic conjugated polymer [9, 9-bis (6'-methyl imidazolium bromide) hexyl) fluorene-co-4,7-(2,1,3-benzothiadiazole)] (PFBT-MI) was designed and synthesized via Suzuki cross-coupling polymerization in good yields without any tedious purification steps. PFBT-MI showed excellent photophysical responses towards SDS and SDBS with a detection limit of 0.12 µM/(34 ppb) and 0.13 µM/(45 ppb) respectively. Furthermore, occurrence of FRET from the donor (fluorene) to acceptor (BT units), via surfactant induced aggregation results in naked-eye detection of these common anionic surfactants (SDS/SDBS) as the color changes from blue to yellowish green in aqueous solution. The polymer-surfactant nanoaggregates thus formed via electrostatic as well as hydrophobic interactions has been explored for the sensitive detection of spermine (considered as an excellent biomarker for early cancer diagnosis) with detection limit of 66 ppb (0.33 µM) which is much below the range 1-10 µM pertinent for the early diagnosis of cancer in urinary samples. This, highly sensitive technique would facilitate the direct and non-invasive detection of spermine from urine rapidly and is likely to have great significance in early cancer diagnosis.

4.1 Introduction

Spermine, a biogenic polyamine, usually found in eukaryotic cells and body fluids, plays a vital role in the regulation of several cellular processes like cell growth and proliferation.[1-4] These polyamines are among the most abundant organic polycations found in human body and are known to be involved in numerous stages of protein synthesis, stabilization of nucleic acid conformations and cytoskeleton structures.[4] It has been observed that enhanced levels of spermine in urine and blood are liable to many types of cancer. Thus, it is regarded as an excellent biomarker for early cancer detection and an indicator for assessing the efficiency of cancer chemotherapy during the long-term continuation of patients.[5-11] Currently, spermine and its analogues are being detected using classical analytical methods *viz.* immunoassays, mass spectrometry, electrophoresis and chromatographic techniques.[5,12-15] Since, these techniques are complex, tedious, time consuming and expensive, establishment of an alternate fluorescent based method for selective and ultrasensitive detection of spermine in body fluids is highly significant in the present context.

Anionic surfactants comprising of non-polar alkyl chain (hydrophobic tail) and an anionic polar group (hydrophilic head), form a major source of environmental pollutant due to their widespread use in personal, home/vehicle cleaning agents, industrial and agricultural processes.[16] Moreover, they are also known for their interaction with biomolecules like nucleic acids, proteins and peptides with the ability to even penetrate cell membranes.[17-21] Among all anionic surfactants, sodium dodecyl benzenesulfonate (SDBS) and sodium dodecyl sulfate (SDS) are most abundant owing to their extensive industrial scale production and frequent applications in various sectors. Hence, their determination at very low levels in the waste water, food preparations, pharmaceuticals, as masking agents in drug abuse, in biological mediums etc., is highly significant since they are considered as "emerging pollutants".[22,23] Apart from the efforts in developing methods to reduce their environmental impact, yet another key aspect is the introduction of new and improved strategy for their detection in the surroundings. Although, various sophisticated surfactant detection methods[24-27] are available, most of them are inefficient and suffer from severe drawbacks like employing large amounts of halogenated solvents, delayed signal response, tedious procedures and irreproducibility. Hence, the development of more efficient and reliable method for trace detection of anionic surfactants that can overcome the limitations found in the existing methods is highly desirable.

Fluorescence technique is regarded superior among various detection methods owing to their simplicity, high sensitivity and rapid signal response time. In this context, few probes for sensing anionic surfactants have been established recently.[28-31] However, they usually depend on the change in the intensity of single emission band that might result in erratic quantitative analysis due to autofluorescence, environmental effects and instrumental fluctuation. A prospective solution to this problem is the development of suitable ratiometric probe that exhibits spectral shifts, since it provides a relative measurement of the intensities of two different emission bands and eliminate most of the possible artefacts. Interestingly, FRET assisted ratiometric detection of anionic surfactants (SDS and SDBS) using CPE has never been reported, thus, providing huge opportunities to be explored.

Recently, conjugated polyelectrolytes (CPEs) have emerged as excellent materials[32] in the field of sensing due to their numerous features such as remarkable sensitivity, high quantum efficiency, photostability etc. These materials combine the optoelectronic properties of neutral conjugated polymers (CPs) as well as electrostatic behaviour of polyelectrolytes, thus, providing an exceptional platform for the sensing of chemical and biological species.[33-44] The delocalized backbone chain of CPEs also favour rapid intra-chain and inter-chain energy transfer processes compared to small molecules.[45] However, the inter-chain Förster resonance energy transfer (FRET) is considered as more efficient than intra-chain FRET due to stronger electronic coupling and enhanced transfer range in the former[46-48] which is also highlighted by Bazan[49] and Swager's group[8] in their pioneer work on the detection of charged species. Thus, an alternate method for the detection of spermine and anionic surfactants comprising of CPE is highly significant.

Herein, we have developed a new water soluble cationic CP poly[9,9-bis(6'-methyl imidazolium bromide) hexyl) fluorene-co-4,7-(2,1,3-benzothiadiazole)] (PFBT-MI), comprising 20 mol% of benzothiadiazole (BT) via Suzuki polymerization method. The blue emitting polymer PFBT-MI displayed significant changes in its photophysical properties as well as morphology after selective interaction with anionic surfactants *viz.* SDS and SDBS followed by spermine. The formation of stable polymer-surfactant complex via Columbic as well as hydrophobic interaction induces the process of aggregation that enables the increment of local BT concentration in aqueous solution. This leads to the favorable inter-chain FRET from the donor (fluorene) to acceptor (BT units), giving rise to a blue-to-yellowish green emission that was subsequently utilized for

the detection and quantification of SDS and SDBS in aqueous solution. Furthermore, the polymer-surfactant assembly was successfully used for the trace detection of biogenic amine spermine in urine specimens with high selectivity and sensitivity. To the best of our knowledge, this is the first report based on FRET assisted ratiometric detection of most common anionic surfactants (SDS and SDBS) *viz-a-viz* sensing of spermine using polymer-surfactant assembly.

4.2 Experimental

4.2.1 Materials and measurements

All chemicals were acquired from Aldrich, Merck, Ranbaxy (India) and were used as received. UV-Visible and emission spectra were recorded on a Perkin Elmer Lambda-25 and Horiba Fluoromax-4 spectrofluorometer, respectively using 10 mm path length quartz cuvettes with a slit width of 3 nm at room temperature. Milli-Q water was used in all sensing experiments. The ^{1}H NMR (600 MHz and 400 MHz) and ^{13}C NMR (150 MHz and 100 MHz) spectra were obtained on Bruker Ascend 600 spectrometer and Varian-AS400 NMR spectrometer, respectively. Gel permeable chromatography (GPC) was performed in Waters-2414 instrument (Polystyrene calibration). Zetasizer Nano ZS90, Model No. ZEN3690, Malvern was used to perform DLS based size and charge measurements. Lifetime measurements were performed using an Edinburgh Instruments F900 spectrometer with a laser source (λ_{ex}=375 nm). Morphological characterization was done using Zeiss sigma field emission scanning electron microscope (FESEM) at an accelerating voltage of 2 kV. Transmission electron microscopic (TEM) images were obtained on JEOL 2100 UHR-TEM instrument, operating at 200 KV.

4.2.2 Synthetic procedure

Monomers 2,7-dibromo-9,9-bis(6-bromohexyl)-9H-fluorene (M1) and 2,7-Bis[9,9′-bis(6″-bromohexyl)fluorenyl]-4,4,5,5-tetramethyl[1.3 .2]dioxaborolane (M2) were prepared using established procedure.[50]

4.2.2a Synthesis of Poly[9,9-bis(6'-bromohexyl)fluorene-co-4,7-(2,1,3-benzothiadiazole)] (P1)

Polymer P1 was synthesized via reported procedure.[50] M1 (97.5 mg, 0.15 mmol), M2 (186.0 mg, 0.25 mmol), 4,7-dibromo-2,1,3-benzothiadiazole (29.0 mg, 0.1 mmol), [Pd(PPh_3)$_4$] (5 mg), and potassium carbonate (345 mg, 2.5 mmol) were kept in a 50 mL two neck round-bottom flask. A mixture of water (5 mL) and THF (15 mL) was added to

the flask using syringe and degassed thrice by freeze thaw cycle to remove any oxygen. The reaction mixture was then stirred vigorously at 75 °C for 24h followed by precipitation into excess of methanol repeatedly. The precipitate was then filtered, washed and dried under vacuum for 12h to afford the neutral dark brownish coloured polymer. (0.220 g, 70.0%)

^{1}H NMR (600 MHz, $CDCl_3$, δ ppm): 8.06-7.47 (m), 7.96 (b), 7.87 (b), 7.69 (b), 7.52 (b), 7.47 (b), 3.30 (b), 2.16 (b), 1.93 (b), 1.69 (b), 1.26 (b), 0.88 (b), 0.71 (b), 0.59 (b).

^{13}C NMR (150 MHz, $CDCl_3$, δ ppm): 154.57, 152.35, 139.25, 132.22, 130.52, 128.78, 126.23, 124.20, 121.77, 121.75, 121.40, 120.34, 55.73, 40.19, 34.13, 32.77, 29.85, 29.23, 27.91, 25.03, 23.63.

GPC in THF, polystyrene standard: Mw= 1.4103×10^4, PDI-2.1.

4.2.2b Synthesis of Poly [9,9-bis(6'-methyl imidazolium bromide)hexyl)fluorene-co-4,7-(2,1,3 benzothiadiazole)] (PFBT-MI)

Brominated polymer P1 (0.05 g, 0.031 mmol, 1 eq.) dissolved in excess of 1-methyl imidazole was refluxed under stirring condition at 80 °C for 24h. The reaction mixture was then decanted into excess chloroform and stirred for 1 h to get precipitate. The yellow precipitate was then washed several times with chloroform to remove trace quantities of methyl imidazole so as to obtain pure functionalized polymer PFBT-MI (0.043 g, 66.0%).

^{1}H NMR (600 MHz, CD_3OD, δ ppm): 8.23-7.52 (m), 4.62 (b), 4.09 (b), 3.87 (m), 2.26 (b), 2.12 (b), 2.04 (b), 1.71 (b), 1.17 (b), 0.78 (b).

^{13}C NMR (150 MHz CD_3OD, δ ppm): 154.45, 152.99, 151.82, 151.32, 140.34, 136.51, 136.28, 136.06, 130.57, 128.42, 126.26, 123.83, 122.65, 110.03, 55.60, 49.63, 44.83, 40.32, 39.85, 35.30, 29.77, 29.02, 25.92, 23.58.

4.2.3 Preparation of stock solutions for sensing studies

A stock solution of 10 mM for each analyte (surfactants, anions, metal ions, polyamines and various cancer biomarkers) was prepared in Milli-Q water and diluted to desired concentrations whenever required. A solution of PFBT-MI (6.6 µM) in repeat units (RUs) in Milli-Q water was placed in a 3 mL cuvette (10 mm width) to record the fluorescence spectrum by exciting at 350 nm. Various analyte solutions were then introduced to monitor the changes in the fluorescence intensity. Similarly, the absorbance spectra of

PFBT-MI (6.6 µM) in Milli-Q water was recorded at room temperature in presence of SDS, SDBS and spermine to monitor the changes in absorbance.

4.2.4 Method used for detection limit calculation

Different PFBT-MI samples (6.6 µM) each containing SDS (0, 2, 4, 6 and 8 µM) and SDBS (0, 2, 4, 6 and 8 µM) were prepared separately in Milli-Q water. The fluorescence spectrum for each sample was recorded by exciting at 350 nm at room temperature. The calibration curve for surfactants was then obtained from the plot of change in fluorescence intensity vs concentration of SDS/SDBS. The detection limit (LOD) value was determined using below equation.

$$LOD = 3 \times \sigma/k$$

where, k is slope of the curve and σ denotes the standard deviation of five repeated fluorescence measurements for PFBT-MI solution in the absence of surfactants. Similarly, various PFBT-MI/SDS (6.6 µM/18 µM) samples each containing spermine (0, 1.6, 3.3, 5.0 and 6.6 µM) were prepared and used to obtain the detection limit plot for spermine.

4.3 Result and discussion

4.3.1 Synthesis and characterization of polymer PFBT-MI

The synthetic method for newly synthesized cationic polymer PFBT-MI is shown in **Scheme 4.1.** The monomers M1, M2 and 4,7-dibromo-2,1,3-benzothiadiazole was taken in the ratio of 0.3:0.5:0.2 and copolymerized by Suzuki cross-coupling polymerization to yield neutral polymer PFBT (P1). N-methyl imidazole was then strapped onto the side chain of PFBT using post functionalization method to obtain pure cationic polymer PFBT-MI in high yields without any tedious purification methods. PFBT-MI was found to be soluble in polar solvents like water, dimethyl sulfoxide, methanol etc. All the products were well characterized by ^{1}H and ^{13}C NMR spectroscopy (**Figure A4.1-A4.6**). The molecular weight (M_w) of the precursor polymer PFBT was found to be 14103 g/mol with PDI-2.1 by GPC using THF as solvent and polystyrene as standard (**Figure A4.7**). The polymer PFBT-MI shows absorption maxima at 350 nm in aqueous solution that corresponds to the fluorine fragment of the polymer and a band ranging from 415-530 nm which is the characteristic of BT unit. PFBT-MI displays absorption at 350 nm and 435 nm with emission maxima at 415 nm (λ_{ex}=350 nm) and no peak in the region 500-650 nm

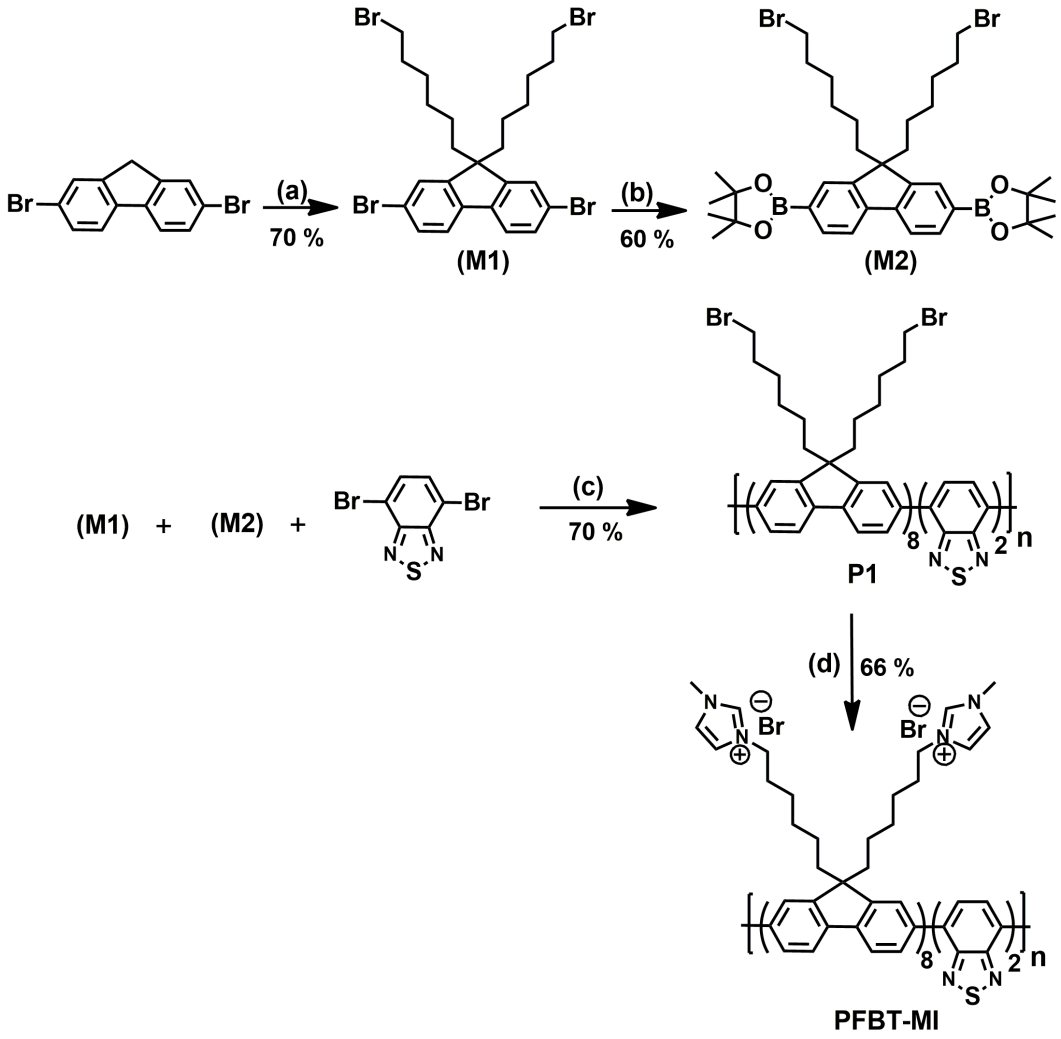

Scheme 4.1 Synthesis of poly[9,9-bis(6′-methyl imidazolium bromide)hexyl)fluorene-co-4,7-(2,1,3-benzothiadiazole)] (PFBT-MI) (a) 1,6-Dibromohexane, 50 % aq. NaOH, TBAI, 70 °C, 4h. (b) Bis(pinacolato)diborane, [Pd(dppf)Cl_2], KOAc, dioxane, 85 °C, 12h. (c) Tetrakistriphenylphosphine palladium(0), 2M K_2CO_3 (aq.), THF, reflux, 24h. (d) PFBT, 1-methyl imidazole, reflux, 24h.

(**Figure A4.8**), which indicates that polymer chains in dilute solution does not aggregate, thus preventing inter-molecular FRET to occur.

4.3.2 Effect of pH on the fluorescence of PFBT-MI

The effect of pH on the emission of PFBT-MI was monitored at 415 nm prior to sensing experiments by varying the pH of the solution from 1-14. The fluorescence intensity increases as the pH varies from 1-4 while the intensity decreases by further increasing the pH of the solution from 9-14.

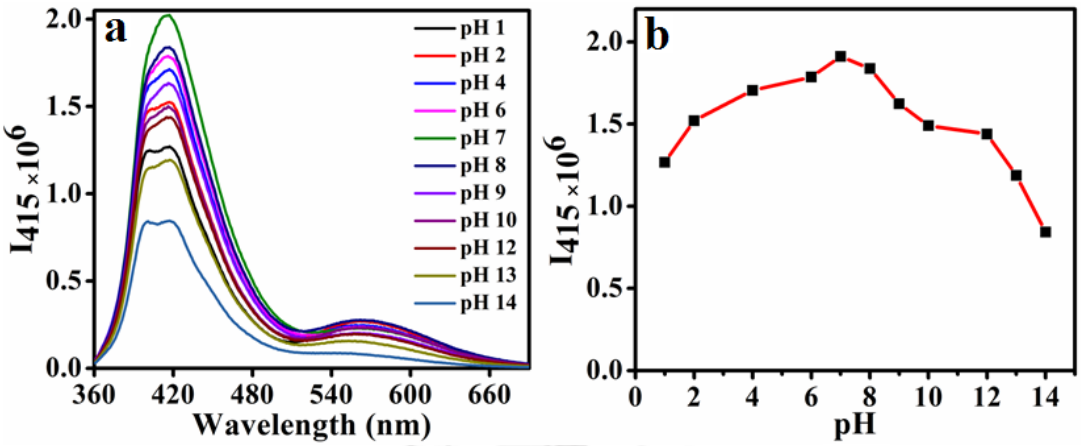

Figure 4.1 (a) Fluorescence emission spectra of PFBT-MI in presence of varying (pH 1-14) and (b) its corresponding plot showing the variation of emission intensity at 415 nm with pH.

However, the intensity remains unchanged in the pH range of 5-8. These results demonstrated that PFBT-MI exhibits excellent emission in the pH range 5-8 **(Figure 4.1**), confirming its ability to work efficiently under physiological conditions.

4.3.3 Sensing of SDS and SDBS

The molecular state of PFBT-MI in water was studied by dynamic light scattering that shows an observed distribution of ~1 nm (**Figure A4.9**) which can be assigned to the hydrodynamic diameter of a single polymer chain. This unimolecular state of polymer in water explains the presence of weak FRET efficiency from fluorene to the BT unit since inter-chain FRET is negligible. Therefore, no new peak was observed at higher wavelength in water for polymer only. Upon successive addition of SDS and SDBS to the aqueous solution of PFBT-MI, a new peak appeared at 545 nm while the emission peak at 415 nm disappeared completely with the formation of an isoemissive point at 500 nm. The intensity of the emission band at 545 nm reaches its maximum value and saturated on adding total of 18 μM SDS and 21 μM SDBS, respectively (**Figure 4.2a & 4.2b**). The detection limits calculated for SDS and SDBS were found to be 0.12 μM (34 ppb) and 0.13 μM (45 ppb) respectively which is much lower than the standard methylene blue method[51] (**Figure 4.2c & 4.2d**). Interestingly, the solution colour progressively changed from blue to yellowish green with increasing SDS/SDBS concentration that could be easily visualized by naked eye under UV-light (lamp excitation-365 nm), thus, allowing colorimetric detection of SDS/SDBS (**Figure 4.3**). This change in colour of PFBT-MI upon introducing SDS/SDBS reflects the occurance of an efficient energy transfer from

fluorene fragment (donor) to BT units (acceptor) of the polymer due to an increased aggregation of polymer chains facilitated by polymer-surfactant complexation. It is well-know that a prerequisite for the phenomenon of FRET to occur is the spectral overlap between the emission of donor and absorption of acceptor along with a suitable distance (< 10 nm) between them.[52] As shown in **Figure A4.8** there is a spectral overlap between the emission of fluorene moiety with the absorption of BT unit. To confirm the event of FRET, lifetime of the polymer in presence and absence of SDS were examined as shown in **Figure 4.4.** Upon exciting by 375 nm, the decay monitored for PFBT-MI at 415 nm shows a reduction in the average life time after adding SDS while as the lifetime increases when monitored at 545 nm which explains the transfer of energy from fluorine unit to BT moiety via polymer- surfactant complexation.

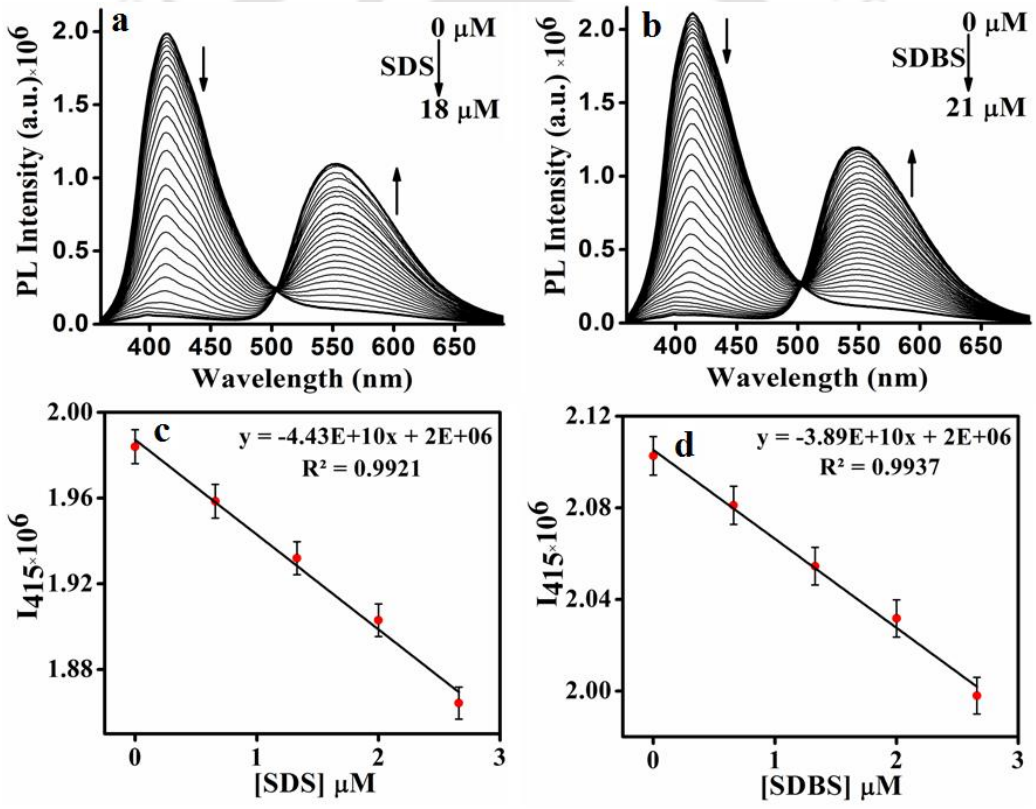

Figure 4.2 Fluorescence spectra of PFBT-MI (6.6 µM) with increasing concentration of (a) SDS (18 µM) and (b) SDBS (21 µM) in aqueous solution. Detection limit plot for (c) SDS and (d) SDBS at lower concentrations.

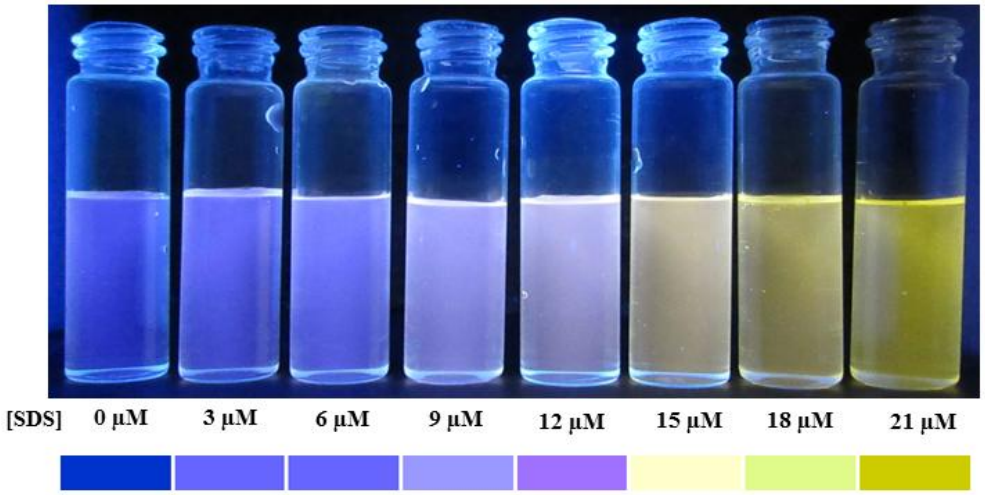

Figure 4.3 Change in the color of PFBT-MI (6.6 µM) solution under the excitation of UV light (365 nm) after adding variable concentration of SDS.

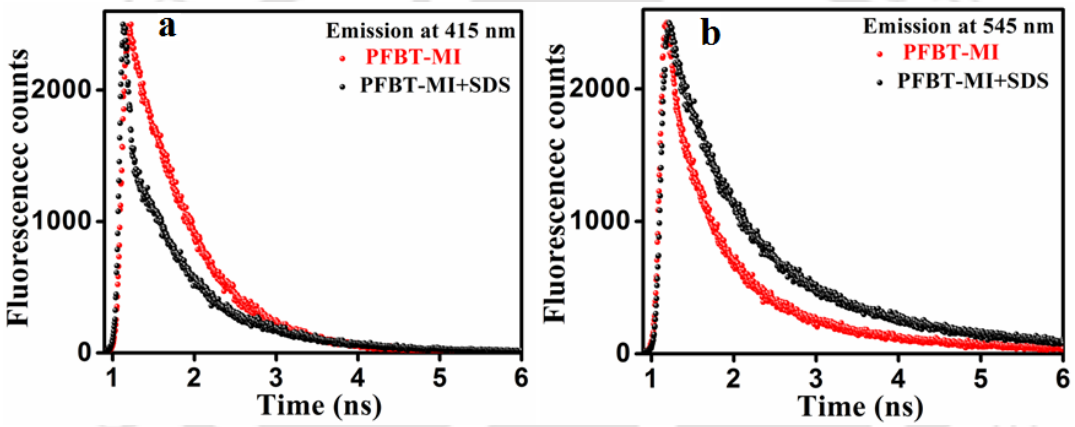

Figure 4.4 Decay curves of PFBT-MI in the presence and absence of SDS monitored at an emission wavelength of (a) 415 nm and (b) 545 nm.

To check the practicability of this probe in real environmental conditions, selectivity studies were performed using various common analytes usually found in natural water systems. Widespread surfactants (cetyltrimethylammonium bromide (CTAB), triton-X-100, stearate, laurate and palmate), anions (I^-, Cl^-, F^-, SO_4^-, SO_4^{2-}, PO_4^{3-}, PO_4^{2-}, PO_4^- , N_3^-, NO_3^-, BF_4^- , PF_4^-, p-toluenesulfinate, benzene sulfinate, pyrophosphate and citrate) and common metal ions (Co^{2+}, Cu^{2+}, Zn^{2+}, Fe^{3+}, Pb^{2+}, Cr^{3+}, Mn^{2+}, Cd^{2+}, Ln^{3+}, Eu^{3+} and Yb^{3+}) were checked and found ineffectual towards the emission of PFBT-MI (**Figure 4.5a & 4.5b**), since imidazolium units attached to the fluorophores typically acts[46,47,53] as specific recognition site for SDS and SDBS.

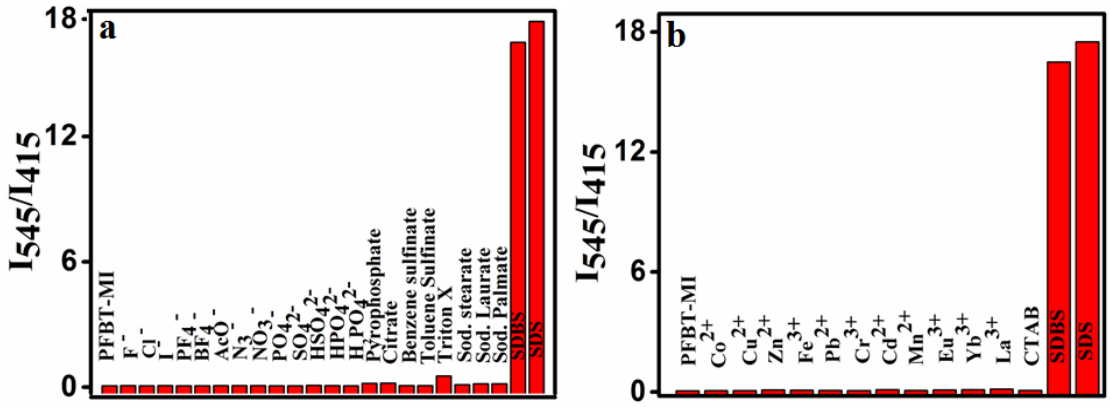

Figure 4.5 Bar diagram depicting effect of various (a) anions (20 μM) and (b) cations (20 μM) including various cationic, anionic and neutral surfactants (20 μM) on the emission of PFBT-MI (6.6 μM).

4.3.4 Detection of Spermine

Surfactants usually form non-covalent assemblies with amphiphilic polymers and solubilize them in aqueous solution with enhanced quantum yield. The photophysical properties of encapsulated fluorophores in such assemblies are tunable[54–56] and can be employed to detect chemical or biological species that has the capability of amending these assemblies.[57] Thus, fluorescent-surfactant assemblies have recently emerged as an excellent platform for detecting various chemical[58-60] and biological analytes.[61] Furthermore, this method reduces the dependence on molecular design *viz-a-viz* synthesis of new fluorophores and thus enables detection in aqueous media. Utilizing this intrinsic advantage, we prepared PFBT-MI/SDS nanoaggregates as an exceptional probe for the selective and sensitive detection of spermine in aqueous medium among various other amines like spermidine, putrescine, dodecylamine, hexylamine, L-Arginine, melamine, N,N-dimethyl ethylenediamine (DMEA), hexamethylene tetraamine (HMTA) and pyrophosphate (PPi). PFBT-MI-SDS nanoaggregates exhibits strong emission centered at 545 nm (λ_{ex}=350 nm) that was quenched on sequentially adding the aliquots of spermine (**Figure 4.6a**). This may be due to the formation of non-fluorescent complex between the positively charged analyte molecule (spermine) and the polymer-surfactant nanoaggregates. Greater the positive charge on polyamine, the stronger will be its electrostatic interaction which is in well agreement with quenching efficiency by other amines (**Figure 4.6b**) and forms the basis for the selective detection of spermine. Nearly 42% quenching was observed on adding 20 μM of spermine into the polymer-surfactant nanoaggregates that reaches to 86% at total 120 μM spermine.

To study the efficiency of quenching, Stern-Volmer (S-V) plot was obtained via I_0/I vs [Q] where, I_0 and I represents fluorescence intensity of PFBT- MI/SDS complex in the absence and presence of spermine and Q is the respective concentration of spermine. The S-V constant (K_{sv}) value thus obtained for spermine was 0.35 $\times 10^5$ M^{-1}, confirming high sensitivity of the polymer/surfactant assembly towards spermine (**Figure 4.6c**). The detection limit (0.33 µM/66 ppb) calculated for spermine (**Figure 4.6d & Figure A4.10**) was found to be far below the range 1-10 µM applicable for timely diagnosis of cancer in urinary samples.[62] Moreover, we have also monitored the effect of few other well-known cancer biomarkers[63,64] such as transferrin, prothrombin, leucine, isoleucine and valine on the emission of PFBT-MI/SDS

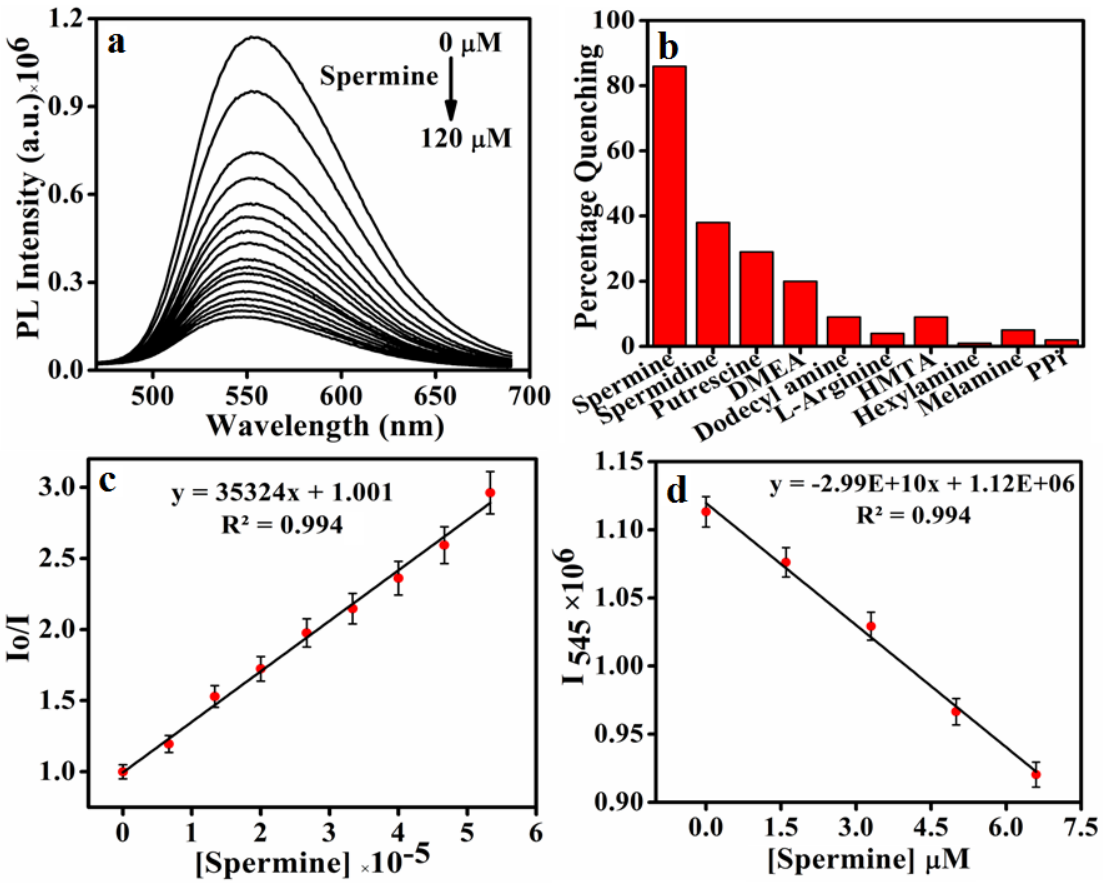

Figure 4.6 (a) Fluorescence spectral changes of PFBT-MI/SDS in aqueous solution with different concentrations of spermine. (b) Percentage fluorescence quenching (at λ_{em}=545 nm) with spermine (120 µM) and other amines (120 µM). (c) Stern-Volmer plot for spermine with PFBT-MI/SDS (6.6 µM/18 µM). (d) Detection limit plot for spermine.

complex. It was established (**Figure A4.11**) that these biomarkers have insignificant effect on the emission of PFBT-MI/SDS complex, indicating viability of this system for the detection of cancer biomarker spermine under realistic conditions.

4.3.5 Complexation studies

To understand the complexation process, the interaction between the polymer, surfactant and spermine was monitored via UV-Vis, FESEM, TEM and DLS studies. Upon successive addition of SDS and SDBS to the aqueous solution of PFBT-MI, the 350 nm absorbance peak decreases gradually with a bathochromic shift of 5 nm while the peak at 430 nm showed a significant red shift of ~20 nm (**Figure 4.7a & 4.7b**). These red shifts in the absorption spectra can be attributed to the complexation of PFBT-MI molecules on binding with surfactants via hydrophobic and/or hydrophilic interactions driven by Columbic attractions resulting in increased conjugation length of the PFBT-MI owing to aggregation-induced planarization of the polymer chains.[65,66] This was confirmed by FESEM and TEM studies which indicated the formation of spherical nanoaggregates having an average diameter of 230 nm in aqueous solution with the net negative charge on their surface. Hence, these polymer-surfactant nanoaggregates are presumed to have greater affinity for positively charged spermine at the interface. On introducing spermine to PFBT-MI/SDS solution, the absorption peak at 350 nm and 450 nm displayed a hypochromic shift and a hyperchromic shift was observed in the range 510-600 nm with an isosbestic point at 488 nm, demonstrating the favorable interaction between spermine and PFBT-MI/SDS nanoaggregates (**Figure 4.7c & 4.7d**). Since, the polymer chains are expected to remain intact at the core with surfactant molecules at the outer side, the chances for spermine molecules to interact with polymer are very less. To further confirm this presumption, a control study was performed by monitoring the change in the emission of polymer PFBT-MI after adding spermine. Interestingly, spermine did not cause any significant effect on the emission of PFBT-MI (**Figure A4.12**) probably due to the absence of any favorable electrostatic interaction. Thus, it can be concluded that spermine interacts with polymer-surfactant assembly at the surface and caused fluorescence quenching.

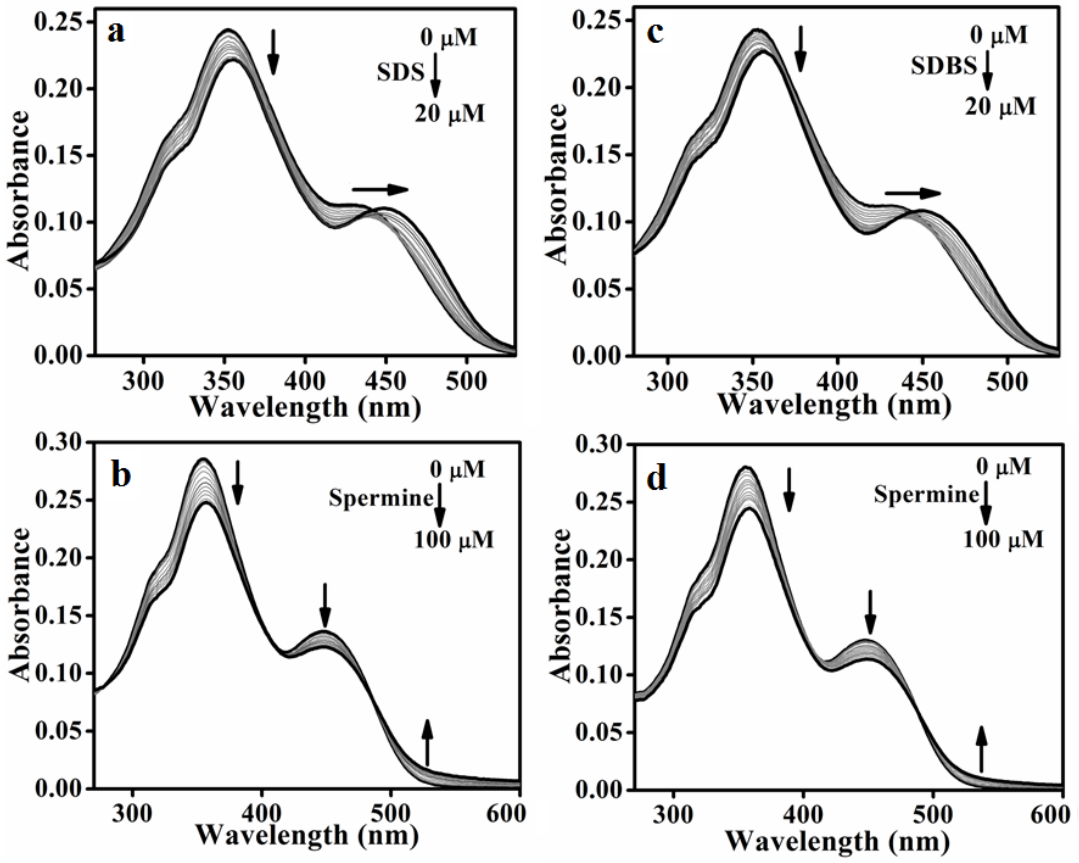

Figure 4.7 UV-vis titration spectra of PFBT-MI (6.6 μM) with increasing concentration of (a) SDS (20 μM) (b) SDBS (20 μM). Change in the absorption spectra of (c) PFBT-MI-SDS and (d) PFBT-MI-SDBS on introducing different concentrations of spermine (100 μM).

The morphological studies revealed that the average diameter of the spherical aggregate increases from 230 to 280 nm on introducing spermine while the net negative charge on surface decreases from -15.5 to -6.5. DLS experiments further confirms the formation of nanoaggregates with an average diameter of 250 and 300 nm for PFBT-SDS and PFBT-SDS-spermine respectively which is slightly greater than observed from TEM (Figure 3.8b & c) and FESEM (**Figure 4.9b & 4.9c**) whereas PFBT-MI alone exists as a single polymer chain in water with a hydrodynamic diameter of ~1 nm with no definite shape as shown in **Figure 4.8a & 4.9a)**. The above results indicate that the polymer-surfactant complex did not disassemble in presence of spermine and remains intact on the surface via electrostatic interaction. The overall sensing mechanism for the detection of SDS/SDBS and spermine is shown in **Figure 4.10.**

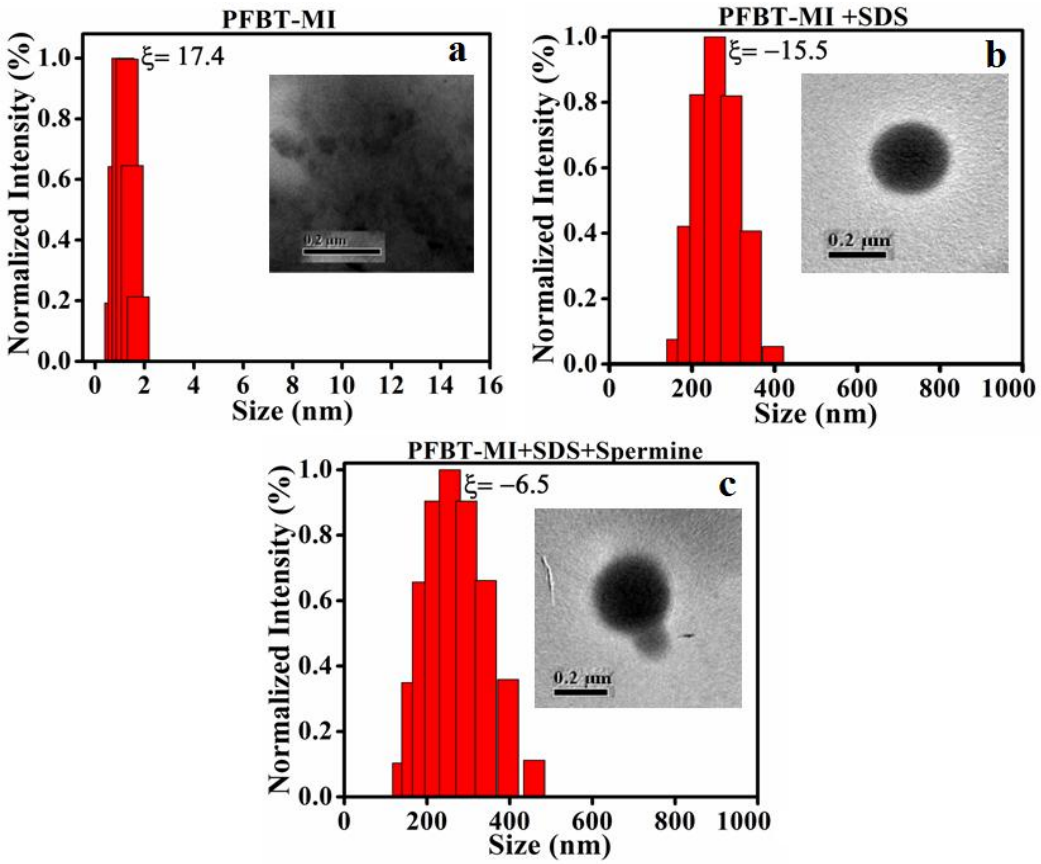

Figure 4.8 Dynamic light scattering measurements showing hydrodynamic diameter of (a) PFBT-MI, (b) PFBT-MI+SDS, (c) PFBT-MI+SDS+spermine as 2 nm, 250 nm, and 300 nm respectively. (Inset: TEM images showing an average diameter of 230 and 280 nm respectively for PFBT-MI+SDS and PFBT+SDS+Spermine).

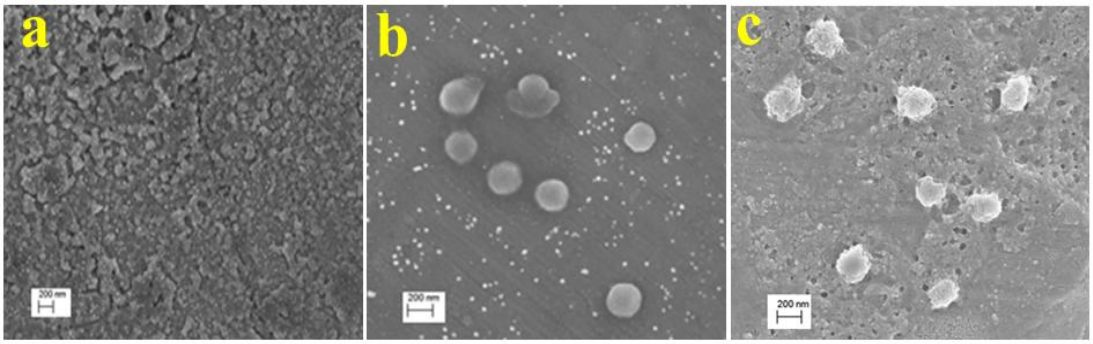

Figure 4.9 FESEM images of (a) PFBT-MI (b) PFBT-MI+SDS (c) PFBT-MI+SDS+Spermine.

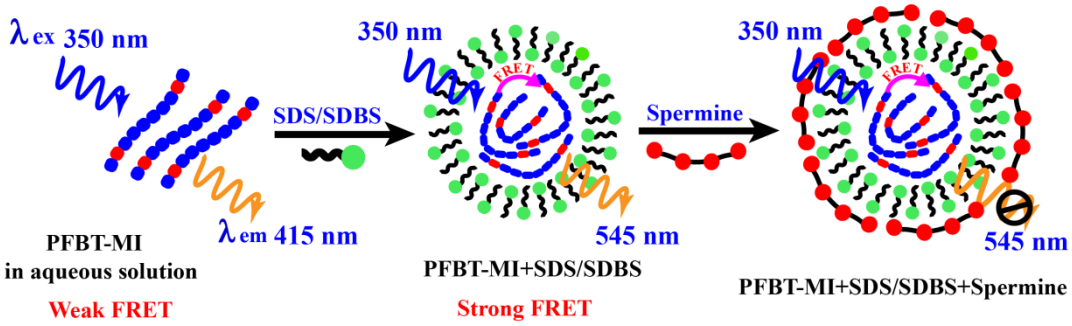

Figure 4.10 Schematic representation of the overall sensing mechanism of SDS/SDBS and spermine.

4.3.6 Detection of Spermine in urine specimens

To validate the non-invasive nature and practical utility of PFBT-MI system, sensing studies for the detection of spermine were also performed in urine samples, since spermine is considered as one of the important biomarker for cancer detection usually found and tested in urine. Three urine samples were collected from three different individuals and used as such without further treatment. No significant change in emission of PFBT-MI was observed after introducing undoped urine specimen, indicating the absence of spermine in the original sample (**Figure A4.13**). Each urine specimen was spiked independently with known concentrations of spermine and sensing experiment was performed in aqueous medium. The fluorescence spectra were then recorded after adding known volumes of these spiked samples to the solution of PFBT-MI/SDS (6.6 µM/18 µM) (**Figure 4.11a**) and the peaks were.

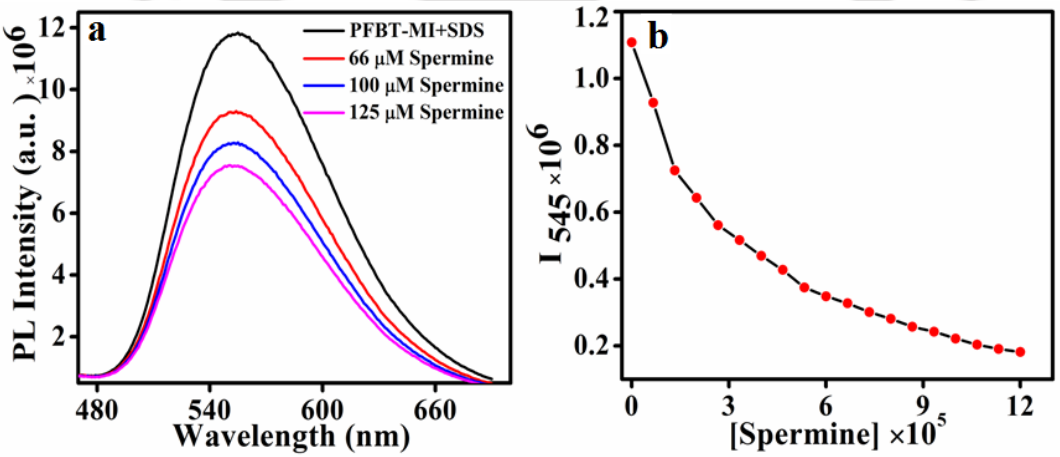

Figure 4.11 (a) Fluorescence quenching of PFBT-MI/SDS (6.6 µM/18 µM) assembly on addition of different urine samples spiked with known concentrations of spermine and (b) calibration plot for spermine.

Table 4.1 Determination of spermine in urine specimen.

Urine Samples	Spermine added (10^{-7}M)	Spermine found[a] (10^{-7}M)	Recovery (%)	RSD (%)
U1	66	71	107	4
U2	100	105	105	5
U3	125	133	106	7

compared with the standard calibration curve (**Figure 4.11b**) after taking three replicate measurements (**Table 4.1**). These results demonstrate that PFBT-MI based system can be employed as an exceptional probe to monitor traces of spermine in the urinary specimens that can be helpful in early diagnosis of cancer.

4.4 Conclusion

In conclusion, a newly developed cationic conjugated polyelectrolyte [9,9-bis(6'-methyl imidazolium bromide)hexyl)fluorene-co-4,7-(2,1,3-benzothiadiazole)] (PFBT-MI) displayed emission colour change from blue to yellowish green in the presence of most common anionic surfactants SDS and SDBS in 100% aqueous solution and enables naked-eye detection and quantification of these surfactants in real time. The detection of SDS/SDBS at parts per billion levels [SDS - (0.12 µM/34 ppb) and SDBS - (0.13 µM/45 ppb)] is attributed to the inter-molecular FRET due to the aggregation of polymer chains assisted by SDS/SDBS via strong electrostatic as well as hydrophobic interactions. Furthermore, PFBT-MI/SDS ensemble serves as a unique platform for the non-invasive, rapid and sensitive detection of spermine over other relevant amines, which is much lower than the range required for early cancer diagnosis and validates the reliability of the present system for real time practical applications.

References

(1) Russell, D. H.; Durie, B. G. M. Polyamines as Biochemical Markers of Normal and Malignant Growth, Raven Press: New York, **1978**.

(2) Seiler, N.; Delcros, J. G.; Moulinoux, J. P. *Int. J. Biochem Cell Biol*. **1996**, *28*, 843.

(3) Stefanelli, C.; Bonavita, F.; Stanic, I.; Mignami, M.; Facchinin, A.; Pignatti, C.; Flamigni, F.; Calderera, C. M. *FEBS Lett*. **1998**, *437*, 233.

(4) Cipolla, B. G.; Ziade, J.; Bansard, J. Y.; Moulinoux, J. P.; Staerman, F.; Quemener, V.; Lobel, B.; Guille, F. *Cancer* **1996**, *78*, 1055.

(5) Kawakita, M.; Hiramatsu, K. *J. Biochem*. **2006**, *139*, 315.

(6) Byun, J. A.; Choi, M. H.; Moon, M. H.; Kong, B.; Chung, B. C. *Cancer Lett*. **2009**, *273*, 300.

(7) Paik, M. J.; Kuon, D.; Cho, J.; Kim, K.-R. *Amino Acids* **2009**, *37*, 407.

(8) Satrijo, A.; Swager, T. M. *J. Am. Chem. Soc.* **2007**, *129*, 16020.

(9) Tanima, D.; Imamura, Y.; Kawabata, T.; Tsubaki, K. *Org. Biol. Chem.* **2009**, *7*, 4689.

(10) Zyryanov, G. V.; Palacios, M. A.; Anzenbacher, P. *Angew. Chem. Int. Ed*. **2007**, *46*, 7849.

(11) Palacios, M. A.; Nishiyabu, R.; Marquez, M.; Anzenbacher, P. *J. Am. Chem. Soc*. **2007**, 129, 7538.

(12) Chiu, T. C.; Lin, Y. W.; Huang, Y. F.; Chang, H. T. *Electrophoresis* **2006**, *27*, 4792.

(13) Ma, Y.; Liu, G.; Du, M.; Stayton, I. *Electrophoresis* **2004**, *25*, 1473.

(14) Teti, D.; Visalli, M.; McNair, H. *J. Chromatogr. B Analyt. Technol. Biomed. Life Sci*. **2002**, *781*, 107.

(15) Khuhawar, M. Y.; Qureshi, G. A. *J. Chromatogr., B: Biomed. Sci. Appl.* **2001**, *764*, 385.

(16) Rosen, M. J.; Li, F.; Morrall, S. W.; Versteeg, V. *J. Environ. Sci. Technol*. **2001**, *35*, 954.

(17) Patel, R.; Patel, K. S. *Analyst* **1998**, *123*, 1691.

(18) Chan, W. H.; Lee, A. W. M.; Lu, J. *Anal. Chim. Acta.* **1998**, *361*, 55.

(19) Sakai, T.; Harada, H.; Liu, X.; Ura, N.; Takeyoshi, K.; Sugimoto, K. *Talanta* **1998**, *45*, 543.

(20) Cserháti, T.; Forgács, E.; Oros, G. *Environ. Int*. **2002**, *28*, 337.

(21) Nielsen, A. D.; Borch, K.; Westh, P. *Biochim. Biophys. Acta, Protein Struct. Mol. Enzymol.* **2000**, *1479*, 321.

(22) Oshima, M.; Motomizu, S.; Doi, H. *Analyst* **1992**, *117*, 1643.

(23) Taguchi, S.; Takahashi, K.; Hata, N.; Kasahara, I. *Analyst* **2001**, *126*, 2078.

(24) Clesceri, L. S., Greenberg, A. E., Eaton, A. D. *Standard Methods for the Examination of Water and Wastewater*, 20th ed.; American Public Health Association: Washington, D.C., **1999**.

(25) Heinig, K.; Vogt, C. *Electrophoresis* **1999**, *20*, 3311.

(26) Villar, M.; Callejón, M.; Jiménez, J. C.; Alonso, E.; Guiráum, A. *Anal. Chim. Acta* **2007**, *599*, 92.

(27) Moldovan, Z.; Avram, V.; Marincas, O.; Petrov, P.; Ternes, T. *J. Chromatogr. A* **2011**, *1218*, 343.

(28) Evans, R. C.; Knaapila, M.; Willis-F, N.; Kraft, Mario.; Terry, A.; Burrows, H. D.; Scherf, U. *Langmuir* **2012**, *28*, 12348.

(29) Chen, X.; Kang, S.; Kim, M. J.; Kim, J.; Kim, Y. S.; Kim, H.; Chi, B.; Kim, S-J.; Lee, J. Y.; Yoon, J. *Angew. Chem. Int. Ed*. **2010**, *49*, 1422.

(30) Hussain, S.; Malik, A. H.; Iyer, P. K. *ACS Appl. Mater. Interfaces* **2015**, *7*, 3189.

(31) Gao, M.; Wang, L.; Chen, J.; Li, S.; Lu, G.; Wang, L.; Wang,Y.; Ren, L.; Qin, A.; Tang, B. Z. *Chem. Eur. J*. **2016**, *22*, 5107.

(32) Rochat, S.; Swager, T. M. *ACS Appl. Mater. Interfaces* **2013**, *5*, 4488.

(33) Jiang, H.; Taranekar, P.; Reynolds, J. R.; Schanze, K. S. *Angew. Chem., Int. Ed.* **2009**, *48*, 4300.

(34) Marques, A. T.; Pinto, S. M. A.; Monteiro, C. J. P.; Melo, J. S. S.; Burrows, H. D.; Scherf, U.; Calvete, M. J. F.; Pereira, M. M. *J. Polym. Sci., Part A: Polym. Chem.* **2012**, *50*, 1408.

(35) Malik, A.H.; Hussain, S.; Kalita, A.; Iyer, P. K. *ACS Appl. Mater. Interfaces* **2015**, *7*, 26968.

(36) Heeley, M. E. H.; Gallaher, J. K.; Nguyen, T. L.; Woo, H. Y.; Hodgkiss, J. M. *Chem. Commun.* **2013**, *49*, 4235.

(37) Henson, Z. B.; Zhang, Y.; Nguyen, T. Q.; Seo, J. H.; Bazan, G. C. *J. Am. Chem. Soc.* **2013**, *135*, 4163.

(38) Gaylord, B. S.; Heeger, A. J.; Bazan, G. C. *J. Am. Chem. Soc*. **2003**, *125*, 896.

(39) Liu, B.; Bazan, G. C. *Chem. Mater*. **2004**, *16*, 4467.

(40) Thomas, S. W.; Joly, G. D.; Swager, T. M. *Chem. Rev*. **2007**, *107*, 1339.

(41) Ho, H.-A.; Najari, A.; Leclerc, M. *Acc. Chem. Res*. **2008**, *41*, 168.

(42) McQuade, D. T.; Pullen, A. E.; Swager, T. M. *Chem. Rev*. **2000**, *100*, 2537.

(43) Zhu, C.; Liu, L.; Yang, Q.; Lv, F.; Wang, S. *Chem. Rev*. **2012**, *112*, 4687.

(44) Liang, J.; Li, K.; Liu, B. *Chem. Sci.* **2013**, *4*, 1377.

(45) Pu, K. Y.; Liu, B. *Biosens. Bioelectron*. **2009**, *24*, 1067.

(46) Schwartz, B. J. *Annu. Rev. Phys. Chem.* **2003**, *54*, 141.

(47) Hennebicq, E.; Pourtois, G.; Scholes, G. D.; Herz, L. M.; Russell, D. M.; Silva, C.; Setayesh, S.; Grimsdale, A. C.; Mullen, K.; Bredas, J. L.; Beljonne, D. *J. Am. Soc. Chem.* **2005**, *127*, 4744.

(48) Praveen, V. K.; George, S. J.; Varghese, R.; Vijayakumar, C.; Ajayaghosh, A. *J. Am. Soc. Chem.* **2006**, *128*, 7542.

(49) Liu, B.; Bazan, G. C. *J. Am. Chem. Soc*. **2004**, *126*, 1942.

(50) Pu, K. Y.; Liu, B. *Macromolecules* **2008**, *41*, 6636.

(51) Standard Methods for the Examination of Waters and Wastewaters, 19th ed.; American Public Health Association, Baltimore, Maryland, **1995**, *5540*.

(52) Förster, T. Intermolecular Energy Migration and Fluorescence. *Ann. Phys.* **1948**, *437*, 55.

(53) Coll, C.; Martínez-Máñez, R.; Marcos, M. D.; Sancenón, F.; Soto, J. *Angew. Chem. Int. Ed.* **2007**, *46*, 1675.

(54) Wang, J.; Qian, X.; Qian, J.; Xu, Y. *Chem. −Eur. J.* **2007**, *13*, 7543.

(55) Xu, Y.; Li, B.; Xiao, L.; Li, W.; Zhang, C.; Sun, S.; Pang, Y. *Chem. Commun*. **2013**, *49*, 7732.

(56) Singh, Y.; Gulyani, A.; Bhattacharya, S. *FEBS Lett*. **2003**, *541*, 132.

(57) Rusu, A. D.; Moleavin, I. A.; Hurduc, N.; Hamel, M.; Rocha, L. *Chem. Commun.* **2014**, *50*, 9965.

(58) Hu, R.; Feng, J.; Hu, D.; Wang, S.; Li, S.; Li, Y.; Yang, G. *Angew. Chem. Int. Ed.* **2010**, *49*, 4915.

(59) Ding, L.; Wang, S.; Liu, Y.; Cao, J.; Fang, Y. *J. Mater. Chem. A* **2013**, *1*, 8866.

(60) Ding, L.; Bai, Y.; Cao, Y.; Ren, G.; Blanchard, G. J.; Fang, Y. *Langmuir* **2014**, *30*, 7645.

(61) Cao, J.; Ding, L.; Hu, W.; Chen, X.; Chen, X.; Fang, Y. *Langmuir* **2014**, *30*, 15364.

(62) Russell, D. H *Nat. New Biol*. **1971**, *233*, 144.

(63) Mayers, J. R.; Wu, C.; Clish, C. B.; Kraft, P.; Torrence, M. E.; Fiske, B. P.; Yuan, C.; Bao, Y.; Townsend, M. K.; Tworoger, S. S.; Davidson, S. M.; Papagiannakopoulos, T.; Yang, A; Dayton, T. L.; Ogino, S.; Stampfer, M. J.; Giovannucci, E. L.; Qian, Z. R.; Rubinson, D. A.; Ma, J.; Sesso, H. D.; Gaziano, J. M.; Cochrane, B. B.; Liu, S.;

Wactawski-Wende, J.; Manson, J. E.; Pollak, M. N.; Kimmelman, A. C.; Souza, A.; Pierce, K.; Wang, T. J.; Gerszten, R. E.; Fuchs, C. S.; Heiden, M. G. V.; Wolpin, B. M. *Nature Medicine* **2014**, *20*, 1193.

(64) Chen, Y.-T.; Chena, H.-W.; Domanski, D., Smith, D. S.; Liang, K.-H.; Wua, C.-C.; Chen, C.-L.; Chung, T.; Chen, M.-C.; Chang, Y.-S.; Parker, C. E.; Borchersc, C. H.; Yu, J.-S. *J. Proteomics* **2012**, *75*, 3529.

(65) Miteva, T.; Palmer, L.; Kloppenburg, L.; Neher, D.; Bunz, U. H. F. *Macromolecules* **2000**, *33*, 652.

(66) Rughooputh, S. D. D. V.; Hotta, S.; Heeger, A. J.; Wudl, F. *J. Polym. Sci., Part B: Polym. Phys*. **1987**, *25*, 1071.

Appendix

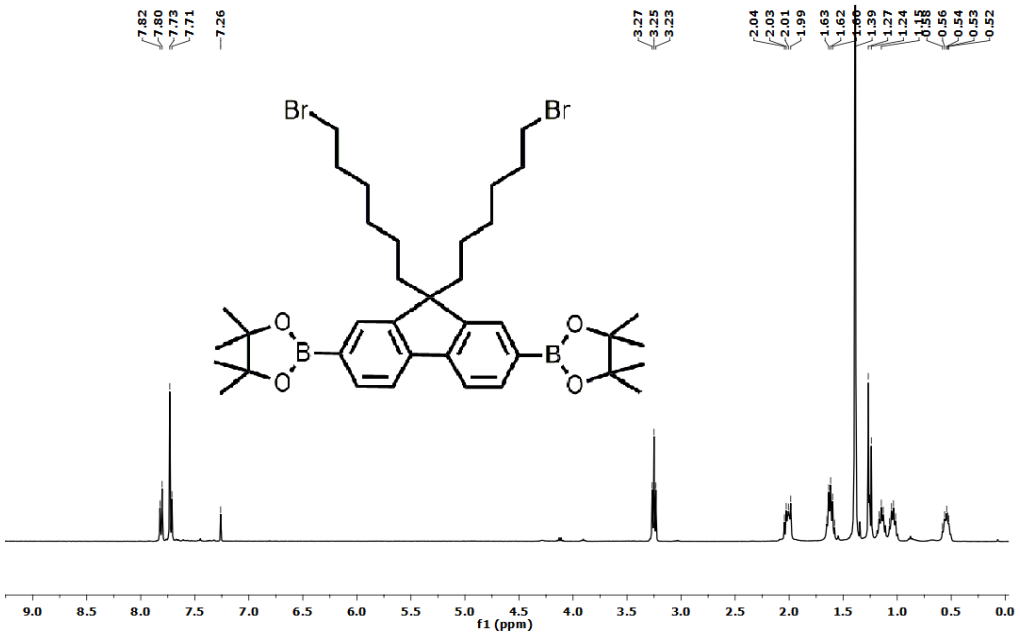

Figure A4.1 ^{1}H NMR spectra of M2.

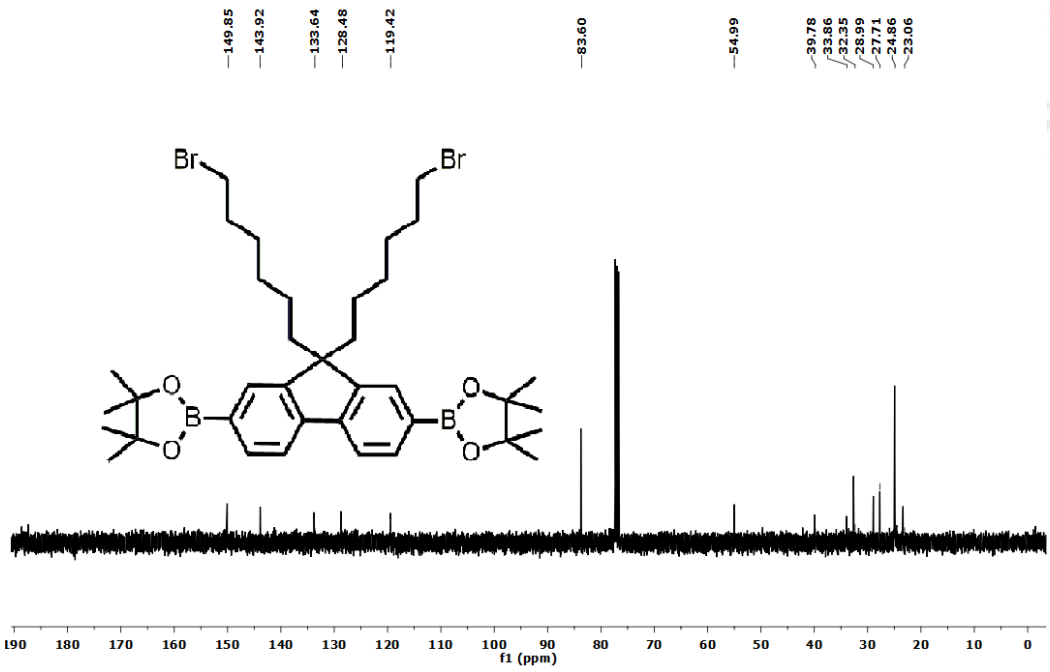

Figure A4.2 ^{13}C NMR spectra of M2.

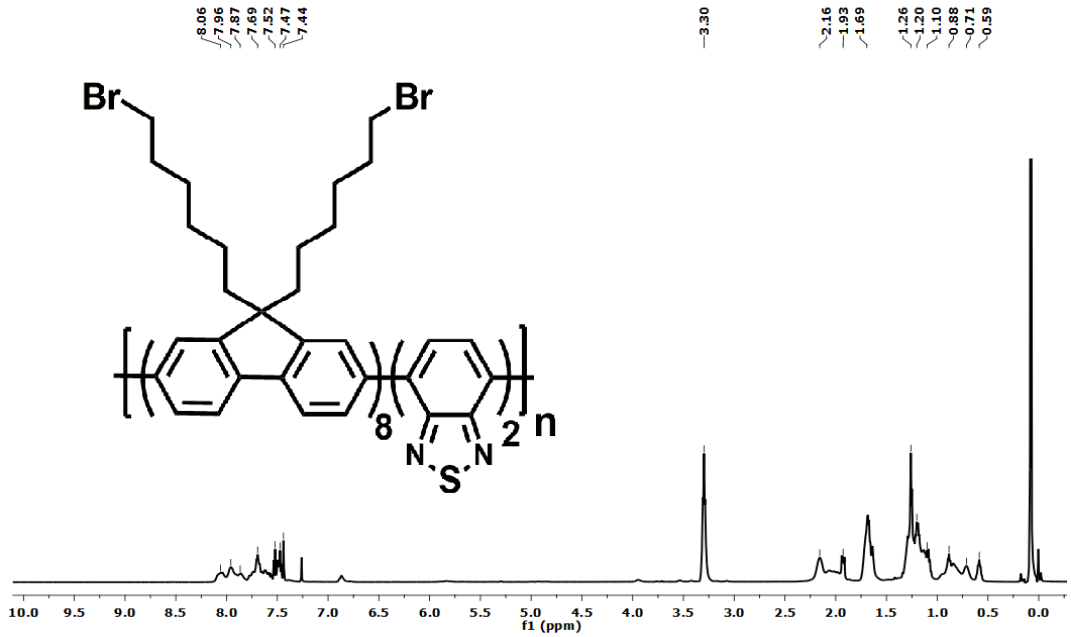

Figure A4.3 ^{1}H NMR (600 MHz, $CDCl_3$) spectrum of PFBT.

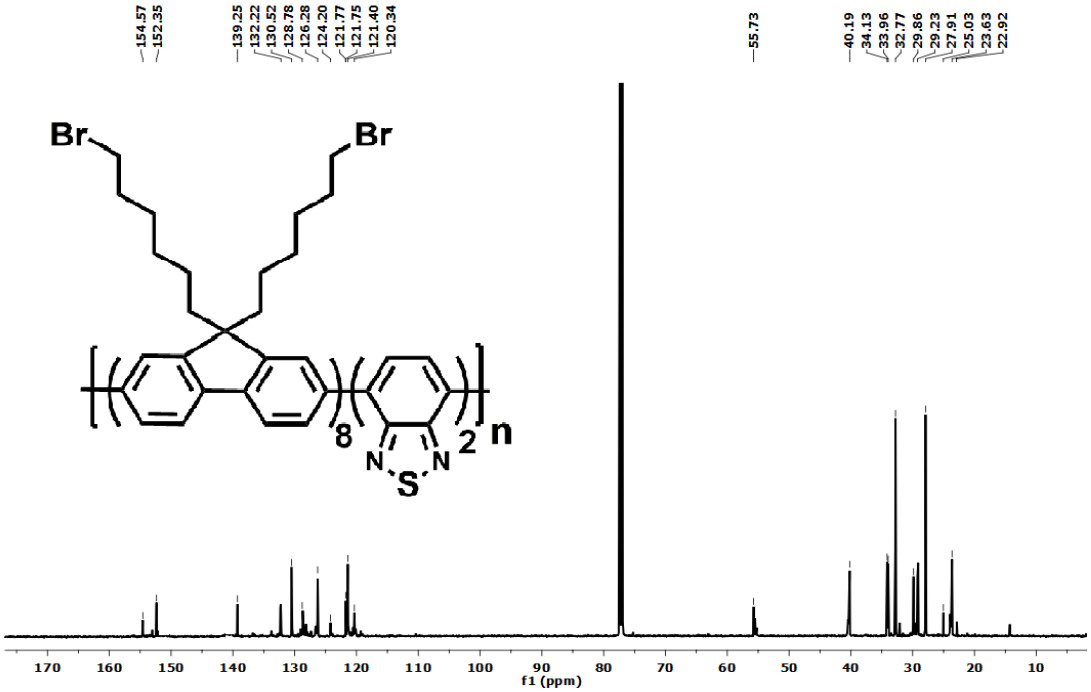

Figure A4.4 ^{13}C NMR (150 MHz, $CDCl_3$) spectrum of PFBT.

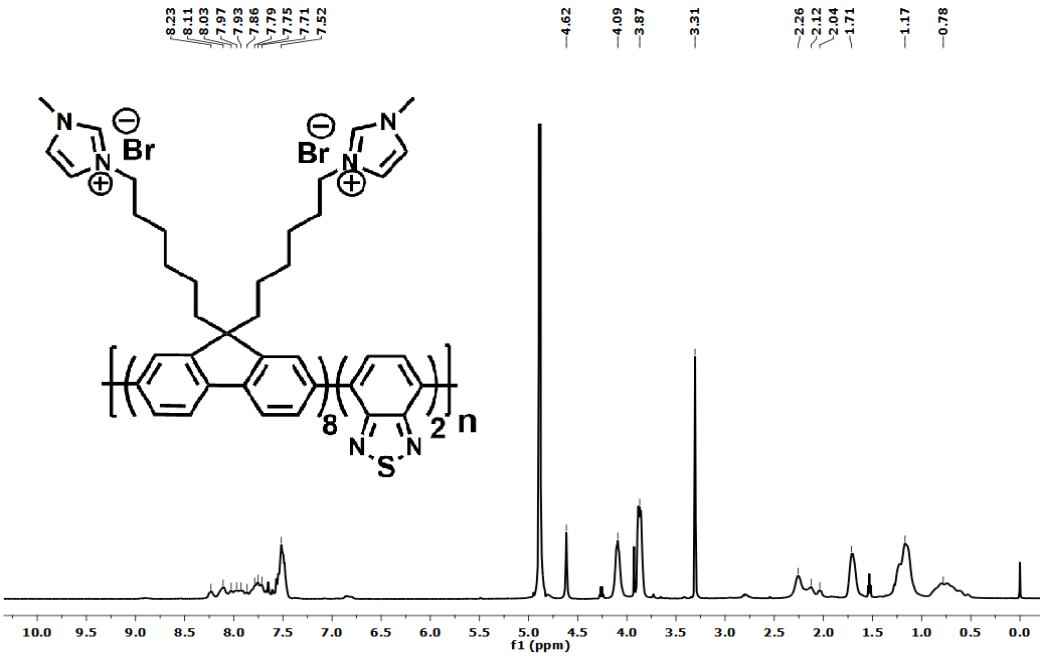

Figure A4.5 ^{1}H NMR (600 MHz, CD_3OD) spectrum of PFBT-MI.

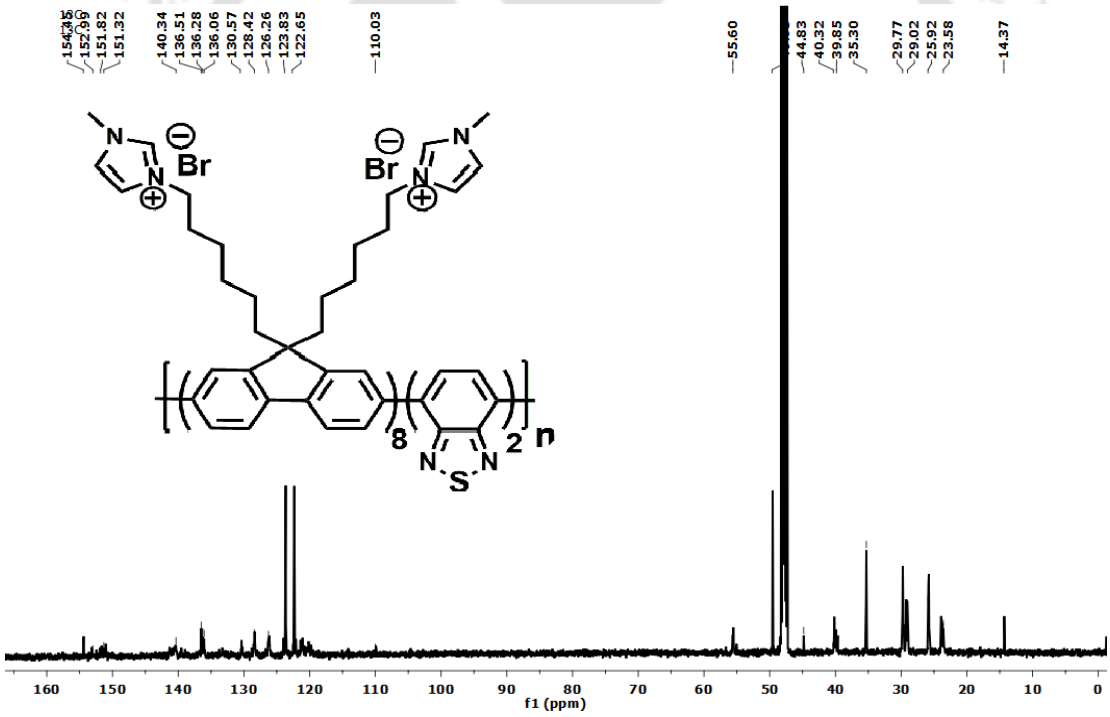

Figure A4.6 ^{13}C NMR (150 MHz, CD_3OD) spectrum of PFBT-MI.

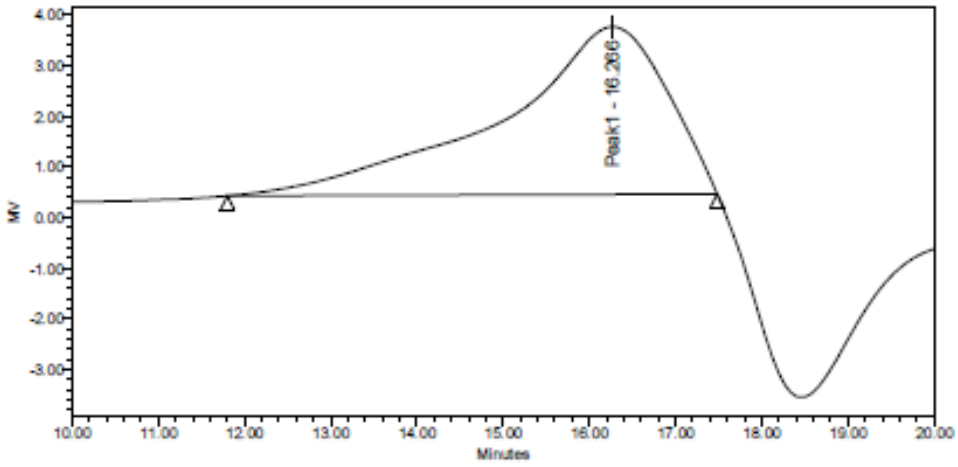

GPC Results

	SampleName	Mn	Mw	MP	Mz	Mz+1	Polydispersity
1	PPBT-C6_Br	6707	14103		29529	43058	2.102760

Figure A4.7 GPC chromatogram of PFBT.

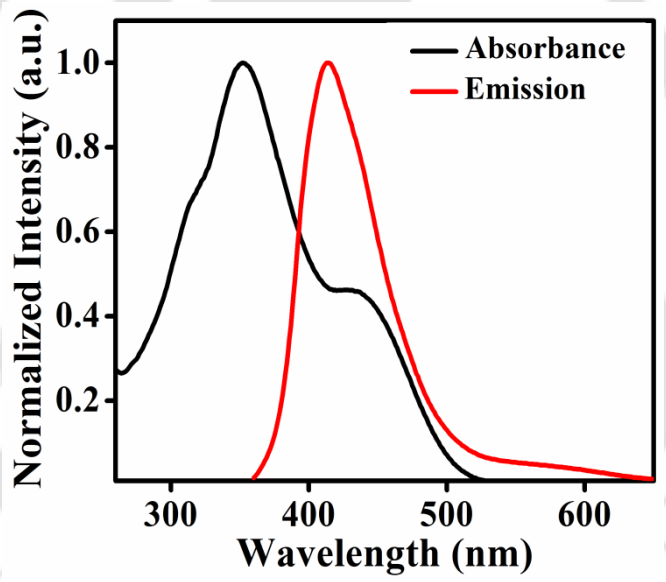

Figure A4.8 Spectral overlap between the emission of fluorene unit with the absorption of BT unit of PFBT-MI in water.

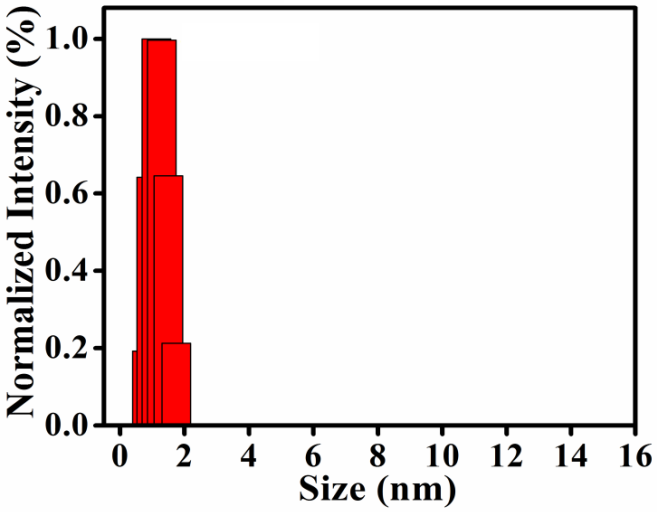

Figure A4.9 Dynamic light scattering showing the hydrodynamic distribution of PFBT-MI in water as ~1 nm confirming the existence of polymer as a single chain.

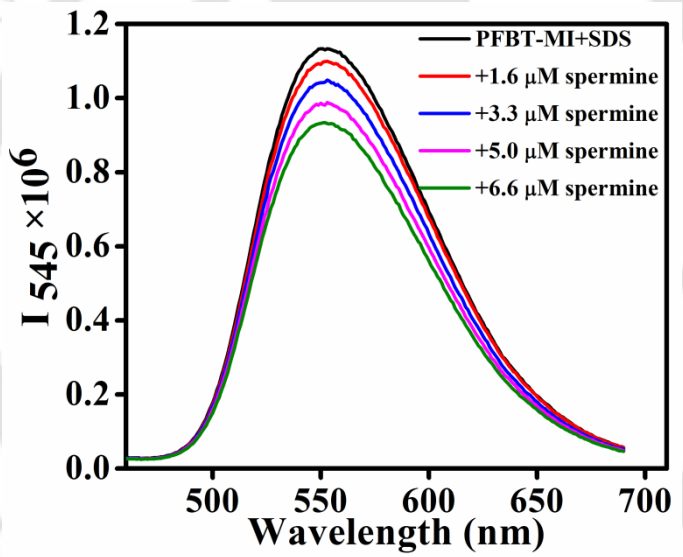

Figure A4.10 Changes in the emission spectra of PFBT-MI/SDS (6.6 μM/ 18 μM) with various concentrations of spermine (0, 1.6, 3.3, 5.0, 6.6 μM) in aqueous solution.

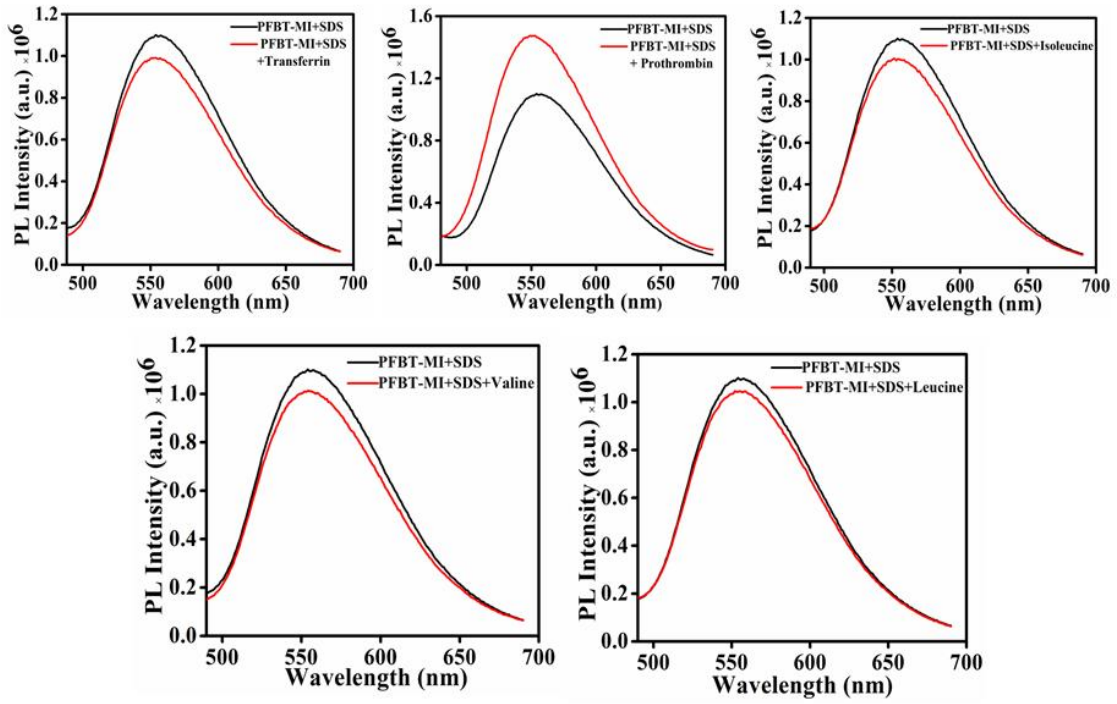

Figure A4.11 Effect of various cancer biomarkers (120 μM) on the emission of PFBT-MI/SDS complex.

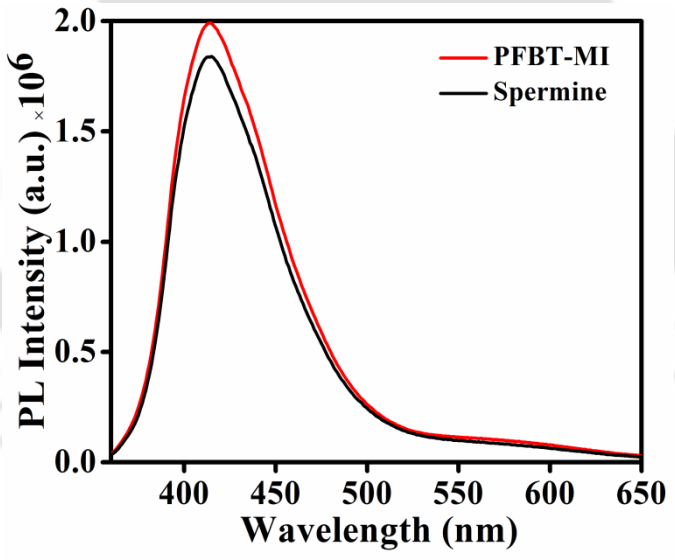

Figure A4.12 Control experiment showing the effect of spermine on the fluorescence emission of PFBT-MI.

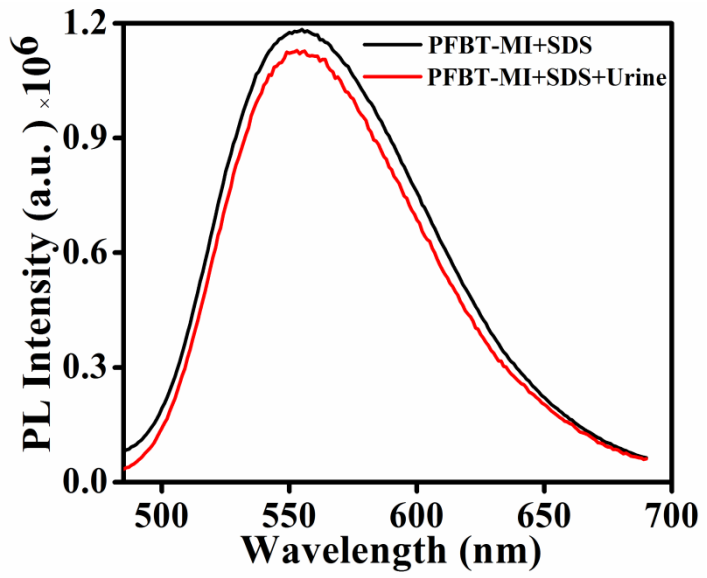

Figure A4.13 Control experiment showing the effect of undoped-urine specimen (10 μL) on the emission of PFBT-MI/SDS assembly (6.6 μM/18 μM).

Chapter 5

Development of Latent Fingerprints on Various Substrates using AIEE Active Conjugated Polyelectrolyte

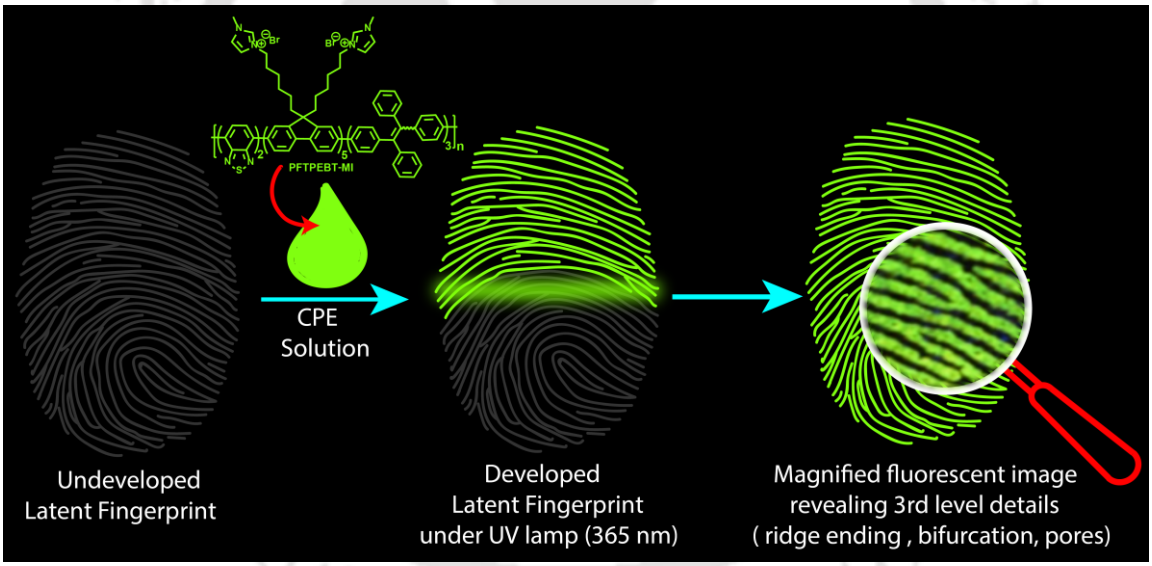

Malik, A. H.; Kalita, A.; Iyer, P. K. *ACS Appl. Mater. Interfaces* **2017**, *9*, 37501-37508.

Abstract

The development of highly efficient latent fingerprint (LFP) technology remains extremely vital for medical, forensic and criminal investigation. A highly convincing, straightforward, rapid and cost-effective method has been established for the quick development of latent fingerprint on multiple substrates including plastic, glass, aluminum foil, metallic surfaces, etc. without any additional treatment, based on AIEE active conjugated polyelectrolyte PFTPEBT-MI, revealing clearly the third-level details (ridges, bifurcations and pores) with high selectivity, high contrast and no background interference even by blood stains confirming the ability of the proposed technique for efficient LFPs detection. The LFP development process was accomplished simply by immersing fingerprint loaded substrate into the CPE solution for 1 minute followed by shaking off the residual polymer solution and then dried in air. The CPE were readily transferred to the LFPs because of the strong electrostatic and hydrophobic interaction between the CPE molecules and the fingerprint components revealing distinct fluorescent images.

5.1 Introduction

Latent fingerprints (LFPs) detected at the site of crime are considered as imperative physical circumstantial evidence in forensic investigation and criminal justice[1-4] because of the distinctiveness in the ridge pattern for each individual and thus, are unique and vital in cracking any criminal case and accurately identify the prime suspect and convict. Predominantly, LFPs if found are not easily visible to naked eye under ambient light, hence, additional tedious efforts are required for enhanced visualization and confirmation. Improvements in existing methods and techniques have been attempted for the identification of LFPs which include ninhydrin spraying,[5] powder dusting,[6] iodine/cyanoacrylate fuming,[7-9] and fluorescent dye staining.[10] Although these methods were extensively used under specific circumstances, all of them are fraught with numerous limitations, which primarily are very low sensitivity, low contrast, easy damaging of fingerprint details, require long processing time, post-treatments to develop, etc. yet are not considered as "beyond a reasonable doubt" proof to convict him or her guilt as guilty. Therefore, development of simple, rapid, highly sensitive, cost-effective and reliable technique with low background interference for LFPs on multiple surfaces is highly desirable and remains in foremost demand as *de facto* proof and a challenge in the field of forensic research.

Conjugated polyelectrolytes (CPEs) consisting of a hydrophobic π backbone possess unique optical properties, which along with hydrophilic ionic side groups, enhance their solubility in aqueous solution as well as makes it liable to exhibit strong electrostatic interactions with various charged species like proteins, amino acids, surfactants, etc. Thus, CPEs have emerged as key materials in the fields of biological sensors and bioimaging entities because of their excellent biocompatibility, low cytotoxicity, strong emission brightness and resistance to photo bleaching.[11-22] Countless efforts by researchers in the development of new fluorescent reagents and methods for developing LFP, more efficiently have appeared.[23-30] However, due to the lack of selectivity towards fingerprint components and involvement of other post-treatments reduces the developing efficiency and increases the cost of the technique proportionally. Considering the above beneficial properties, CPEs can also be applied in the detection of LFPs because LFPs contain sweat (comprising of charged biomolecules[31-33] and sebum (consisting of oily mixture of wax esters, triglycerides, and cholesterol esters[34,35]) components as a mixture

so as to have both hydrophilic and lipophilic interactions possible with appropriately chosen CPE.

Herein, we explored a new strategy using aggregation induced enhanced emission (AIEE) based CPE (PFTPEBT-MI) for comprehensible and "beyond a reasonable doubt" visualization of LFPs on various surfaces without any post-treatment[36,37] or fingerprint transfer process[23,38] for the development on different substrates such as glass, aluminum foil, steel sheet, coins, adhesive tape (both transparent and colored) and OHPC sheets by immersing the fingerprint laden substrate into aqueous solution of polymer for ~1 minute, withdrawing it, shaking the residual solution off and subsequently drying it in air.

The present method is simple and has numerous advantages over previously reported techniques. Firstly, the AIEE based CPE emits strongly on the solid substrate by avoiding the phenomenon of ACQ thus diminishing the background interference for LFPs detection. Secondly, no post-treatment or fingerprint transfer process is required for developing LFPs because of the presence of AIEE active moiety in the polymer backbone. Thirdly, the visualization of LFPs on the substrate preferentially depends upon the adhesion of the CPE to the ridges of fingerprints. Since this (PFTPEBT-MI) polymer is amphiphilic in nature, it can interact strongly with LFPs via both electrostatic and lyophilic interactions resulting in the enhanced contrast of fingerprints on various substrates.

5.2 Experimental

5.2.1 Materials and measurements

All the chemicals were purchased from Aldrich, Merck (India) and were used as received. UV-Visible and Fluorescence spectra were recorded on a Perkin Elmer Lambda-25 and Horiba Fluoromax-4 spectrofluorometer, respectively using 10 mm path length quartz cuvettes with a slit width of 3 nm at room temperature. Milli-Q water was used in all experiments. The ^{1}H NMR (600 MHz) spectra were obtained on Bruker Ascend 600 spectrometer. Zetasizer Nano ZS90, Model No. ZEN3690, Malvern was used to calculate the zeta potential of the polymer. FESEM images were recorded on a Sigma Carl ZEISS scanning electron microscope. Different substrates used for depositing fingerprints, such as glass slides, adhesive tapes (colored and transparent), aluminum foil, steel plate, OHPC sheet, and metal coins were purchased from local market. The digital photographs of

developed fingerprints were taken by Nikon D5200 camera under a hand held ultraviolet lamp (365 nm) purchased from Sigma.

5.2.2 Synthetic procedure

5.2.2a Synthesis of M1 & M2

Synthesis of monomer M1 & M2 was carried out using a previously established procedure shown in chapter 3.

5.2.2b Synthesis of M3

M3 was prepared by a reported procedure.[39] In short, 4-Bromobenzophenone (1 g, 3.8 mmol) and zinc powder (0.74 g, 11.0 mmol) were added into a 100 mL two-necked round bottom flask. The flask was degassed and flushed with argon 2-3 times, after which anhydrous THF (40 mL) was injected. The mixture was cooled to −5 °C and titanium tetrachloride (0.60 mL, 5.7 mmol) was added gradually. The mixture was heated up to 25 °C and kept for half an hour and then refluxed at 80 °C overnight. The reaction mixture was quenched with 10% K_2CO_3 (aq.) and extracted with DCM. The organic layer was washed with water and dried over anhydrous sodium sulfate. The solvent was evaporated under reduced pressure and the residue was purified by silica gel column chromatography to get a white solid compound (1.31 g, 70%).

^{1}H NMR (600 MHz, $CDCl_3$, δ ppm): 7.29-7.23 (m, 4H; Ar H), 7.17-7.12 (m, 6H; Ar H), 7.03-7.00 (m, 4H; Ar H), 6.92-6.89 (m, 4H; Ar H).

5.2.2c Synthesis of PFTPEBT

PFTPEBT was synthesized via Suzuki coupling polymerization as reported.[40] M2 (0.100 g, 0.13 mmol), M3 (0.038 g, 0.08 mmol), 4,7-dibromo-2,1,3-benzothiadiazole (0.015 g, 0.05 mmol), [$Pd(PPh_3)_4$] (0.007 g) and potassium carbonate (0.215 g, 1.5 mmol) were kept in a 50 mL two neck round-bottom flask. A mixture of water and THF (1:3) was added to the flask using syringe and degassed thrice by flashing argon and freeze thaw cycle to remove any oxygen. The reaction mixture was then refluxed and stirred vigorously at 80 °C for 24h followed by repeated precipitation into excess of methanol 3-4 times. The precipitate was then filtered, washed with water/chloroform and dried under vacuum overnight to get the dark yellowish coloured polymer (0.114 g, 75%).

^{1}H NMR (600 MHz, $CDCl_3$, δ ppm): 8.06 (b), 7.97-7.89 (b), 7.81 (b), 7.68 (b), 7.54-7.47 (b), 7.16-7.12 (b), 7.03 (b), 6.98 (b), 6.89 (b), 6.82 (b), 3.27 (b), 2.17-2.05 (b), 1.67 (b), 0.88 (b), 0.81 (b), 0.66 (b)

5.2.2d Synthesis of PFTPEBT-MI

Brominated polymer PFTPEBT (0.05 g, 0.051 mmol) was taken into 25 mL RB. To it 2 mL of 1-methyl imidazole was added and heated under stirring condition at 80 ºC for 24h. The whole reaction mixture was then poured into excess of chloroform kept in a separate 50 mL beaker and stirred for 2-3h to get precipitate. The light brownish precipitate was then washed several times with chloroform to remove trace quantities of methyl imidazole so as to obtain pure functionalized polymer PFTPEBT-MI (0.044 g, 75%).

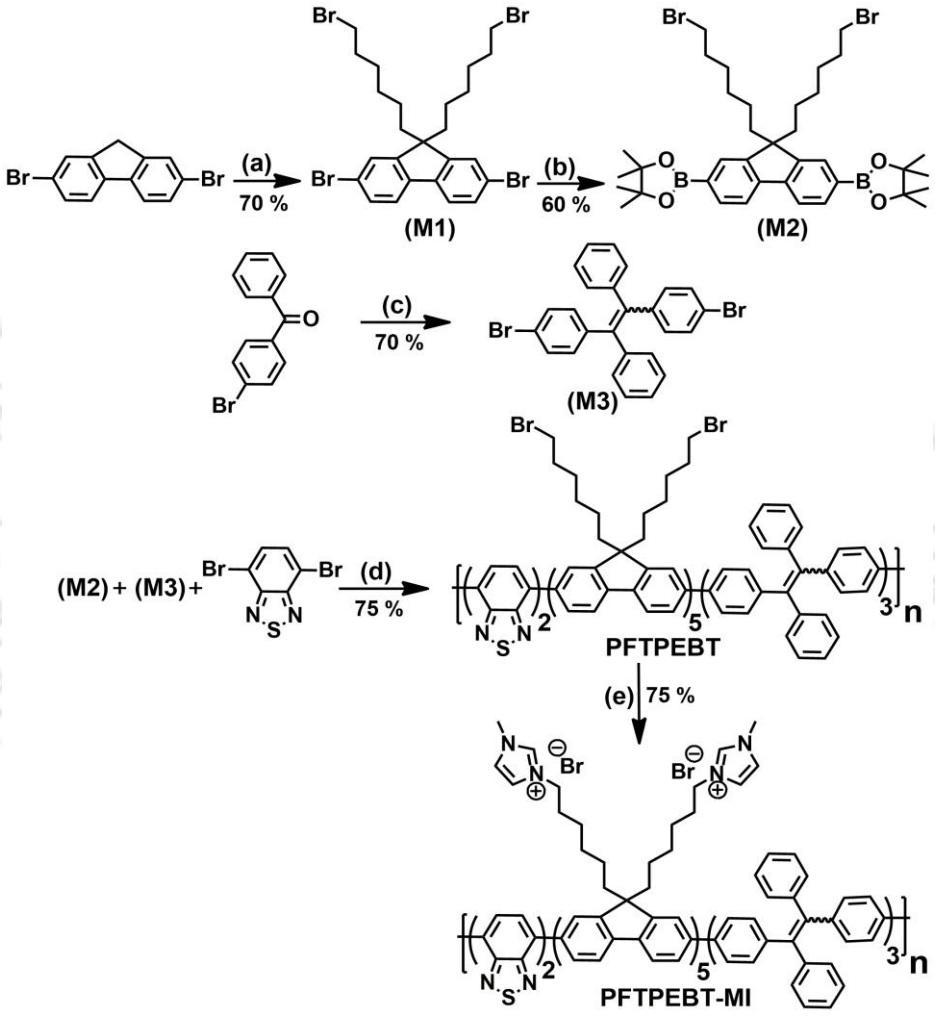

Scheme 5.1 Synthesis of PFTPEBT-MI (a) 1, 6-Dibromohexane, 50% aq. NaOH, TBAI, 70 ºC, 4h. (b) bis(pinacolato)diborane, [Pd(dppf)Cl_2], KOAc, dioxane, 85 °C, 12h. (c) $TiCl_4$, Zn powder, THF, reflux, 12h (d) Tetrakis(triphenylphosphine) palladium(0), 2M K_2CO_3 (aq.), THF, reflux, 24h. (e) PFTPEBT, 1-methyl imidazole, reflux, 24h.

^{1}H NMR (600 MHz, CD_3OD, δ ppm): 8.84 (b), 8.23 (b), 8.07-8.01 (b), 7.91 (b), 7.85-7.81 (b), 7.75 (b), 7.70 (b), 7.46 (b), 7.12 (b), 4.04 (b), 3.83 (b), 2.15-2.09 (b), 1.65 (b), 1.16-1.09 (b), 0.83-0.59 (b).

5.2.3 Preparation of stock solutions

Stock solution of PFTPEBT-MI was prepared in Milli-Q water at concentrations of 10 mM. The absorption and fluorescence measurements of the PFTPEBT-MI were carried out in a 3 mL quartz cuvette (1 cm × 1 cm) containing 33 μM of PFTPEBT-MI.

5.2.4 LFPs collection and development

Prior to fingerprint deposition on various substrates, the donors were asked to wash hands thoroughly with the soap and rinse with water and ethanol then blown dry. Fingerprints were obtained by gently rubbing the fingertips across nose and forehead and then pressing onto different surfaces with minimum pressure. The fingerprint laden substrates were brought in contact with the developing solution (0.2 mM) by directly immersing it into the petri dish for 1 minute and then the substrate was taken out and dried in air to splash off the excess solution and then air dried. For practical applications polymer solution was added into a spray bottle, together with 20−30% (v/v) of methanol to hasten water evaporation, and then sprayed onto the substrate. Photographs of the developed fingerprints were taken under UV lamp (365 nm) using digital camera.

5.2.5 Abrasion tests

Physical abrasion test was performed by mounting double sided adhesive tape on to the substrate containing developed fingerprints and then peeling off the tape from the surface while chemical abrasions were done by treating the developed fingerprint substrates with various solvents like chloroform, acetone, THF, and toluene after that digital images were taken under UV lamp (365 nm) before and after abrasion.

5.3 Result and discussion

5.3.1 Synthesis and characterization of polymer PFTPEBT-MI

With an aim to develop highly efficient latent fingerprint technology that would advance the existing method used in forensic investigation a polymer probe with high brightness and large stokes shift that can offer superior contrast for the visualization of LFPs was essential. The synthetic procedure for the newly synthesized cationic polymer PFTPEBT-MI is shown in **Scheme 5.1**. Monomers M2, M3 and 4,7-dibromo-2, 1, 3-benzothiadiazole were taken in the ratio of 0.5:0.3:0.2 and polymerized by Suzuki cross-

coupling polymerization reaction to yield PFTPEBT. N-methyl imidazole was then introduced onto the side chain of PFTPEBT via post functionalization method to obtain cationic polymer PFTPEBT-MI in good yields without any hectic purification methods. PFTPEBT-MI (**Figure 5.1a**) was found to be soluble in polar solvents like water, dimethyl sulfoxide, methanol etc. All the products were characterized by ^{1}H NMR spectroscopy (**Figure A5.1-A5.3**). The zeta potential of PFTPEBT-MI was calculated to be 33 mV±1.52 at 25 ºC in water (**Figure A5.4**). The polymer PFTPEBT-MI shows absorption maxima at 350 nm and 460 nm in aqueous solution and as well as in solid state (as film). The polymer PFTPEBT-MI shows absorption maxima at 350 nm and 460 nm in aqueous solution as well as in solid state (as film). PFTPEBT-MI displays emission maxima at 555 nm and 565 nm (λ_{ex}=450 nm) in liquid (aqueous solution) and solid state (as film) respectively with Stokes shift of ~100 nm (**Figure 5.1b**). PFTPEBT-MI appeared dark yellowish colour in concentrated aqueous solution as well as in thin film state under the illumination of UV light (365 nm) (**Inset: Figure 5.1b**). To explore the AIEE character of the polymer, emission studies of PFTPEBT-MI were recorded in water-THF mixture as shown in **Figure 5.2a & 5.2b**. It is clear that the fluorescence intensity of this polymer is less in pure water (good solvent), the intensity suddenly increases when THF (poor solvent) fraction (f_{THF}) was 30% and the fluorescence intensity remains constant on further increasing the f_{THF} up to 90%, which is further confirmed by the appearance of bright fluorescence under the irradiation of 365 nm UV lamp as shown in the inset of **Figure 5.2c**. The enhancement in the fluorescence intensity with increase in f_{THF} is due to the formation of polymer aggregates (**Figure A5.5**) that endows the intense emission.

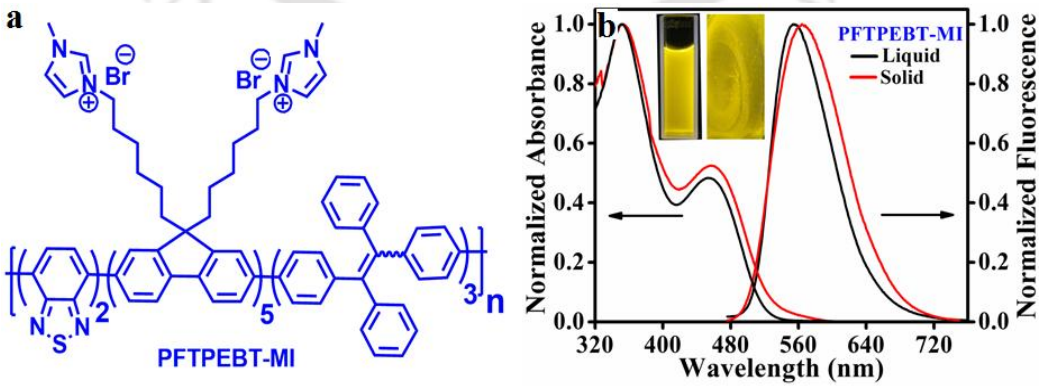

Figure 5.1 (a) Structure of polymer PFTPEBT-MI. (b) Absorption and emission spectra of PFTPEBT-MI in water. Inset: Colour of polymer in solid and liquid state under the irradiation of UV lamp (365 nm).

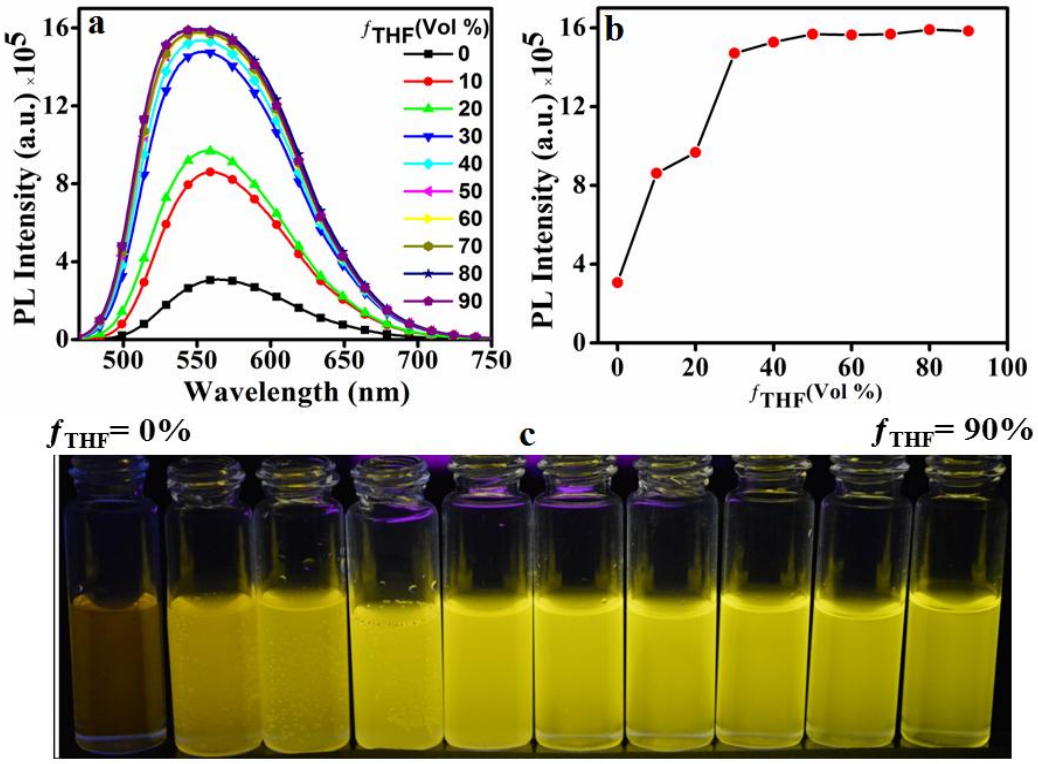

Figure 5.2 (a) Fluorescence spectra of the PFTPEBT-MI (33 μM) in water and water-THF mixture with varying fractions of THF. (b) Plot of fluorescence intensity against fraction of THF. (c) Digital photograph of PFTPEBT-MI in water/THF mixtures with different THF fractions from 0% to 90% (in vol%) at 365 nm UV irradiation.

5.3.2 Development of LFPs and digital magnification

LFPs were prepared from sebum and sweat components together by rubbing the finger with nose and forehead and depositing the fingerprints initially on four different substrates such as aluminium foil, glass slide, adhesive tape and coins as mentioned in the experimental section. Fluorescence image of the developed fingerprints displayed yellowish green colour under UV radiation (365 nm) with apparently high contrast between the fluorescent ridges and non-fluorescent furrow without any post-treatment method which could be clearly distinguished on various substrates having different background colours by naked eye as shown in **Figure 5.3**. The appearance of bright and quality fluorescence images of LFPs is due to the preferential increase in the local concentration of PFTPEBT-MI on the fingerprint ridges rather than on the furrows as observed in fluorescence microscope and FESEM images (**Figure 5.4**) by the process of adhesion, which may be attributed to both hydrophobic and electrostatic interactions between PFTPEBT-MI and the chemical components of the fingerprints.[41] The hydrophobic interactions arise from the interactions between the fatty components (wax

esters, fatty acids, squalene, and cholesterol) of the LFPs and the conjugated backbone of PFTPEBT-MI which contains AIEE active moiety, whereas the electrostatic interactions ascend from the sweat components (amino acids, proteins, glucose, etc.) and the functional groups of PFTPEBT-MI. Using this method, fingerprints with high resolution were obtained with distinct level 1-3 details which is a prerequisite for the identification of individuals. Usually fingerprints are characterized at three levels of details.[42] Level 1 detail is not unique enough for recognition and it includes cores and deltas. Level 2 includes ridge ending and bifurcation, which are the most characteristic features. Level 3 provides quantitative data for exact fingerprint recognition and it includes ridge path deviations, sweat pores and edge contours. The level 3 details of the fingerprint, features as a representative example of one developed in **Figure 5.5a** (left) and the regional magnified images are shown in **Figure 5.5b** (right) which include core (level 1), ridge ending, bifurcation and island (level 2) as well as pore (level 3), thus providing prima facie evidence to prove the case during trial without contradiction and validating the practicability of the present system for the LFP recognition. To further investigate whether the external abrasions will affect the developing fingerprints or not, physical abrasion test (**Figure A5.6)** was performed as mentioned in the experimental section to the developed fingerprints on various substrates such as aluminium foil, glass slide, adhesive tape (transparent), steel plate, OHPC sheet, coins, and adhesive tape (blue color) and digital images were captured before and after abrasion under 365 nm UV lamp as shown in **Figure 5.6**. Though in some cases the fluorescent images of the fingerprints captured were scratched to some extent but still all the fingerprint patterns are very clear even after applying external abrasion.

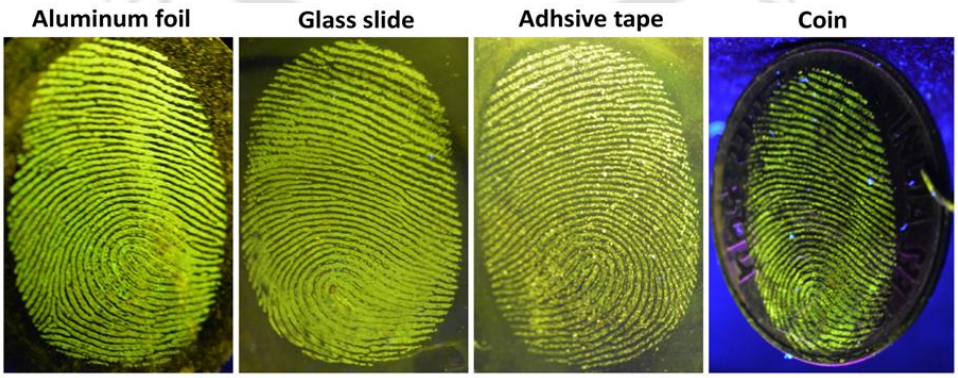

Figure 5.3 Fluorescence images of LFPs developed with PFTPEBT-MI on different substrates such as aluminum foil, glass slide, adhesive tape and coin.

Similarly, chemical abrasion test was performed by treating the developed LFP substrate such as glass slide with various chemicals such as THF, chloroform, acetone and toluene as shown in **Figure 5.7**, no such interference was observed. Furthermore, we also developed blood laden fingerprints as shown in **Figure 5.8**. It is clear that even the blood stained fingerprints can be developed easily without any interference. Therefore, our strategy is effective in developing LFP on various substrates with negligible effect even in the presence of external interferences

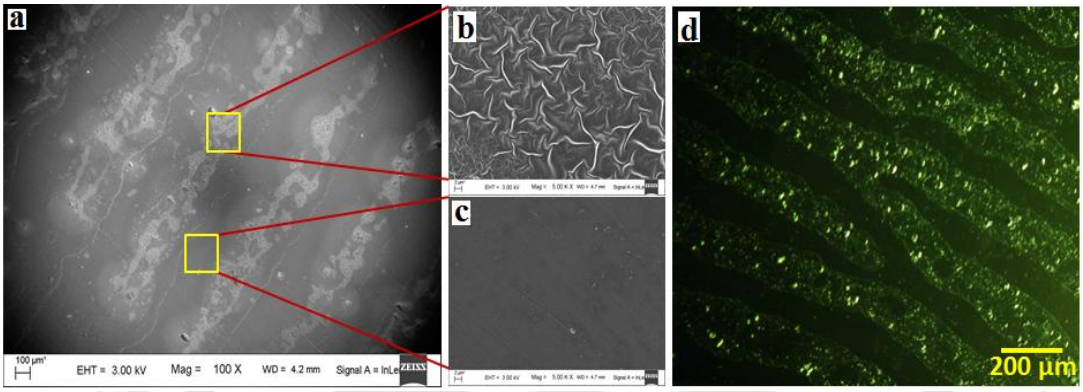

Figure 5.4 (a) FESEM images of developed LFPs showing adhesion of CPE on (b) ridges rather than on (c) furrows with a lower and higher magnification. (d) Fluorescence microscopic images of the developed LFPs.

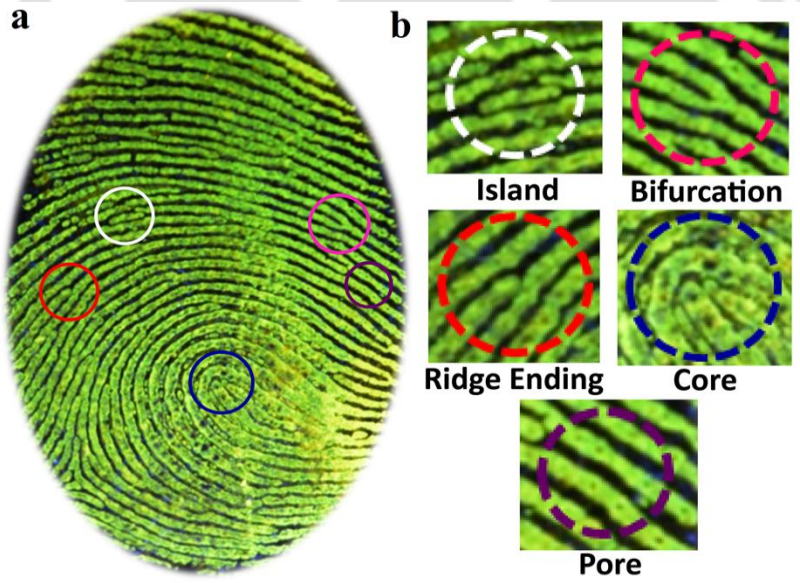

Figure 5.5 High-resolution photographs of LFPs after developing with PFTPEBT-MI showing level 1-3 details including island, bifurcation, core, ridge ending, and pores under the excitation of UV radiation (365 nm).

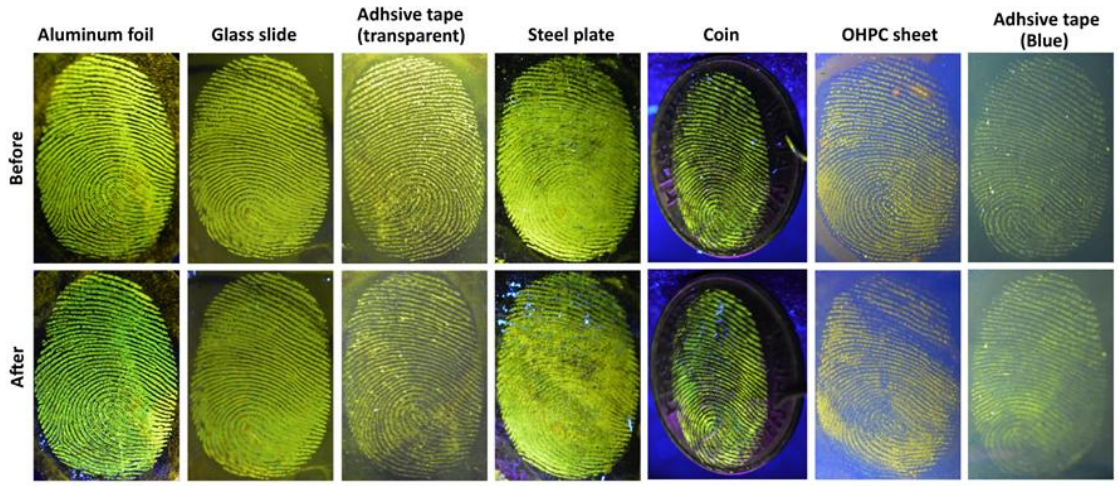

Figure 5.6 Digital photographs of LFPs developed with PFTPEBT-MI on different substrates before and after abrasion with double sided tape under UV irradiation (365 nm).

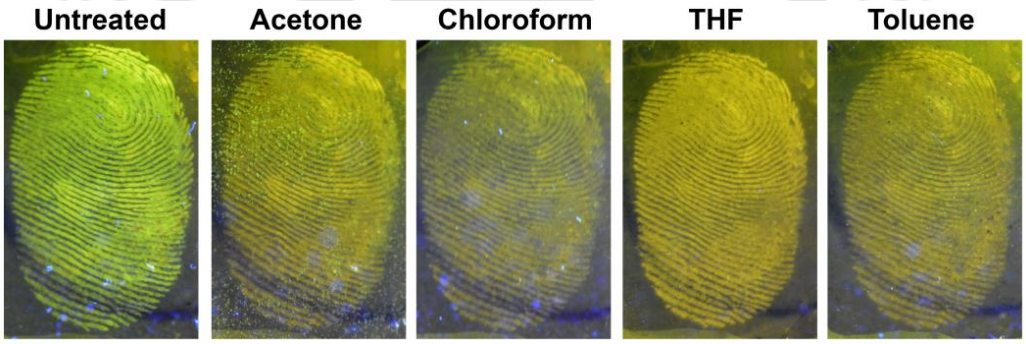

Figure 5.7 Chemical abrasion of the developed fingerprint on a glas slide upon treatment with various solvents.

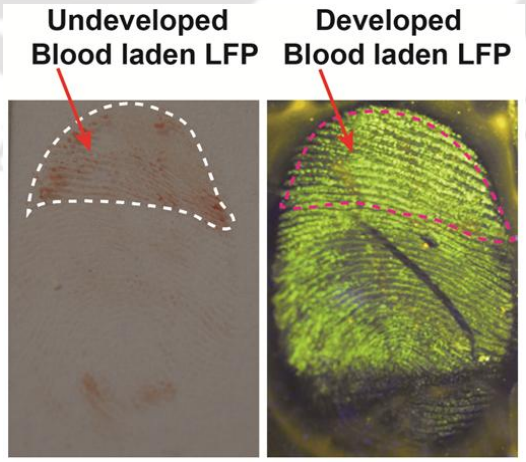

Figure 5.8 Blood laden LFPs developed on a glas slide.

5.3.3 Application of PFTPEBT-MI for LFP development

To evaluate the practicability of PFTPEBT-MI assay for detection of latent fingerprints as the weight of evidence in real samples the CPE solution was added into a spray bottle, along with 20%-30% (v/v) of methanol for quick evaporation of residual polymer solution and then sprayed onto the substrate such as drinking glass and tin can (soft drink container) to develop LFPs. As shown in **Figure 5.9a**, the fluorescence generated by CPE in the fingerprint patterns could be clearly observed. Although the blank ink on the tin can interfere with the visualization of LFPs, yet the fingerprint details could be clearly recognized with high resolution and high contrast. Similarly results could also be seen on a drinking glass, as shown in **Figure 5.9b**. These results confirmed that CPE PFTPEBT-MI can be applied to a variety of samples and will have widespread use in forensic sciences.

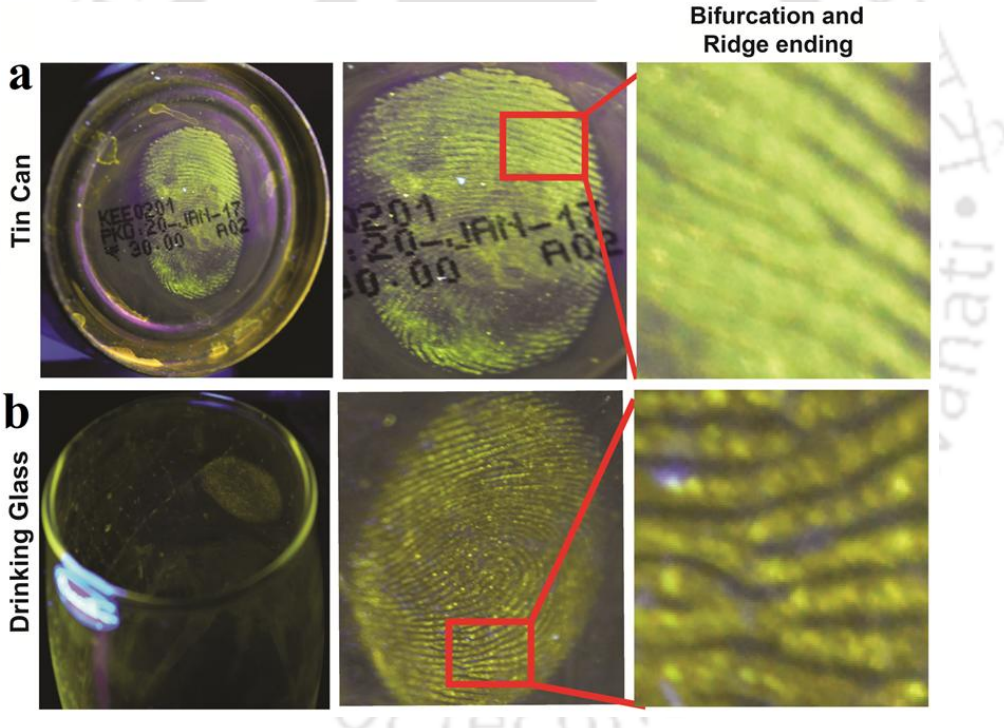

Figure 5.9 Images of LFPs developed with PFTPEBT-MI (a) tin can and (b) drinking glass. The left and middle set of each image represent the photographs of latent fingerprints under 365 nm light irradiation. The right set shows the enlarged fluorescence images of latent fingerprints with third level details.

5.4 Conclusion

In conclusion, a highly convincing, sensitive, environmentally friendly and cost-effective approach for the enhanced visualization of latent fingerprint based on AIEE active

conjugated polyelectrolyte PFTPEBT-MI was successfully developed by simply dipping the fingerprint laden substrate into the polymeric solution or spraying the polymer on the surface of evidence. The high fluorescence brightness and large Stokes shift contributed to the high-resolution imaging of latent fingerprints without any post-treatment such as fume treatment, surfactants, etc. for latent fingerprint development, therefore providing highly reliable and concrete evidence (1-3 level), which makes the identification of an individual suspect very easy and beyond doubt. Thus, PFTPEBT-MI polymer could be effectively applied in developing LFPs with high-sensitivity on practically any surface such as glass, aluminum foil, steel, coins, adhesive tape etc. with negligible interference including blood, in the presence of even harsh external abrasions which could hinder in the identification of personal information, thereby demonstrating successfully the durability and unmatched ability of this approach. We anticipate that the present method could be used in the detection of LFP and further find its utility for various forensic applications.

References

(1) Faulds, H. *Nature* **1880**, *22*, 605.

(2) Saferstein, R. *Criminalistics*: *An Introduction to Forensic Science*, 9th ed.; Prentice Hall: Upper Saddle River, NJ, **2006**.

(3) Ortiz-Bacon, D. L.; Swanson, C. L. In *Encyclopedia of Forensic Sciences*, 2nd ed.; Siegel, J. A., Saukko, P. J., Eds.; Elsevier: Waltham, MA, **2013**.

(4) Hazarika, P.; Russell, D. A. *Angew. Chem., Int. Ed.* **2012**, *51*, 3524.

(5) Oden, S.; Hofsten, B. V. *Nature* **1954**, *173*, 449.

(6) Sodhi, G. S.; Kaur, J. *Forensic Sci. Int.* **2001**, *120*, 172.

(7) Jasuja, O. P.; Kaur, A.; Kumar, P. *Forensic Sci. Int.* **2012**, *223*, e47.

(8) Fung, T. C.; Grimwood, K.; Shimmon, R.; Spindler, X.; Maynard, P.; Lennard, C.; Roux, C. *Forensic Sci. Int.* **2011**, *212*, 143.

(9) Tahtouh, M.; Kalman, J. R.; Reedy, B. J. *J. Polym. Sci., Part A: Polym. Chem.* **2011**, *49*, 257.

(10) Frick, A. A.; Busetti, F.; Cross, A.; Lewis, S. W. *Chem. Commun*. **2014**, *50*, 3341.

(11) Jiang, H.; Taranekar, P.; Reynolds, J. R.; Schanze, K. S. *Angew. Chem., Int. Ed*. **2009**, *48*, 4300.

(12) Feng, F.; Tang, Y.; Wang, S.; Li, Y.; Zhu, D. *Angew. Chem., Int. Ed*. **2007**, *46*, 7882.

(13) Hoven, C. V.; Garcia, A.; Bazan, G. C.; Nguyen, T.-Q. *Adv. Mater*. **2008**, *20*, 3793.

(14) Zhu, C.; Liu, L.; Yang, Q.; Lv, F.; Wang, S. *Chem. Rev*. **2012**, *112*, 4687.

(15) Lee, B. H.; Jung, I. H.; Woo, H. Y.; Shim, H.-K.; Kim, G.; Lee, K. *Adv. Funct. Mater*. **2014**, *24*, 1100.

(16) Liu, B.; Bazan, G. C. *Chem. Mater*. **2004**, *16*, 4467.

(17) Thomas, S. W.; Joly, G. D.; Swager, T. M. *Chem. Rev*. **2007**, *107*, 1339.

(18) Ho, H.-A.; Najari, A.; Leclerc, M. *Acc. Chem. Res*. **2008**, *41*, 168.

(19) McQuade, D. T.; Pullen, A. E.; Swager, T. M. *Chem. Rev*. **2000**, *100*, 2537.

(20) Zhu, C.; Liu, L.; Yang, Q.; Lv, F.; Wang, S. *Chem. Rev*. **2012**, *112*, 4687.

(21) Liang, J.; Lia, K.; Liu, B. *Chem. Sci.* **2013**, *4*, 1377.

(22) Rochat, S; Swager, T. M. *ACS Appl. Mater. Interfaces* **2013**, *5*, 4488.

(23) Kwak, G.; Lee, W. E.; Kim, W. H.; Lee, H. *Chem. Commun*. **2009**, *16*, 2112.

(24) Yang, S. Y.; Wang, C. F.; Chen, S. *Angew. Chem.* **2011**, *123*, 3790.

(25) Choi, M. J.; Smoother, T.; Martin, A. A.; McDonagh, A. M.; Maynard, P. J.; Lennard, C.; Roux, C. *Forensic Sci. Int*. **2007**, *173*, 154.

(26) Lee, J.; Lee, C. W.; Kim, J. M. *ACS Appl. Mater. Interfaces* **2016**, *8*, 6245.

(27) Dilag, J.; Kobus, H.; Ellis, A. V. *Forensic Sci. Int.* **2009**, *187*, 97.

(28) Algarra, M.; Jiménez-Jiménez, J.; Moreno-Tost, R.; Campos, B. B.; Esteves da Silva, J. C. G. *Opt. Mater.* **2011**, *33*, 893.

(29) Wang, J.; Wei, T.; Li, X.; Zhang, B.; Wang, J.; Huang, C.; Yuan, Q. *Angew. Chem.* **2014**, *126*, 1642.

(30) Bettinelli, M.; Carlos, L.; Liu, X. G. *Phys. Today* **2015**, *68*, 38.

(31) Choi, M. J.; Sun, Y. S.; Kim, C. S.; Choi, M. S.; Sung, N. D.; Park, S. W. *Anal. Sci. Technol.* **2007**, *20*, 147.

(32) Choi, M. J.; Ha, J.; Yoo, S.; Park, S. W. *Anal. Sci. Technol.* **2007**, *20*, 434.

(33) Shirreffs, S. M.; Maughan, R. J. *J. Appl. Physiol.* **1997**, *82*, 336.

(34) Greene, R.; Downing, D.; Pochi, P.; Strauss, J. *J. Invest. Dermatol.* **1970**, *54*, 240.

(35) Nicolaides, N. *Science* **1974**, *186*, 19.

(36) Chen, H.; Chang, K.; Men, X.; Sun, K.; Fang, X.; Ma, C.; Zhao, Y.; Yin, S.; Qin, W.; Wu, C. *ACS Appl. Mater. Interfaces* **2015**, *7*, 14477.

(37) Wang, M.; Li, M.; Yu, A.; Wu, J.; Mao, C. *ACS Appl. Mater. Interfaces* **2015**, *7*, 28110.

(38) Kim, B. S.; Jin, Y.-J.; Uddin, M. A.; Sakaguchi, T.; Woo, H. Y.; Kwak, G. *Chem. Commun.* **2015**, *51*, 13634.

(39) Hu, R.; Lam, J. W. Y.; Liu, J.; Sung, H. H. Y.; Williams, I. D.; Yue, Z.; Wong, K. S.; Yuen, M. M. F.; Tang, B. Z. *Polym. Chem.* **2012**, *3*, 1481.

(40) Pu, K. Y.; Liu, B. A. *Macromolecules* **2008**, *41*, 6636.

(41) Choi, M. J.; McDonagh, A. M.; Maynard, P.; Roux, C. *Forensic Sci. Int.* **2008**, *179*, 87.

(42) Zhang, D.; Liu, F.; Zhao, Q.; Lu, G.; Luo, N. *IEEE Trans. Instrum. Meas.* **2011**, *60*, 863.

Appendix

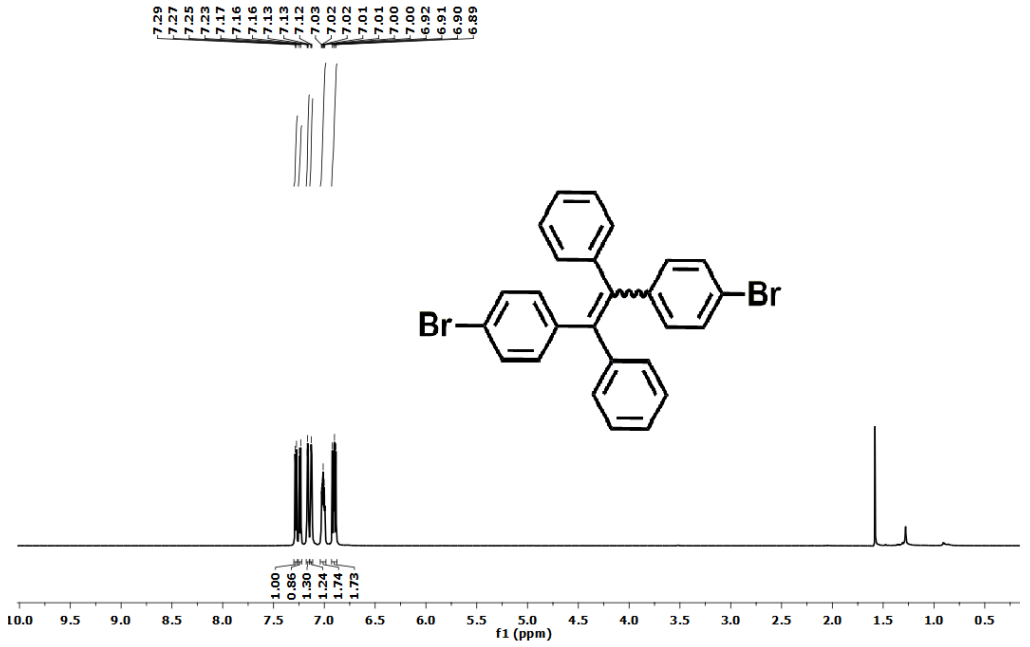

Figure A5.1 ^{1}H NMR spectra of M3.

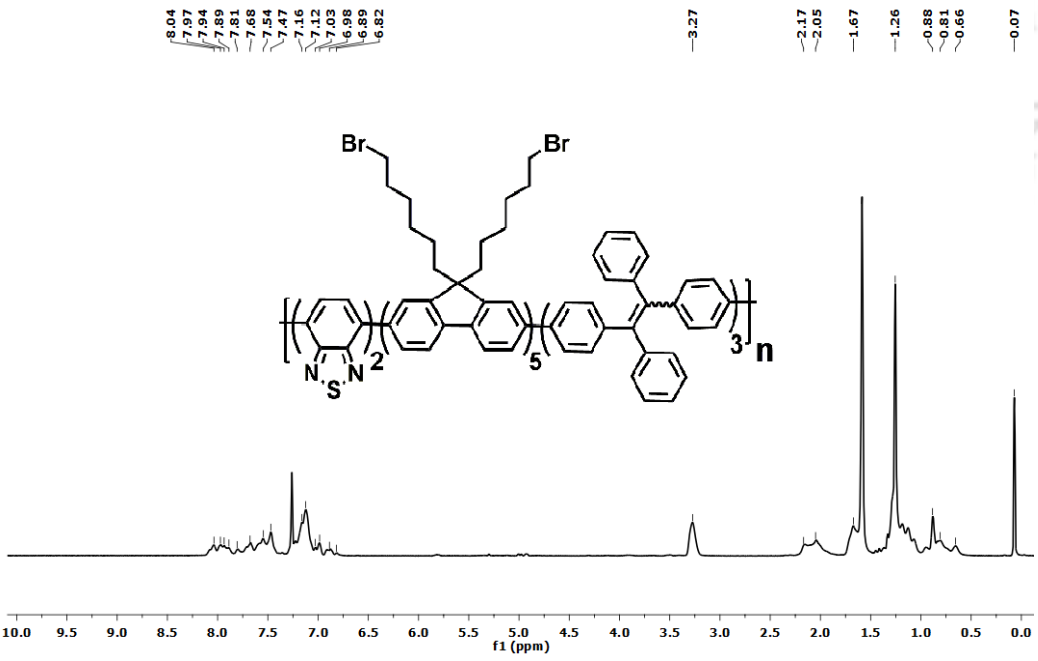

Figure A5.2 ^{1}H NMR spectra of PFTPEBT.

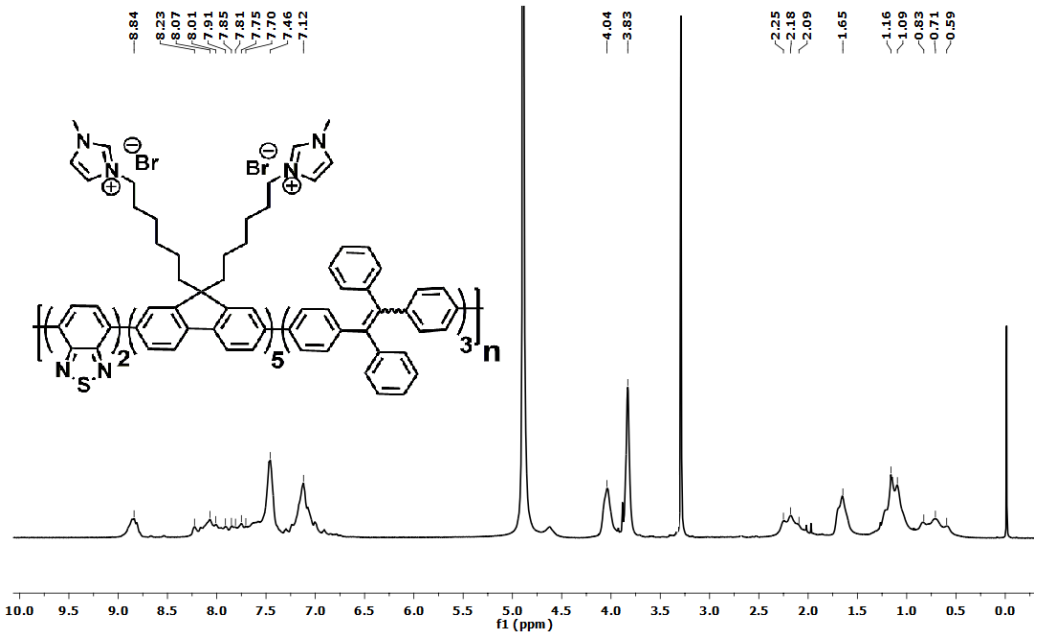

Figure A5.3 ^{1}H NMR spectra of PFTPEBT-MI.

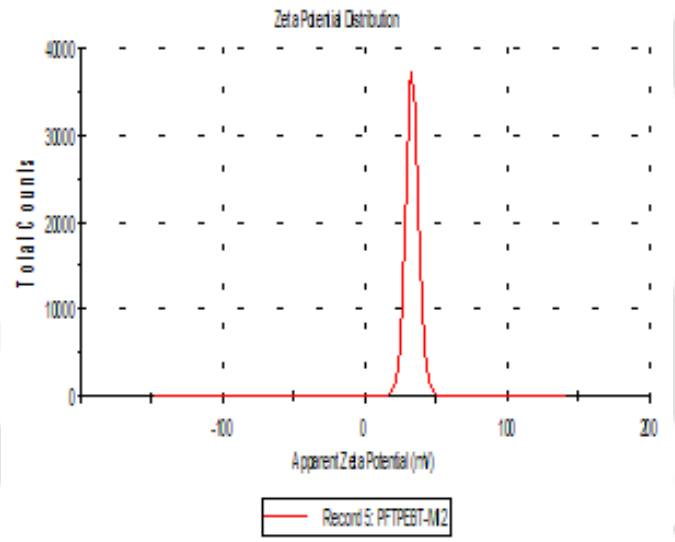

Figure A5.4 Zeta potential of PFTPEBT-MI.

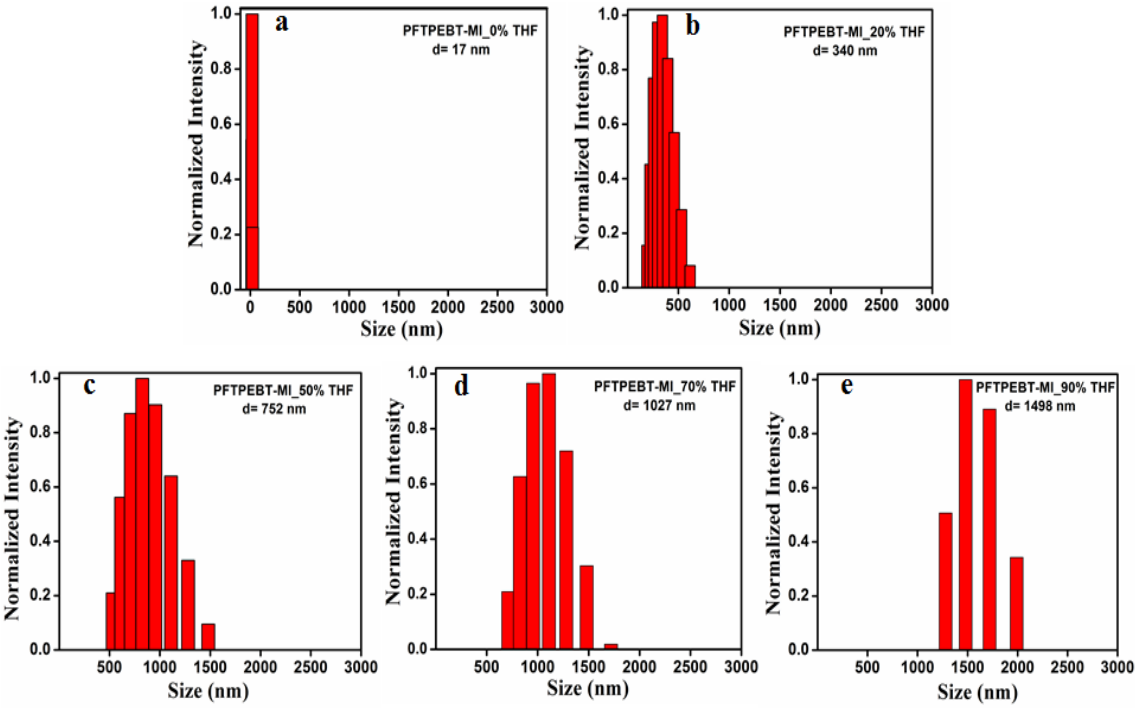

Figure A5.5 Formation of polymer aggregates with increasing fraction of THF (a-e).

Figure A5.6 Physical abrasion of the developed fingerprint substrate using a double sided tape.

Publications

1. Hussain, S.; **Malik, A. H**.; Iyer, P. K. Highly precise detection, discrimination, and removal of anionic surfactants over the full pH range *via* cationic conjugated polymer: An efficient strategy to facilitate illicit–drug analysis, *ACS Appl. Mater. Interfaces* **2015,** *7*, 3189–3198.

2. Hussain, S.; **Malik, A. H**.; Afroz, M. A.; Iyer, P. K. Ultrasensitive detection of nitro explosive–picric acid *via* conjugated polyelectrolyte in aqueous media and solid support, *Chem. Commun.* **2015**, *51*, 7207–7210.

3. **Malik, A. H**.; Hussain, S.; Tanwar, A. S.; Layek, S.; Trivedi, V.; Iyer, P. K. An anionic conjugated polymer as a multi–action sensor for the sensitive detection of Cu^{2+} and PPi, *Analyst* **2015**, *140*, 4388–4392.

4. Kalita, A.; Hussain, S.; **Malik, A. H**.; Subbarao, N. V. V.; Iyer, P. K. Vapor phase sensing of ammonia at the sub–ppm level using a perylene diimide thin film device, *J. Mater. Chem. C.* **2015**, *3*, 10767–10774.

5. **Malik, A. H**.; Hussain, S.; Kalita, A.; Iyer, P. K. Conjugated polymer nanoparticles for the amplified detection of nitro–explosive picric acid on multiple platforms, *ACS Appl. Mater. Interfaces* **2015**, *7*, 26968–26976.

6. Hussain, S.; **Malik, A. H**.; Iyer, P. K. FRET–assisted selective detection of flavins *via* cationic conjugated polyelectrolyte under physiological conditions, *J. Mater. Chem. B* **2016**, *4*, 4439–4446.

7. **Malik, A. H**.; Hussain, S., Iyer, P. K. Aggregation–induced FRET *via* polymer–surfactant complexation: A new strategy for the detection of spermine, *Anal. Chem.* **2016**, *88*, 7358–7364.

8. Tanwar, A. S.; Hussain, S.; **Malik, A. H**.; Afroz, M. A.; Iyer, P. K. An inner–filter effect based selective detection of nitroexplosive–picric acid in aqueous solution and solid support using conjugated polymer, *ACS. Sens.* **2016**, *1*, 1070–1077.

9. Kalita, A.; Hussain, S.; **Malik, A. H**.; Barman, U.; Goswami, N.; Iyer, P. K. Anion–exchange induced strong π–π interactions in single crystalline naphthalene diimide for nitroexplosive sensing: An electronic prototype for visual on–site detection, *ACS Appl. Mater. Interfaces* **2016**, *8*, 25326–25336.

Publications

10. **Malik, A. H**.; Iyer, P. K. Conjugated Polyelectrolyte Based Sensitive Detection and Removal of Antibiotics Tetracycline from Water, *ACS Appl. Mater. Interfaces* **2017**, *9*, 4433–4439.

11. **Malik, A. H**.; Kalita, A.; Iyer, P. K. Development of Well-Preserved, Substrate-Versatile Latent Fingerprints by Aggregation-Induced Enhanced Emission-Active Conjugated Polyelectrolyte, *ACS Appl. Mater. Interfaces* **2017**, *9*, 37501-37508.

Conferences & Seminars

1. Presented a ***POSTER*** in "Research Conclave '17" organized by Students' Academic Board (SAB), IIT Guwahati during 16–19 March 2017.
2. Attended the full agenda of **ACS on campus** (An Initiative from the American Chemical Society) at Indian Institute of Technology Guwahati, Guwahati, India on January 16, 2017.
3. Delivered an ***ORAL*** talk in Frontiers in Chemical Sciences (FICS 2016) conducted by Department of chemistry, Indian Institute of Technology Guwahati during 08-11 Dec 2016.
4. Participated in "2nd National Workshop on NEMS/MEMS and Theranostics Devices" (NWNTD–2016) organized by Centre for Nanotechnology, IIT Guwahati during 21–22 March 2016.
5. Presented a ***POSTER*** in "Research Conclave '16" organized by Students' Academic Board (SAB), IIT Guwahati during 17–20 March 2016.
6. Attended "National Workshop on Advanced Probing Techniques in TEM" organized jointly by IIT Guwahati and Electron Microscopy Society of India during 15–16 February 2016.
7. Presented a ***POSTER*** in Materials and Research Society of India (MRSI) symposium on "Advanced Materials for Sustainable Applications" held at NEIST, Jorhat during 18–21 February 2016.
8. Delivered ***ORAL*** talk in Global Research Mind Seminar held at Kyushu Institute of Technology Japan on 19 January 2016.
9. Delivered an ***ORAL*** talk in "4th International Conference on Advanced Nanomaterials and Nanotechnology" (ICANN–2015) organized by Centre for Nanotechnology, IIT Guwahati during 08–11 December 2015.
10. Presented a ***POSTER*** in 68th Annual Session of Indian Institute of Chemical Engineers (CHEMCON 2015) held at Indian Institute of Technology during Dec 27-30, 2015.
11. Attended "2–Day Familiarization Workshop on Nanofabrication Technologies" held at Tezpur University during 25–26 April 2015 funded by the Dept of Electronics and

Information Technology (DeitY), the Ministry of Communication and Information Technology (MCIT), Govt. of India.

12. Presented a ***POSTER*** at Annual Chemical Engineering Festival (Reflux 2015) during 27-29 March, 2015 organized by Department of Chemical Engineering, IIT Guwahati, India.

13. Presented a ***POSTER*** in "International Symposium on Polymer Science and Technology" (MACRO 2015) organized jointly by the Kolkata and Kharagpur chapters of the SPSI at the Indian Association for the Cultivation of Science (IACS), Kolkata during 23–26 January, 2015.

14. Attended "National Conference on Recent Advances in Cancer Biology and Therapeutics" (RACBT) organized by Department of Biotechnology, IIT Guwahati on 5th December, 2014.

Awards & Achievements

1. Received ***Departmental Best Poster Award*** in Research Conclave '16 organized by Students' Academic Board (SAB), IIT Guwahati during 15–19 March 2017.
2. Received ***Institute Best Poster Award*** in Research Conclave '16 organized by Students' Academic Board (SAB), IIT Guwahati during 17–20 March 2016.
3. Awarded ***Full Grant*** from Department of Science and Technology (DST), Govt. of India for delivering an ***ORAL*** talk in Global Research Mind Seminar 2016 held at Kyushu Institute of Technology Japan.
4. Delivered an ***Invited Lecture*** in the 2nd Indo-Sweden Joint International Workshop held at IIT Guwahati on 2nd December 2015.
5. Received ***Best Poster Award i***n Annual Chemical Engineering Festival "Reflux 2015" organized by Department of Chemical Engineering, IIT Guwahati during 27–29 March 2015.

Title: Conjugated Polymer Nanoparticles for the Amplified Detection of Nitro-explosive Picric Acid on Multiple Platforms

Author: Akhtar Hussain Malik, Sameer Hussain, Anamika Kalita, et al

Publication: Applied Materials

Publisher: American Chemical Society

Date: Dec 1, 2015

PERMISSION/LICENSE IS GRANTED FOR YOUR ORDER AT NO CHARGE

This type of permission/license, instead of the standard Terms & Conditions, is sent to you because no fee is being charged for your order. Please note the following:

- Permission is granted for your request in both print and electronic formats, and translations.
- If figures and/or tables were requested, they may be adapted or used in part.
- Please print this page for your records and send a copy of it to your publisher/graduate school.
- Appropriate credit for the requested material should be given as follows: "Reprinted (adapted) with permission from (COMPLETE REFERENCE CITATION). Copyright (YEAR) American Chemical Society." Insert appropriate information in place of the capitalized words.
- One-time permission is granted only for the use specified in your request. No additional uses are granted (such as derivative works or other editions). For any other uses, please submit a new request.

BACK CLOSE WINDOW

TH-1653_126122024

Title: Conjugated Polyelectrolyte Based Sensitive Detection and Removal of Antibiotics Tetracycline from Water

Author: Akhtar Hussain Malik, Parameswar Krishnan Iyer

Publication: Applied Materials

Publisher: American Chemical Society

Date: Feb 1, 2017

PERMISSION/LICENSE IS GRANTED FOR YOUR ORDER AT NO CHARGE

This type of permission/license, instead of the standard Terms & Conditions, is sent to you because no fee is being charged for your order. Please note the following:

- Permission is granted for your request in both print and electronic formats, and translations.
- If figures and/or tables were requested, they may be adapted or used in part.
- Please print this page for your records and send a copy of it to your publisher/graduate school.
- Appropriate credit for the requested material should be given as follows: "Reprinted (adapted) with permission from (COMPLETE REFERENCE CITATION). Copyright (YEAR) American Chemical Society." Insert appropriate information in place of the capitalized words.
- One-time permission is granted only for the use specified in your request. No additional uses are granted (such as derivative works or other editions). For any other uses, please submit a new request.

BACK CLOSE WINDOW

TH-1653_126122024

Title: Aggregation-Induced FRET via Polymer–Surfactant Complexation: A New Strategy for the Detection of Spermine

Author: Akhtar Hussain Malik, Sameer Hussain, Parameswar Krishnan Iyer

Publication: Analytical Chemistry

Publisher: American Chemical Society

Date: Jul 1, 2016

PERMISSION/LICENSE IS GRANTED FOR YOUR ORDER AT NO CHARGE

This type of permission/license, instead of the standard Terms & Conditions, is sent to you because no fee is being charged for your order. Please note the following:

- Permission is granted for your request in both print and electronic formats, and translations.
- If figures and/or tables were requested, they may be adapted or used in part.
- Please print this page for your records and send a copy of it to your publisher/graduate school.
- Appropriate credit for the requested material should be given as follows: "Reprinted (adapted) with permission from (COMPLETE REFERENCE CITATION). Copyright (YEAR) American Chemical Society." Insert appropriate information in place of the capitalized words.
- One-time permission is granted only for the use specified in your request. No additional uses are granted (such as derivative works or other editions). For any other uses, please submit a new request.

TH-1653_126122024

